The University Of Sheffield.

Design rules for non-aqueous foam formulations

Niall Ward-O'Brien

Thesis submitted for the degree of Doctor of Philosophy

September 2021

Department of Chemistry

University of Sheffield

Supervisor:

Professor Anthony J Ryan

University of Sheffield

Abstract

Foams are a colloidal phase of matter, composed of ga bubbles dispersed within a liquid. They find use in many applications and have excellent properties for alcohol-based hand rubs. However, producing foams in alcohol-water mixtures is challenging, and typically requires siloxane polyether surfactants. In addition, little is known about the structure-property relationships which govern properties such as foamability in these systems. An empirical model was developed that connects chemical, interfacial and foaming behaviour for siloxane polyethers and facilitates the development of higher performance foaming agents.

A set of triblock siloxane polyether surfactants has been characterised. Foam fractionation and solvent extraction were shown to remove impurities from such surfactants and improve foaming performance. In addition, empirical rules were developed to predict which siloxane-polyether surfactants should disperse well in various water-ethanol mixtures.

Several methods were explored to determine the critical micelle concentration for a series of siloxane polyethers. The critical micelle concentration was shown to decline rapidly as the size of the siloxane block and the relative proportion of water in the solvent mixture are increased.

Foaming performance was explored using experimental design and regression modelling. Strong interactions were found between surfactant composition and ethanol content, with siloxane-rich surfactants performing better in ethanol-rich solutions. Significant differences in foamability are observed between different foaming methods.

Du Noüy ring tensiometry and the maximum bubble pressure method are used to measure dynamic surface tension over a range of surface ages. As indicated by the critical micelle concentration, surfactants in water-rich solutions are shown to be more kinetically limited than ethanol-rich solutions. Surface pressures measured at a characteristic time for different foaming methods are shown to accurately predict foamability.

In conclusion, direct links are made between surfactant composition, interfacial behaviour and foaming properties. Solvent composition and foaming method are shown to be important variables in designing a surfactant for good foaming performance in water-ethanol mixtures.

Acknowledgements

I owe many thanks to Tony Ryan for his supervision, support and advice over the last four years – through the ups and downs of the project, he has always been compassionate, engaged and enthusiastic. Thanks to the rest of the RyMyk group for sharing their knowledge and wisdom and being great lab/office company, and to the CDT cohort for their support and friendship.

I also want to acknowledge the technical and administrative staff at the department – in particular, Garry Turner, who designed & built the automated foam test rig, Sandra van Meurs, who assisted with NMR and Sharon Spey & Simon Thorpe, who assisted with mass spectrometry.

More broadly, I also want to thank all the staff and students I've interacted with or been taught by over the last 8 years in the Chemistry Department at Sheffield – I'll miss it.

Thanks to SCJ Professional for part-funding my project, providing many useful materials and an interesting challenge to work on. Thanks to John Hines, Mat Slack and Chris Lang for their ideas, encouragement and willingness to endure very long, dry presentations about foam.

I also have to thank my friends and family – especially Fiona and Fergus – for commiserating with me when things were going wrong and listening to my excited babbling when they weren't. Finally, thanks to Abi, without whom I may have gone completely mad at some point in the last four years, and whose bad influence has apparently corrupted even this thesis with social science-ish overtones.

I'd like to dedicate this thesis to Charles F. Ward, with whom I would have loved to have shared it.

Contents

Abstract 2

Acknowledgements 3

1 Introduction 8

1.1 Overview & levels of analysis 8

1.2 Surfactants 9

1.2.1 Overview and structure 9

1.2.2 Self-assembly 9

1.2.3 Surfactants and foaming 10

1.3 Interfaces 10

1.3.1 Surface tension 10

1.3.2 Surface tension gradients 11

1.4 Foam structure 12

1.4.1 Formation 12

1.4.2 Structure 13

1.5 Foam dynamics and rheology 14

1.5.1 Drainage 14

1.5.2 Coarsening 15

1.5.3 Film rupture and coalescence 15

1.5.4 Rheology of foams 16

1.6 Non-aqueous foams 17

1.7 Alcohol-based hand rubs (ABHRs) 18

1.7.1 ABHRs and hand hygiene 18

1.7.2 ABHR formats 18

1.7.3 Foaming ABHRs 19

2 Literature review 21

2.1 Overview 21

2.2 Methodological considerations in foam research 21
2.2.1 Dynamic versus equilibrium behaviour 21
2.2.2 Foamability and foam stability 22
2.3 Structure-foamability relationships for surfactants 24
2.4 Surfactant behaviour in non-aqueous polar media 25
2.5 Foaming in non-aqueous media 26
2.6 Siloxane surfactants 27
2.7 Conclusion 29
3 Project Aims 32
3.1 Thesis structure 32
4 Surfactant characterisation 34
4.1 Material characterisation 34
4.1.1 Materials and methods 34
4.1.2 Characterisation results and discussion 36
4.2 Impurities and their influence on foaming 46
4.2.1 Methods 46
4.2.2 Purity results and discussion 47
4.3 Surfactant synthesis 55
5 Micelle investigation and characterisation 57
5.1 Materials and methods 57
5.1.1 Equilibrium surface tension 57
5.1.2 Dye solubilisation 57
5.1.3 Small-angle X-ray scattering (SAXS) 58
5.1.4 Dynamic light scattering (DLS) 59
5.2 Results and discussion of micelle characterisation 59
5.2.1 Equilibrium surface tension measurements 59
5.2.2 Dye solubilisation measurements 62

5.2.3 Discussion of SAXS 64
5.2.4 Discussion of DLS 66
6 Foam research 70
6.1 Foam generation methods 70
6.2 Design of Experiments (DoE) 73
6.3 Application of statistical methods 75
6.3.1 Regression 75
6.3.2 Modelling considerations 76
6.3.3 Modelling methods 79
6.4 Foamability results and discussion 83
7 Development of pendant drop tensiometer 101
7.1 Theory 101
7.2 Instrument design and construction 102
7.3 Code interface & algorithmic development 104
7.3.1 In-line calculation 104
7.3.2 Offline calculation 105
7.4 Sample results 109
8 Dynamic surface tension 112
8.1 Theory 112
8.2 Methods 112
8.2.1 Du Noüy ring tensiometry 112
8.2.2 Maximum bubble pressure method (MBPM) 113
8.3 Dynamic surface tension results 113
8.3.1 Du Noüy ring tensiometry 114
8.3.2 Maximum bubble pressure method 118
8.3.3 Relationship with foamability 122
8.4 Time-concentration superposition 125

8.4.1 Theory 125
8.4.2 Methods 126
8.4.3 Results 128
9 Discussion 134
9.1 Substantive outcomes 134
9.1.1 Molecular/surfactant properties 134
9.1.2 Interfacial and solution properties 135
9.1.3 Foam properties 135
9.1.4 Linking surface and foam properties 136
9.2 Methodological developments 137
9.3 Strengths 138
9.4 Key limitations 138
9.5 Future work 139
10 References 140
11 Appendices 146
11.1 Doping Model 147
11.2 Foam pump naïve model 148
11.3 Foam pump informed model 151
11.4 Sparging foam volume model 153
11.5 Sparging foam half-life model 155
11.6 Vortexing foam volume model 157
11.7 Double syringe half-life model 159
11.8 Surface pressure model 160

1 Introduction

Liquid foams are a phase of dispersed matter formed by the mixture of a liquid and a gas phase, in which pockets of gas are separated by thin films of liquid. As with many phases of dispersed matter, foams are inherently thermodynamically unstable and, over time, their components typically seek to separate and thereby minimise their surface area. Foams are made quasi-stable by the presence of surface-active compounds, which act by several mechanisms to prevent film collapse.

This section introduces important background concepts regarding foam structure, the role of surfactants and the advantages of foams as a medium for alcohol-based hand rubs.

1.1 Overview & levels of analysis

Foams can be examined on several length- and time-scales – the smallest (and shortest) is that of the molecular dynamics of surfactant molecules, which assemble at interfaces and films, and includes rapid processes such as surfactant adsorption, Marangoni flows and the effects of disjoining pressures – this can be characterised as the domain of 'chemistry' and will be the broad focus of this work.

At longer length and time scales, one enters the realm of 'physics' – here, foam films are broadly in equilibrium and processes such as drainage, coarsening and film rupture occur over the timescale of minutes or longer. At this level of analysis, the behaviour of surfactant molecules at films is largely abstracted as a surface tension – rather, it is the behaviour of individual bubbles, films and nodes that is of central interest.

At the longest length scale, the details of foam structure blur and the foam becomes essentially a continuous material. This is the realm of foam rheology, in which the complex rearrangements and processes occurring at shorter length scales below influence the viscous and elastic properties of the bulk foam.[1]

This introduction will begin at the molecular level, describing surfactants and their role, extend to the intermediate level of interfaces and films, and then describe foams. Finally, it will outline the research problem which this thesis seeks to address – the behaviour of surfactants in water-ethanol mixtures, and their practical application in alcohol-based hand rubs.

1.2 Surfactants

1.2.1 Overview and structure

Surfactants are a class of compounds of crucial importance to foam formation. By assembling at interfaces, they make foam bubbles resilient and elastic.[2]

Surfactant behaviour is a result of their amphiphilic nature – they possess both solvophilic and solvophobic moieties – see Figure 1. Thus surfactant molecules are driven to the interface by unfavourable interactions with solvent but are prevented from undergoing phase separation by an anchoring solvophilic group. In aqueous solution, such separation is driven by the hydrophobic effect, which describes the significant free energy gains which occur on the removal of hydrophobic moieties from bulk solvent.[1]

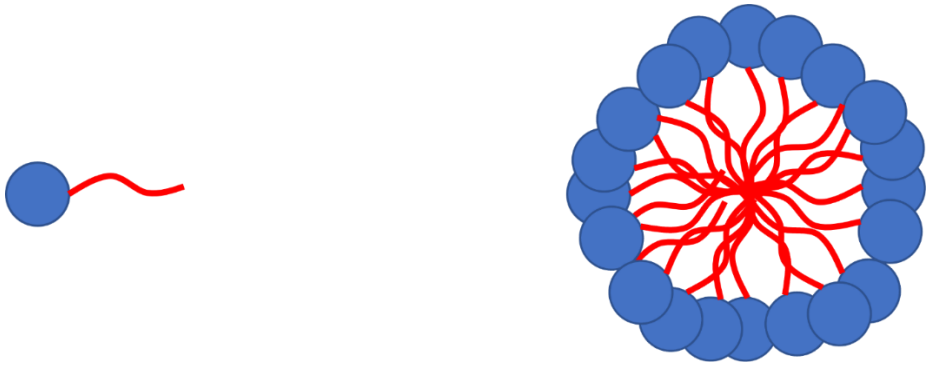

Figure 1. Schematic representation of a typical surfactant molecule and cross-section of a micelle. The hydrophilic head group is represented as a blue circle, and the hydrophobic tail group as a red line. Voids within the micelle are filled with solvent.

For conventional surfactants, the solvophobic portion is typically an alkyl chain, whereas the solvophilic 'head' may be a salt (e.g. a sulfate group) or a hydrophilic oligomer such as poly(ethylene oxide) (PEO). A wide range of important biomolecules, such as proteins and glycolipids, also exhibit surfactant behaviour.[2]

In some applications (e.g., superwetting or in non-aqueous systems) more 'exotic' surfactants are required to achieve satisfactory performance. Such surfactants typically contain super-hydrophobic groups such as siloxanes or fluorocarbons.[3]

1.2.2 Self-assembly

As the concentration of surfactant in a solution increases, the interface becomes saturated with solvophobic moieties and further adsorption becomes impossible. At this point, surfactants form structures within the liquid phase which screen their solvophobic moieties from solvent. Initially, these take the form of micelles, roughly spherical structures in which

surfactants can screen their solvophobic moieties, while presenting solvophilic groups to the solvent – see Figure 1. As surfactant concentration increases further, higher-order structures can also form.[2,4,5] The concentration region at which micelles form is termed the critical micelle concentration (CMC).[2]

The thermodynamics of micelle formation and dissolution are strongly influenced by the solvent environment and nature of the surfactant. Micelle formation depends on unfavourable interactions between solvent molecules and surfactant – thus reducing solvent quality or increasing the size of the solvophobic moiety makes micelle formation more favourable.[6–8]

Polar solvents such as alcohols increase the CMC of nonionic surfactants by increasing the solubility of their solvophobic blocks and thus reducing the free energy gain associated with micellisation.[9]

1.2.3 Surfactants and foaming

Surfactants play a vital role in foam formation and stability. They promote new surface formation, stabilise films against rupture, and give foams their elastic, solid-like properties.[2]

For foam formation to occur, surfactant needs to mobilise at the interface in a timely fashion – and once there, to make it robust and resilient to mechanical stresses.[2]

Different surfactants have markedly different foaming behaviour. Section 2.3 summarises the existing literature on structure-property relationships between surfactants and foam formation.

1.3 Interfaces

1.3.1 Surface tension

In their introduction to *The Physics of Foams*, Weaire and Hutzler observe, "*…for many purposes, a single material property, the surface tension γ, is all that matters. The rest, so to speak, is geometry*." Surface tension is the most important force in the behaviour of foams, responsible for both stabilizing them and pulling them apart.[1]

Surface tension is an ensemble property of liquids that arises from intermolecular attractive forces between solvent molecules. A molecule within the 'bulk' of a liquid experiences essentially isotropic attractive forces from surrounding molecules, but a molecule located at the interface experiences a net directional pull towards the bulk of the material. Thus, liquids

with strong cohesive forces will seek to reduce their surface area, e.g., by beading into a droplet, as molecules are pulled away from the interface. The force with which a liquid seeks to reduce its surface area is described as 'surface tension', and is dependent on the strength of intermolecular attraction in the liquid.[2]

Work is required to mix a gas and liquid. Mixing generates new interfacial area, populated by molecules from the liquid phase which would energetically 'prefer' to be elsewhere. As soon as mixing occurs, surface tension and gravity begin to act, to separate the gas and liquid phases and thereby minimise their surface area.[1]

Surfactants fundamentally alter this behaviour. Whereas a molecule of water in aqueous solution pays an energetic penalty to reside at the interface, surfactants (as a result of their solvophobic moiety) have an energetic *preference* to adsorb there. By moving surfactant to the interface, the molecular ensemble minimises the entropic penalty that arises from interactions between the solvophobic surfactant moiety and bulk solvent. Thus, surfactants stabilise the formation of interfaces and enable the generation of complex structures such as foams.[1]

1.3.2 Surface tension gradients

A low surface tension facilitates the creation of new air-liquid interfaces – this is one reason why it is easier to blow bubbles in water than in liquid mercury. But a low surface tension alone is not sufficient to generate stable foams – rather, it is surface tension *gradients*, the difference in surface tension between a surfactant-laden and a bare interface, which gives rise to the Gibbs-Marangoni effect (described below) and gives foam films a measure of resilience and elasticit.[2] This, in part, explains the difficulty in generating durable foams in ethanol, which has a relatively low surface tension compared to water, and so has less 'headroom' for surface tension gradients.

The Gibbs-Marangoni effect arises from the coupling between surface tension and interfacial surfactant concentration. When a surfactant-laden interface is stretched, the local interfacial surfactant concentration is reduced, and the surface tension will therefore increase. This rise in surface tension creates a counteracting force that resists the further expansion of the interface, and seeks to reduce its area.[2] Further, this variation in surface tension along the interface gives rise to viscous drag, which quickly transports surfactant to depleted areas of the interface ('Marangoni flow'). Thus, interfaces that can generate large surface tension

gradients are viscoelastic and capable of ‘repairing’ local stretching or thinning – giving rise to stable foams.[2]

1.4 Foam structure

1.4.1 Formation

Liquid-gas mixing, the crucial first step of foam formation, can arise through many mechanisms – one recent classification by Drenckhan *et al.* divides these into: physical mechanisms (include beating, co-flow through a tube or stator, and foaming as a result of phase transitions such as gas nucleation); chemical mechanisms (such as when gas is generated by electrochemical reactions); and biological mechanisms (when the gas is generated by organisms such as yeast).[10]

Physical mixing is the most important mechanism of formation for most liquid foams and is typical for alcohol-based hand rubs (see below). Physical mixing mechanisms are simple, repeatable and can take advantage of mechanical work on the part of a user – such as in the case of foam pumps. Within physical mechanisms, gas and liquid phases can be classified as ‘active’ and ‘passive’ participants in the foaming step. Sparging, for example, involves an active (flowing) gas phase bubbled through a passive (stationary) fluid phase. Foams formed by rapid flow of gas and liquid through a tube or frit (‘co-flow’ mechanisms) involve active gas and liquid phases. The formation of foam as ocean waves break onto shore involves a passive gas phase and an active liquid phase.[10]

A number of standardised measures exist for the generation of foams – these include: the Bikerman test, in which air is bubbled through a vertical liquid column, the Ross-Miles test, in which a liquid jet is dropped a fixed distance onto a liquid surface, and the Bartsch test, in which foam is generated by rotating a sealed container.[11–13]

Many crucial foam properties are determined or strongly influenced by the mechanism of foam formation – in particular, the proportion of the foam taken up by liquid (the ‘liquid fraction’), the size and size distribution of the bubbles.[14]

There is also robust evidence that surfactants have ‘preferred’ foaming mechanisms – Patist *et al.* report the case of three common industrial surfactants whose performance ranking could be reversed by switching from one method of foam formation to another. They argue that the methods differ in terms of the rate at which new interfacial area is generated, placing

different demands on the surfactant within the foaming solution.[15] This will be discussed in further detail in section 2.2, see below.

1.4.2 Structure

Films

Foam films are narrow sheets of liquid that form the 'faces' of the foam's cellular structure, separating bubbles from each other. Films are composed of pairs of interfaces, separated by a narrow region of liquid. They become thinner as foams dry – liquid flows out of the space between bubbles, and they are pulled closer together until an opposing 'disjoining' force arises to oppose further thinning.[16]

Wet foams comprise thicker films.[1] Their bubbles are typically spherical in shape, gradually jamming and becoming polyhedral as drying brings them into contact with each other. The packing fraction for bubbles in these spherical foams can be as low as 2/3, with bubble deformation and packing efficiency increasing as the liquid fraction is reduced – see Figure 2.[17]

In the absence of any opposing force, these films will continue to narrow until the interfaces meet, and rupture occurs. However, if the interfaces are sufficiently populated by surfactant, they introduce an opposing force which prevents further thinning of the film beyond a critical thickness. This force, the disjoining pressure, arises from repulsive interactions between solvophilic surfactant groups adsorbed at the interface. Such interactions can be electrostatic (as in the case of ionic surfactants) or steric (in the case of nonionic surfactants).[1]

Denkov and co-workers have suggested that the capacity of a surfactant to generate disjoining pressures and prevent rupture is the definitive characteristic required for good foam formation.[18]

Nodes and borders

"Plateau" nodes and borders are the thicker regions of liquid where films meet, which form a continuous network of channels running through a foam. As with films, Plateau borders arise as identifiable structures during draining, as bubbly liquids dry and bubble-bubble contacts become clearer. Nodes and borders continue to shrink as the foam dries.[1]

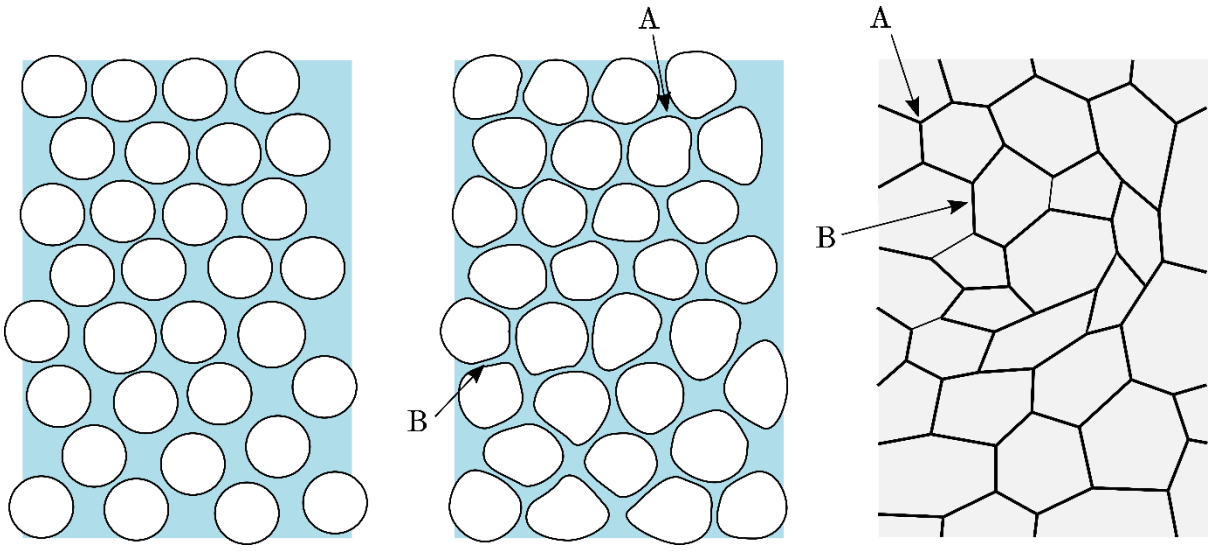

Figure 2. A schematic illustration of a liquid foam undergoing drying. A spherical foam (left) becomes a polyhedral foam (right) as its liquid content reduces and the faces of neighbouring bubbles are pressed into contact. A) indicates Plateau nodes. B) indicates Plateau borders.

The cross-section of Plateau borders is that of a triangle, with its edges becoming concave and curving inwards as the liquid fraction of the foam reduces. They form the main route through which liquid flows, propelled by either capillary pressure or gravity.[14] The walls of Plateau borders can also flow with liquid passing through them, depending on the elasticity of the interface. This propensity to flow can significantly change the 'friction' experienced by liquid passing through the network, as does the fact that Plateau borders shrink and expand in response to the liquid fraction of the local foam.[14]

1.5 Foam dynamics and rheology

Foams are dynamic structures which undergo constant change during and after their formation. This section will detail the three main processes that occur in foams– drainage, coarsening and film rupture/coalescence.

1.5.1 Drainage

Liquid flows occur in foams due to gravity and capillary pressure. The latter force draws liquid from regions of higher liquid content, where borders are enlarged, to regions of lower liquid content, in which borders are narrower. Gravity, on the other hand, draws liquid out of the foam, through the base. Gravity progressively reduces the liquid content of a foam until an equilibrium is reached with the capillary pressure. From a simplified perspective, foams can be treated as a solid, porous material, with Plateau borders and nodes acting as fixed passages through which liquid can flow.[14]

The dynamic nature of liquid foams, however, raises several issues with this model. First, the dimensions and shape (and thus the maximum flow rate) of Plateau borders are not static, but in fact vary with the liquid content of the foam and change due to drainage. Second, resistance to flow can vary between Plateau nodes and borders, again depending on their size and shape. Finally, the walls of nodes and borders are not static but can flow with the liquid passing through them, depending on the rheological properties of these interfaces.[14]

More complex models, which account for these additional features, show that physical factors (e.g., liquid fraction and bubble size) dominate the rate of drainage. These relationships are moderated by properties connected to surfactant behaviour, which affect (for instance) the shear viscosity of interfaces in Plateau nodes and borders.[14]

1.5.2 Coarsening

Films between bubbles in a dry foam are typically thin enough to allow significant gas diffusion between cells. This diffusion is driven by pressure differences between bubbles. Coarsening is analogous to Ostwald ripening in emulsions, and has the net effect of transferring gas from smaller bubbles to larger ones.[14] This increases the mean size of bubbles in the foam over time.

Coarsening is a complex process, affected by bubble geometry and a range of physicochemical factors influencing the permittivity of bubble films – including the film width, the solubility and liquid diffusivity of the gas phase and the surface tension of the interface.[14]

Coarsening and drainage also interact with each other – as foams coarsen, their bubble size distributions change and thus their rate of drainage accelerates. Hence, reducing the rate of coarsening by substituting air for a more slowly diffusing gas can lead to foams with slower drainage processes.[14] In addition, as foams dry, the width of films reduces and coarsening accelerates.

1.5.3 Film rupture and coalescence

Films progressively thin as foams age, and liquid is drawn out of a foam by gravity. Drier, thinner foam films are more vulnerable to antifoams, dust or thermal fluctuation. Foams often collapse from the top, where the foam is most exposed to external disturbance and where drying is fastest.[19]

The equilibrium width of foam films depends on the strength and type of repulsive forces at play between surfactant layers. Ionic surfactants typically show two kinetically stable thicknesses – the 'common black film', arising through electrostatic repulsion, and the 'Newton black film', resulting from short-range repulsive interactions. Nonionic surfactants only possess the latter mechanism.[1] Films are also dynamically stabilized by the Gibbs-Marangoni effect (described above), which confers viscoelastic and self-restoring behaviour on surfactant-laden interfaces.

Film rupture is a violent event, which has knock-on effects on the remaining bulk foam. Statistical analysis of foam rupture events has suggested that they are not independent, but instead occur in connected 'cascades'.[20]

Rupture and coalescence are connected to drainage and coarsening in several respects. Drier portions of the foam are more vulnerable to rupture – thus drainage can promote rupture. In turn, film rupture within a foam leads to the coalescence of bubbles and thus the creation of larger bubbles. In turn, large bubbles drive coarsening by rapidly absorbing gas from the smaller bubbles around them.[14]

1.5.4 Rheology of foams

Once a sufficiently stable foam has been generated it can be characterised by rheology - which involves applying controlled mechanical stress and monitoring the foam's response.[21]

The mechanical processes underlying foam rheology are multiscale and complex, arising from the physical character of interfaces, films and bubbles that undergo morphological change as the bulk foam is distorted.[2] Foams can display elastic, plastic and viscous behaviour, depending on their structure, physicochemical properties and the strength of forces to which they are exposed.[2]

Liquid foams, in general, have been found to possess strain-yielding behaviour - they are largely elastic up to a particular yield strain, at which point the foam begins to flow. Such behaviour is advantageous in applications such as shaving foams, which can be easily deformed but otherwise maintain their original solid structure.[10] This yield strain has been found to depend strongly on the liquid fraction of the foam, increasing as the foam becomes drier (and the bubbles become more 'jammed').[21]

There are significant differences between the bulk rheological properties of foams formed from large, protein-based surfactants and those from small molecules. However, it has been

more difficult to distinguish differences between foams arising from small-molecule surfactants, even when their films apparently possess quite different properties. These findings have led researchers to argue that the physical parameters of a foam (bubble diameter, liquid fraction) have a greater effect on its rheological behaviour than chemical parameters (e.g. surface tension, interfacial viscoelasticity).[21]

These chemical properties are still likely to play an indirect role on foam rheology, however. Two structurally identical foams stabilised by different molecular surfactants may not have measurably different rheological behaviour – but it is only in carefully controlled lab environments that it is possible to generate such structurally identical foams. In most practical applications, surfactants can still exert an effect on rheology *via* their effects on the foaming process. A surfactant which promotes greater foamability, for example, will produce a foam with a lower liquid content and thus indirectly increase the foam's yield stress *versus* a surfactant which generates a smaller (and therefore wetter) foam.

1.6 Non-aqueous foams

Foams in non-aqueous media have received relatively little attention in academic research.[3,22]

Non-aqueous, and especially non-polar, media represent significant challenges for conventional surfactants. This is generally because such solvents have only weak intermolecular interactions – thus the hydrophobic moieties of conventional surfactants are relatively soluble, and are not strongly driven to the interface.[3]

A related issue is the poor performance of ionic surfactants in non-aqueous media: in water, ionic surfactants are a mainstay of foaming formulations and perform well, even at low concentrations. In addition to the increased solubility of their hydrophobic moieties, the reduced dielectric constant of non-polar solvents weakens charge repulsion, reducing ionic surfactants' ability to stabilise films.[22]

Foam research in non-polar media has largely focused on nanoparticle and liquid-crystal stabilised foams. Such particles stabilise foams by physically jamming at interfaces and preventing foam collapse.[22]

Water-ethanol mixtures are quasi-aqueous, possessing semi-polar behaviour. As the fraction of ethanol is increased, however, conventional surfactants become less effective and only specialty siloxane or fluorocarbon surfactants are capable of generate the low surface tensions required to form foams.[3]

The literature on non-aqueous foams and the behaviour of surfactants in non-aqueous media will be explored in more detail below – see sections 2.4, 2.5.

1.7 Alcohol-based hand rubs (ABHRs)

1.7.1 ABHRs and hand hygiene

Rigorous hand hygiene is a crucial practice to reduce prevalence of hospital-acquired infections and prevent disease transmission between patients. The World Health Organization produces detailed hand hygiene guidance for healthcare systems, which includes a "five moments for hand hygiene" campaign, intended to promote a rigorous culture of hand-washing amongst healthcare professionals.[23]

ABHRs are a widely-used and important element of hand hygiene systems in healthcare settings throughout the world, as ethanol and isopropanol are safe and cheap disinfectants with strong antibacterial and viricidal properties.[24] Ethanol is typically present in these formulations at 60-80% w/w in order to optimise for effectiveness against both viruses and bacteria.[23,25]

While the ability of ABHRs to effectively disinfect healthcare professionals' hands is well-evidenced, rates of compliance with demanding healthcare standards have attracted more concern. Studies of healthcare professionals' handwashing behaviour have identified that adherence with guidelines reduces when the intensity of patient care increases, at weekends, and in intensive care settings.[23,26,27] Lower compliance with hand hygiene standards may increase the risk of hospital-acquired infection for both staff and patients.[23] Further, qualitative research with healthcare staff has identified a number of sensory barriers which make the use of ABHRs more unpleasant.[28]

It is important to minimise sensory barriers to the regular and proper use of ABHRs and maintain aesthetic appeal to ensure that they do not become barriers to compliance with hand-hygiene standards.

1.7.2 ABHR formats

ABHRs generally take the form of liquids, gels or foams.

Liquid-based formulations are very simple and cheap, typically consisting of water, ethanol (60-80% by mass) and various fragrances, preservatives and emollients.[29] Liquid ABHRs are not typically preferred by users – they are easy to spill, leading to inadequate hand coverage and slip hazards. In work by Greenaway *et al.*, users associated liquid ABHRs with increased

perceptions of skin irritation, slower adsorption, and negative sensory qualities such as unpleasant smells and skin feel. Many of these properties worsened as the dose volume was increased.[28]

Foams and gels, by contrast, have more solid-like rheological behaviour and thus are more easily handled and applied. In addition, they reduce the rate of alcohol evaporation and loss to spillage versus liquids and thus help to ensure good coverage and disinfection.[29]

Alcohol-based gels can be formulated with a range of gelling agents, such as carbomers or substituted celluloses. Typically, such agents are included at around 0.5-1% by weight.[25] These polymers form physically cross-linked networks within the formulation, inducing semi-solid behaviour.[29]

Foaming formulations use specialty surfactants, such as siloxane polyethers, to promote foam formation. Alcohol-based foams present several advantages over gels and liquid formulations.[28] First, a small quantity of alcohol foam formulation can generate a relatively large corresponding volume of foam, which assists users in achieving good hand coverage. The absence of gelling agents reduces the presence of sticky residues and prevents clogging in the pump. Greenaway also identifies other sensory benefits of foams over gels, with users reporting preferable skin feel and aroma characteristics.[28]

1.7.3 Foaming ABHRs

Foaming ABHRs are typically generated using a foam pump. In one common design, the a user depresses a lever to drive a fixed quantity of liquid formulation and air through a series of mesh gauzes, generating a foam, which is then ejected onto the user's hands.

Foam ABHRs present several technical issues regarding effective foam generation – these will be discussed in detail in section 2.5, below.

Historically, ABHR formulators have relied on specialty surfactants, typically siloxane polyethers, to generate foams. Little is understood about the structure-property relationships for these surfactants in the context of foam formation, including how these relationships might be affected by the balance of water and ethanol in the solution.

The quality of foams can be described in terms of several interlinked properties and dynamic behaviours: physical characteristics such as its liquid fraction and bubble size distribution; foamability – the volume of foam generated in the foaming process; stability – drainage, coarsening and bubble coalescence; and the rheological behaviour of the foam.

I argue, though, that foamability is the primary determinant of 'foam quality' for ABHRs. Formulations with high foamability will form drier-feeling, more polyhedral foams with solid-like rheology, and are less likely to run off the hands of users. By contrast, when foamability is poor, foam ABHRs will feel wet (or may be ejected as a mixture of liquid and foam) and their rheology will be liquid-like, and thus more likely to drip off users' hands – an outcome which is both unappealing to users and results in a reduced dose of ethanol being applied.[21] Foam stability is a far less important criterion, as users will typically massage the foam into their hands over timescales of less than a minute.[23]

2 Literature review

2.1 Overview

The aim of this thesis is to develop design rules which can guide the formulation of foaming water-alcohol mixtures using siloxane polyether surfactants.

Given the scarcity of research on siloxane (or indeed any other) surfactants in water-alcohol mixtures, this literature review will approach the area through several related research questions which have received more attention:

What structure-property relationships have been established linking surfactants and foamability, especially for triblock copolymer surfactants in aqueous media?

What is known about foaming in non-aqueous media?

What is known about the solution and foaming behaviour of surfactants, especially triblock copolymer surfactants, in mixed polar media?

What is known about the solution and foaming behaviour of siloxane surfactants, especially siloxane polyethers?

I will begin by discussing several general methodological issues in foam research, and broader research about foamability and surfactant properties.

2.2 Methodological considerations in foam research

2.2.1 Dynamic versus equilibrium behaviour

Foams are both macroscopic entities, formed from films, bubbles, etc. whose parts move and interact on relatively slow timescales – but also entities whose behaviour depends on the microscopic behaviour of surfactant molecules and their assemblages as they adsorb at interfaces. When foams are formed quickly, these timescales may overlap. New interfaces can be generated very quickly and come under mechanical strain before surfactants can assemble. This explains why the equilibrium properties of surfactants are often not predictive of foaming behaviour, and why different foaming methods can lead to different foamabilities from the same surfactant solution.[30]

Patist *et al*. have shown that by varying the method through which foam is generated – from gentle bubbling to hand-shaking, one can shift from an 'slow' regime of foam generation in which equilibrium properties of surfactants determine foam quality, to a 'fast' regime in

which kinetic properties are more important.[31] Petkova *et al.* , comparing sparging, a planetary mixer and the Bartsch test, found extreme differences in foamabilities for non-ionic surfactants from one method to another.[32]

Małysa *et al.* have argued forcefully that the dynamic nature of processes in foams has been overlooked.[30] They point out, for instance, that the 'static' conditions of isolated film measurements do not effectively model the dynamic forces present in foam formation. Even in situations of rapid adsorption kinetics and (relatively) slow interface generation, the precise method through which foams are formed can lead to non-equilibrium behaviour on interfaces.[30] During sparging, as bubbles rise through solution, viscous drag means that their upper sides have reduced surfactant coverage compared to the lower, for example.

Petkova *et al.* recently made a significant contribution to this discussion in a second paper, in which they compared the foamabilities of a range of ionic and nonionic surfactants with their dynamic interfacial properties.[18] They show that these interfacial properties, compared at appropriate surface ages, are highly predictive of foamability. This work corroborates the claim made by Małysa *et al.* that foaming is best analysed as a dynamic process.[30]

2.2.2 Foamability and foam stability

Foamability and foam stability are closely connected concepts used to characterise foaming solutions. Foamability typically describes the volume of foam generated in a foaming process, or the rate at which foam is generated in said process. Foam stability, on the other hand, typically describes the change in foam volume *following* generation. Both foamability and stability have several conceptual issues.

Foamability

Different methods of foam generation lead to differing volumes of foam being created. This in itself is not surprising, as methods can differ significantly in terms of the vigorousness with which they mix liquid and gas phases - generating new interfacial area requires the performance of work on the solution, and hence applying different amounts of work results in differing amounts of new interfacial area. However, various authors have shown that surfactants have 'preferred' foaming conditions under which they perform well – and moving from one set of conditions to another can result in significant changes in *relative* foamability.[15,32,33] These experiments reframe the property of foamability as resulting from the *interaction* of the foaming process and the surfactant solution, not merely a property of surfactant solutions themselves. This important interaction has been under-explored - for

reason of convenience, it is rare for surfactant scientists and formulators to compare the results of multiple foaming tests when characterising a surfactant solution.

Thus, predicting a surfactant's foaming behaviour requires an understanding of both the properties of the surfactant and of the foaming method required to produce it. One approach to characterising a foaming method is that of the characteristic time, a surface age at which new interfaces must be stable and robust in order to generate a stable foam. Quantifying the characteristic time for a given foaming process is less well-defined. For the Bartsch test implemented by Petkova, they identify the characteristic time as being between 75 and 370 ms – with the lower bound being associated with the onset of coalescence after each shaking cycle, and the upper bound related to the frequency with which the tube is rotated.[18]

Foam stability

Like foamability, foam stability is process-dependent. This relationship is mediated by foam structure. Foams can differ in their liquid content, bubble size, bubble polydispersity and homogeneity – foams generated by homogeneous nucleation, for instance, have tiny, monodisperse bubbles throughout, but those generated by the Ross-Miles test have drier, coarser bubbles towards the top and smaller, wetter bubbles at the base.[10] Bubble size and liquid content strongly influence rates of drainage, and highly polydisperse foams coarsen faster.[14] Thus, one could achieve a range of stabilities from a single surfactant solution by varying the parameters under which foaming occurred. Stability, like foamability, cannot be easily assessed by comparing surfactant performance under only a single foaming condition.

Further, 'stability' can be considered more broadly than just in terms of foam volume. The *volume* of a foam primarily declines through the rupture of films at its top but other internal changes also occur simultaneously. Drainage of liquid through the foam, and the coarsening of bubbles will both change the internal structure and properties of the foam without a noticeable effect on the overall volume. These processes might be equally important for the efficacy of a foam depending on its application.

Disentangling foamability and foam stability

The concepts of foamability and stability are often conflated in academic literature as well as in some common foam tests.

The Bikerman test, for example, is an established method for measuring the 'foaminess' of surfactant solutions – it involves sparing a solution in a glass column over a range of gas flow

rates.[13] A curve is constructed, comparing the steady-state equilibrium of the foam height to the gas flow rate at which it has been generated. Variants on this Bikerman test are common in assessing the foamability of surfactant solutions.

However, the Bikerman test cannot distinguish between solutions with high foamability and those with high stability. In the test, these properties are conflated - the result depending on both the rate of downwards foam decay at the head of the column *and* the rate of foam generation at the base.[13]

Distinguishing between foamability and foam stability is particularly difficult when the timescales of foam formation and collapse overlap. This may be because foam formation is slow or continuous (e.g., in the Bikerman test) or because foam collapse is very fast (if foams are merely transient). When foam generation is relatively rapid – e.g., by foam pump – there is less risk of foamability and stability being conflated.

2.3 Structure-foamability relationships for surfactants

Poloxamers, also known as Pluronics or Synperonics, are a family of triblock copolymer surfactants with the general form nEO-PO_m-nEO. They have received significant attention. Their diversity and commercial availability have allowed for systematic comparison of their surface properties. Of particular note is the work of Alexandridis *et al.*, who compared 25 Pluronics across a range of attributes.[34]

Generating foam by a standardised Ross-Miles test, Alexandridis *et al.* found that Pluronics with the highest foamability have $30 < \mathrm{m} < 45$, and an EO mass fraction, $40\% < x_{\mathrm{EO}} < 80\%$. By contrast, when Pluronics foamability is measured by sparging, larger, more PO-rich surfactants generate foams more effectively than smaller ones.[35,36,37] Such differences arise because the demands of slow and fast foaming methods on surfactants are quite different. Fast foaming methods, like the Ross-Miles test, favour fast-diffusing surfactants over those with higher surface activities – Alexandridis' results indicated no correlation between EST and results in the Ross-Miles test, whereas that correlation is clear in the results from the sparging test.

Alkyl ethoxylates, of the form C_mnEO, have also been subjected to systematic study. Work on these surfactants has generally shown that surfactants with longer EO tails have lower surface activity.[38–40] However, in foamability tests, Kanokkarn *et al.* have shown that

surfactants with greater nEO values were able to reduce surface tension at a faster maximum rate, and that this rate correlated well with foamability in a sparging test.[40]

Work on Pluronics and alkyl ethoxylates highlights some common issues in foam research. The first is the diversity of foaming methods used, and the extent to which the choice of foaming method can influence foaming behaviour (as discussed in section 2.2.1). Second, the value of systematic comparisons is clear – Alexandridis' work reveals the complex, non-monotonic relationship between foamability and surfactant structure. Finally, both Alexanderidis' and Kanokkarn's work emphasise that for many foaming systems, the dynamic properties of surfactants are important in determining foamability.

Taken together, this body of literature indicates two important criteria determine foam formation: surface activity and surfactant dynamics. In general, surfactants with larger nEO values reduce surface tension more rapidly, and therefore perform well in fast foaming processes. However, they also have lower surface activities, and therefore reduce the surface tension less on longer timescales. Depending on the speed of the foam generation method, one or other of these parameters appears to have more effect on foamability.

2.4 Surfactant behaviour in non-aqueous polar media

Numerous studies have investigated the effect of additives such as alcohols on the CMCs and the stabilities of ionic and non-ionic surfactant micelles.[8,41,42,43] The principal effect of short chain alcohols on nonionic surfactants is to solubilise them, lowering the polarity of the solution. Thus, the presence of alcohol reduces the entropic forces that are the main driver of micellisation, so the CMC is elevated.[44,45]

Zana *et al.*, studied the dynamics of Pluronics micelles in water and proposed that the hydrophobic PPO segments of the polymer were required to fold before leaving the core of the micelle and entering solution (or vice versa). The resulting energetic barrier, they reasoned, should depend both on the DP of the hydrophobic block and the quality of the solvent into which the surfactant molecule was diffusing.[46]

While this study characterises solvent quality in terms of distance to critical temperature θ, an analogy can be readily drawn regarding the effect of varying the alcohol content of the solution, which is likely to have a similar effect.

Lin *et al.* published a pair of papers on the effect of polar solvents on the behaviour of a PDMS-graft-polyether surfactant and a Pluronic surfactant. In both cases, adding 2-propanol,

ethanol and formamide resulted in smaller micelles with lower aggregation numbers and increasingly solvated cores.[47,48] Similar results were obtained by Soni *et al.*, who tested the effect of 26 polar additives on the micellisation of a siloxane-graft-polyether and found that water-miscible additives raised the CMC.[49]

2.5 Foaming in non-aqueous media

Foaming in non-aqueous media has received attention for three key reasons: first, the comparative scarcity of foams in non-polar media is a sharp contrast to aqueous foams – thus, there is an opportunity to gain fresh insight into the fundamental determinants and features of foaming behaviour. Second, there are many oil-based substrates for which foaming is a desirable characteristic – *e.g.,* in food technology– but has been challenging to achieve. Finally, by contrast, there are some prominent non-polar systems in which foaming is *not* desirable, but persistently occurs – notably, asphaltene-rich crude oils.[50]

Existing research in non-aqueous foams is of only limited relevance to this thesis. Its focus is principally on highly non-polar media, such as vegetable oils, silicones or paraffins, which are generally not amenable to surfactant-based approaches. Instead, the literature principally investigates surface-active nanoparticles and liquid crystals. In several cases where surfactants appeared to generate foams in non-polar media, it has been shown that liquid crystals are the true cause of foam formation.[22]

While conventional hydrocarbon surfactants are often unable to generate foams in non-aqueous media, specialty surfactants with fluoroalkyl or siloxane moieties are still surface-active and can be effective foamers. While this fact is briefly mentioned in passing in several reviews of non-aqueous foams, it is not elaborated on. To the best of my knowledge, there is little or no academic research in this area.

Several explanations are offered in these reviews to account for the difficulty in generating foams in non-aqueous solutions. Friberg argues that the low surface tension of non-aqueous media means that conventional surfactants do not display surface activity. An alternative way of framing this is that conventional surfactants are too soluble in non-aqueous media, and do not experience the entropic driving force which propels those same surfactants to the air-water interface.[3] In addition, Friberg argues that the relationship between surface tension reduction and foam stability is not clear even in non-aqueous liquids with ‘substantial surface tension’, suggesting that interfacial rheology is a more appropriate tool. This thesis will

demonstrate, in contrast, that surface tension reduction is a useful tool for predicting foaming capacity in water-ethanol systems.

Ethanol, especially in mixtures with water, fits some (but not all) of the descriptors applied to these non-polar media, and often the behaviour of these mixtures is somewhere between that of strictly aqueous and non-polar liquids. Friberg states, for instance, that *"Surface tension as an analytical tool is not available for oil foams; the value of the inherent surface tension of most oils is at such a low level that there is little or no adsorption to the surface of hydrocarbon-based surfactants. Hence, in a non-polar solvent increased concentration of added surfactant does not lead to reduced surface tension…"*.[3] Ethanol-water mixtures, by contrast, do display behaviour that is analogous to that observed in aqueous media, and are amenable to analysis by tensiometry. By changing the volume of ethanol in the mixture, it is possible to gradually adjust the solvent quality and monitor the effect on foaming as the water content of the solvent reduces.

Several papers describe attempts to generate foams in water-ethanol mixtures. These studies employ a range of strategies, using mixtures of conventional surfactants and/or polymers,[51,52] nanoparticles,[53] and perfluorinated surfactants.[54] Only very recently has any of these systems generated substantial foams above 50% ethanol (v/v), and thus produced a solution which could conceivably be used as a disinfectant.[55]

In conclusion, while non-aqueous foams have received some attention, research has tended to focus on foams in non-polar oils and therefore investigated surfactant-free mechanisms for generating and stabilising foams – *i.e.*, surface-active particles and liquid crystals. Speciality surfactants, such as fluoroalkanes and siloxanes, have received little attention in these systems. Foams in mixed polar liquids, such as water and ethanol, have gained some attention but no systematic study has been reported.

2.6 Siloxane surfactants

Siloxane surfactants have been the subject of several decades of research, particularly in view of their super-spreading properties.[56] Much of this research has focused on the development novel structures, terminal groups and synthetic approaches.[57–61]

The most widely explored siloxane architectures are comb (or 'graft') and 'tri-siloxane' structures. Relatively little research has been conducted on linear architectures such as diblock or triblock surfactants.[56]

Several published papers investigate, with varying levels of systematicity, the relationship between the composition and structure of siloxane polyethers and their surface properties, though almost always in water. Typically, these studies compare 2-4 surfactants with varying nEO or nPDMS, though some (e.g. Chung *et.al.*[62]) are more extensive.

In this literature, there is a consensus that maximum surface activity – that is, the minimum *equilibrium* surface tension - is achieved with shorter siloxane blocks and shorter EO blocks. This is likely because smaller solvophobic groups are likely able to achieve higher packing efficiency at the interface.[63,64] This finding is not universal though. For example, Chung *et al.* found that only the length of the EO moieties in their series of comb surfactants had a significant effect on surface activity, and Tan *et al.* concluded that surface activity *increases* with both PDMS and EO length.[62,65] Kanellopoulos *et al.* report that, for a series of triblock siloxane polyethers, surface activity reached a maximum when the number of siloxane repeat units was between 36 and 64, with a significant reduction in activity being observed when this number increased.[66]

Differences in chain architecture may explain some of the discrepancies between these studies, which separately consider graft, diblock or triblock siloxane polyethers. As no current research systematically compares the surface behaviour of siloxane surfactants with differing architectures, it is not clear what effect this parameter is likely to have on surface activity.

There are several limitations on the applicability of this literature to this thesis. First, it is almost exclusively limited to aqueous media. Second, much of the exploration focuses on comb or tri-siloxane-type surfactants. Finally, and most significantly, very little research investigates structure-property relationships with *dynamic* properties such as the dynamic surface tension. Given the dynamic nature of the foaming process, it remains to be seen whether the structure-property relationships that hold true for equilibrium behaviour are useful predictors of foamability. One study which does examine dynamic surface tension suggests that surfactants with fewer PDMS units reduce the surface tension more rapidly.[57]

Only a small number of studies compare the foaming behaviour of siloxane polyethers, and generally only comment on their *low* foamability, which is an advantage in many industrial settings. Such isolated foaming results do not provide structure-property relationships.[57,67]

Several studies have investigated the mechanism by which siloxanes assemble at air-water interfaces. This research has generally concluded that at low surface pressures, the siloxane

moiety lies across the interface with EO chains alongside it. As surface pressure increases, EO units are increasingly forced into solution, to be replaced with densely-packed siloxane moieties.[68] Similar behaviour is evident in Pluronics.[69]

Wang *et al.* used AFM to measure the steric forces generated by comb-type siloxane polyether surfactants at an oil-water interface, while systematically increasing the ethanol composition of the aqueous solvent. They found that siloxanes, contrary to hydrocarbon surfactants, maintained relatively high steric repulsion, even up to high loadings of ethanol. While the repulsion of siloxane surfactants with EO hydrophilic chains monotonically declined as the ethanol content was increased, those with mixed EO/PO chains instead exhibited a maximum as the ethanol content was increased.[70]

Despite this apparent preference for more ethanol-rich mixtures, however, Wang *et al.* finds that the EO-only and mixed EO/PO surfactants produced emulsions of similar stability in 80% ethanol.[70]

In summary, research on siloxane polyether surfactants is almost entirely water-based, and largely directed towards the synthesis of surfactants with novel architectures and chemistries. Only a limited body of research is concerned with establishing structure-property relationships between siloxane surfactants and surface behaviour. Systematic comparisons which *do* exist focus principally on equilibrium surface tension, and the diversity of architectures that are considered makes comparisons difficult. For larger siloxane surfactants, smaller EO groups appear to lead to greater surface activity, while larger siloxane blocks may reduce surface activity. Smaller surfactants also tend to have faster *dynamic* behaviour, though no systematic comparisons have been reported in the literature.

2.7 Conclusion

This review has surveyed a number of research areas that are related to my research question. These include addressing broad methodological questions in foam science, and examination of recent work that addresses broader questions concerning foamability. Work that seeks to link the structure of surfactants to their foamabilities is also summarised, as is research on the behaviour of surfactants in non-aqueous polar media and recent work on foaming in non-aqueous solutions. Finally, the (largely water-based) body of research on siloxane-containing surfactants is considered. This overview highlights several saliant points of relevance to this thesis.

First, foam properties are the result of a strongly coupled interaction between surfactant properties and the foaming method that is employed. Surfactants must be able to establish significant elasticities (see Małysa *et al.*[30]) and/or disjoining pressures (see Petkova *et al.*[18]) on the characteristic timescale of the foaming method, with the result that surfactants may have distinct 'preferences' for one foaming method over another.

This finding emphasises the need to carefully consider (and ideally compare) the effect of the foaming process when drawing conclusions about surfactant behaviour in general. It also suggests that equilibrium behaviour is of only limited relevance to the study of foaming processes, especially for fast foaming methods, and that measuring dynamic behaviour may be more fruitful when developing design rules.

Second, there is a general trend in the direction of surfactant-foaming method 'preferences'. More hydrophilic surfactants tend to be the most effective foamers in rapid foaming methods, such as the Ross-Miles or Bartsch tests. By contrast, more hydrophobic surfactants are the best foamers when foams are generated relatively slowly, e.g., by sparging.

This consistency highlights an apparent trade-off which seems to exist for many nonionic surfactant systems – surfactants that can reduce the dynamic surface tension more quickly, also exhibit lower surface activity (i.e., equilibrium surface tension), and vice versa. If foam formation is slower than attainment of the equilibrium surface tension, this suggests that optimising a surfactant for fast foaming processes will inevitably make it less effective in slow foaming processes, and vice versa.

In the cases of Pluronics, this interplay between dynamic and equilibrium properties results in relatively small, EO-rich surfactant performing best in a Ross-Miles test, while larger, more PO-rich surfactants outperform them in sparging tests – with tests with the latter method correlating better with the *equilibrium* surface tension. It is plausible that a similar relationship exists for siloxane-polyether surfactants, but the literature is less clear on the relationship between surfactant structure and surface activity, and there is almost no literature on their foaming behaviour.

All the conclusions above are valid for purely aqueous solutions of surfactants. What effect does the introduction of ethanol have on these relationships? Primarily, the effect of ethanol is to solubilise the hydrophobic moieties of surfactants. This influence can be easily seen via its effect on micellisation behaviour, with higher loadings of alcohols or other polar additives raising the CMC of nonionic surfactants. This probably has an acceleratory effect on

surfactant adsorption kinetics: more unimer surfactant is present in solution and can rapidly adsorb to an interface without the kinetic barrier of first leaving a micelle. Further, improved solvent quality may lower the kinetic barrier to chain exit from micelles, thus making more surfactant able to access the nascent interface.

However, conventional surfactants invariably perform poorly in ethanol-water mixtures. A number of hypotheses have sought to explain this result – Friberg has argued it is a result of conventional surfactants' low surface activity, while Sethumadhavan has argued that the low stability of ethanol foams is the result of interfacial turbulence, resulting from ethanol evaporation.[52] A further argument, complementary to Friberg's, is that the low surface tension of ethanol provides little opportunity for the formation of surface tension gradients, which drive the elastic properties of surfactant-laden films.

I hypothesise that ethanol concentration has a dual effect on surfactants – both accelerating their kinetics through solubilisation and reducing their capacity to generate surface tension gradients. This dual effect likely interacts with the trade-off between fast, hydrophilic surfactants and slow, hydrophobic surfactants.

Siloxane surfactants, by virtue of their high conformational flexibility, can maintain surface activity and foamability in ethanol-rich solutions. However, little is so far known about how the surface-property relationships established for traditional surfactants (or for siloxane polyethers in water) apply under these conditions, nor is it clear how these rules change in different solvent environments.

3 Project Aims

In this project I aim to develop design rules for water-ethanol foams – that is, empirically rooted conceptual tools which enable a formulator to select the appropriate surfactant and surfactant loading for a specific ABHR (or other foaming alcohol) application. I will mostly target foamability in this research, as it is strongly related to perceived foam quality.

As described in section 1.1, foaming behaviour can be analysed on various length- and timescales: the 'molecular' scale of surfactants and solvent, their behaviour and composition; a meso-scale of interfacial behaviour and adsorption kinetics; and a macro-scale – the films and bubbles that make up the foam itself. Each arises, in a complex fashion, from the behaviour and properties of the scales below.

The molecular scale is directly adjustable by formulators – by changing the balance of water and ethanol, and/or the nature and loading of the surfactant in use – whereas the macro-scale, that of foam behaviour and properties, is of most interest to users.

A successful set of design rules will link these regimes – the molecular, interfacial and foam scales - allowing a formulator to make changes to ingredients and to successfully predict the properties of the new foam. I aim to 'map' meso- and macro-scale properties (such as equilibrium surface tension or foamability) as formulation characteristics are adjusted, thereby revealing the underlying relationships between these levels of analysis.

Having mapped these three levels, I will seek to draw links between them, determining which interfacial properties are most useful for predicting good foamability in a given environment, and in turn, which siloxane surfactants best generate said interfacial properties.

3.1 Thesis structure

This thesis applies and develops a range of analytical, instrumental and statistical methodologies. These methods will be described as they arise, in each chapter, rather than in a separate thesis section.

Chapter 4 describes characterisation of the surfactants' molecular properties and investigates into the effects of homopolymer contaminants on their performance.

Chapter 5 describes attempts to characterise the static and dynamic properties of siloxane-polyether micelles, and the influence of solvent mixture on the CMC.

Chapter 6 describes the use of experimental design and regression modelling to explore the foaming behaviour of the surfactants through a range of foaming methods.

Chapter 7 describes the development of a pendant drop tensiometer for measurements of dynamic surface tension between 1 second and ~5 minutes.

Chapter 8 describes dynamic surface tension measurements using the maximum bubble pressure and Du Noüy ring methods and connects this data to foaming behaviour. It will also discuss concentration-time superposition analysis and its application to surface tension data.

Chapter 9 presents the conclusions of my work in terms of formulation design rules and fundamental understanding of interfacial and surfactant behaviour. The strengths and limitations of this work and directions for future exploration will also be discussed.

4 Surfactant characterisation

This chapter details research into the molecular properties and nature of the siloxane polyether surfactants used during this project, followed by work on isolating and testing impurities in these surfactants. Finally, it will briefly discuss the synthesis of a siloxane polyether surfactant and its foaming performance.

4.1 Material characterisation

4.1.1 Materials and methods

*Nominal surfactant content**

The surfactants used in this study were triblock siloxane polyethers, provided by Supplier A (Table 1) and Supplier B (Table 2) both provided courtesy of SCJohnson Professional, Denby, UK. They are described below. Each has the nominal structure $(EO/PO)_m$-$CH_2CH_2CH_2$-$(PDMS)_n$-$CH_2CH_2CH_2$-$(EO/PO)_m$.

Table 1. A summary of the properties of surfactant samples received from Supplier A Ltd.

Designation	***Nominal molar mass, g mol^{-1}***	**nPDMS**	**mEO *(per arm)***	**nPO *(per arm)***	***Appearance***
Di1010	1800	10	10	0	Viscous, clear fluid
Di1018	3200	10	0	18	
Di1508	2000	15	8	0	
Di2012	2700	20	12	0	
Di2510	2800	25	10	0	
Di4515	6500	45	15	15	

* A note on terminology: the commercial naming system for siloxane polyethers used by Supplier A has been adopted throughout this thesis. Surfactant names have the form "Di[n][m]", where n is the number of siloxane repeat units and m is the number of polyether repeat units. The sole exception to this rule is Di4515, which contains 15 EO and 15 PO units per arm.

Table 2. A summary of the properties of surfactant samples received from Supplier B.

Designation	***Nominal molar mass, g mol^{-1}***	**nPDMS**	**nEO *(per arm)***	**nPO *(per arm)***	***Appearance***
Di3012	3400	30	12	0	Grey-yellow solid
Di3514	4000	35	14	0	Grey-yellow solid
Di4016	4500	40	16	0	Waxy white solid
Di4518	5000	45	18	0	Waxy white solid

Surfactants synthesised by Supplier B were designed on the basis of interim modelling results from this project and were later characterised and incorporated into some foamability modelling. Thus, results presented in chapters 5 and 7 will focus on the six surfactants received from Supplier A.

Solvents (dichloromethane, ethanol, methanol, hexane) were purchased from Sigma Aldrich and used as received. Ultrapure (milli-Q) water was used for analysis.

Nuclear-Magnetic Resonance Spectroscopy (NMR)

NMR spectra were in deuterated methanol and chloroform were recorded using a 400 MHz Bruker Avance III HD spectrometer.

Quantitative 1H NMR spectroscopy was used to characterise the surfactants and to analyse the foam fractionation and solvent extraction experiments presented below. The relative balance of EO and PDMS in the sample were compared by reference to the relative areas of peaks in the region occupied by EO protons (chemical shift 3-4 ppm) and the area of peaks in the region occupied by PDMS protons (chemical shift ~0 ppm). The expected ratio of these areas for Di2510 was 1:1.88 – that is, 1 EO proton per 1.88 PDMS protons.

Gel Permeation Chromatography (GPC)

GPC analysis was carried out in HPLC-grade tetrahydrofuran (THF) containing butylated hydroxytoluene, using an Agilent Technologies 1260 Infinity GPC equipped with a refractive

index (RI) detector. All samples were made up to approx. 2 mg / ml before being checked for solubility by dynamic light scattering and filtered twice with a 2.5 μm Whatman syringe filter prior to analysis.

GPC data were normalised with respect to the retention time of the reference peak, typically ~21-22 mins. Retention times are presented in terms of the difference between the analyte and reference peaks.

Matrix-Assisted Laser Desorption-Ionisation Time-Of-Flight Mass Spectroscopy (MALDI TOF-MS)

MALDI-TOF MS studies were conducted using a Bruker Reflex III MALDI-TOF MS instrument in a range of solvents using a dithranol matrix.

Differential Scanning Calorimetry (DSC)

DSC analysis of surfactants Di2510, Di3012, Di3514, Di4016 and Di4518 were conducted using a TA Instruments TRIOS DSC, with Tzero aluminium hermetic pans. All samples comprised 10 mg neat surfactant.

All temperature ramps were carried out at 10°C min^{-1}. Samples were first equilibrated at 20°C, before cooling to -80°C. After equilibrating again, samples were then heated to 60°C and equilibrated. Finally, they were cooled to 20°C and allowed to equilibrate.

4.1.2 Characterisation results and discussion

Most siloxane polyethers used in this study are clear, viscous liquids, soluble in a range of water-ethanol solutions. The four polymers synthesised by Supplier B – Di3012, Di3514, Di4016 and Di4518 are waxy, white solids at room temperature, becoming clear liquids on heating. While Di3012 and Di3514 dissolve well in water-ethanol mixtures, Di4016 and Di4518 do not.

All ten surfactants were subjected to MALDI-MS and GPC analysis. In GPC, molecules elute in order of radius of gyration, with larger molecules eluting first. Thus, the first peak in each trace was assumed to belong to the complete surfactant molecule. Good correlations with expected surfactant masses were observed for all surfactants except Di4518 (see Figure 3, below).

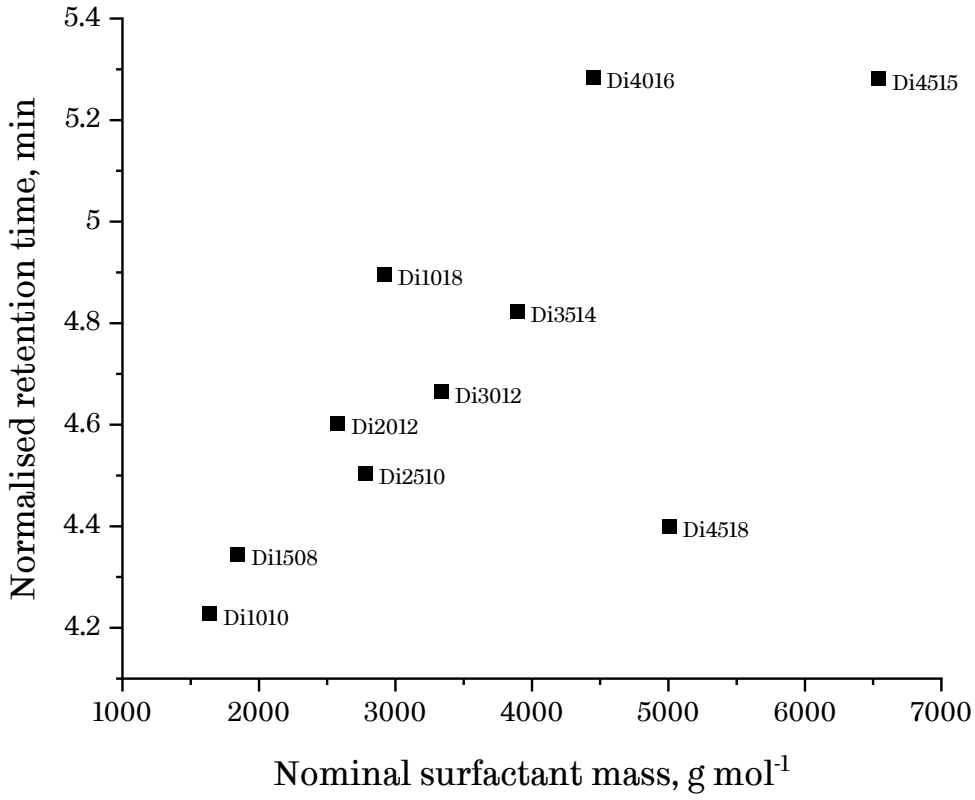

Figure 3. Normalised GPC retention times for siloxane surfactants against their nominal molar mass. Retention times for siloxane polyether surfactants correlate well with expected masses for all surfactants except Di4518.

MALDI showed broad peaks above 2000 g mol^{-1} for all surfactants, with characteristic 76- and 44-unit spacings, suggesting a series of molecules separated by units of PDMS and EO (see Figure 5). Peaks could be identified corresponding to the nominal masses of Di1010, Di1018, Di1508, Di2012 and Di2510.

For larger surfactants, only noise could be observed around the nominal mass of the complete surfactant molecule. This may be due to poor desorption/ionization of larger molecules from the matrix or could be a consequence of isotope pattern broadening and polydispersity. Silicone has three stable isotopes – ^{28}Si, ^{29}Si and ^{30}Si, with abundances of 92.2%, 4.7% and 3.1% respectively. For a surfactant molecule with ~40 silicon atoms, this results in a broad series of overlapping mass peaks which can easily overlap.

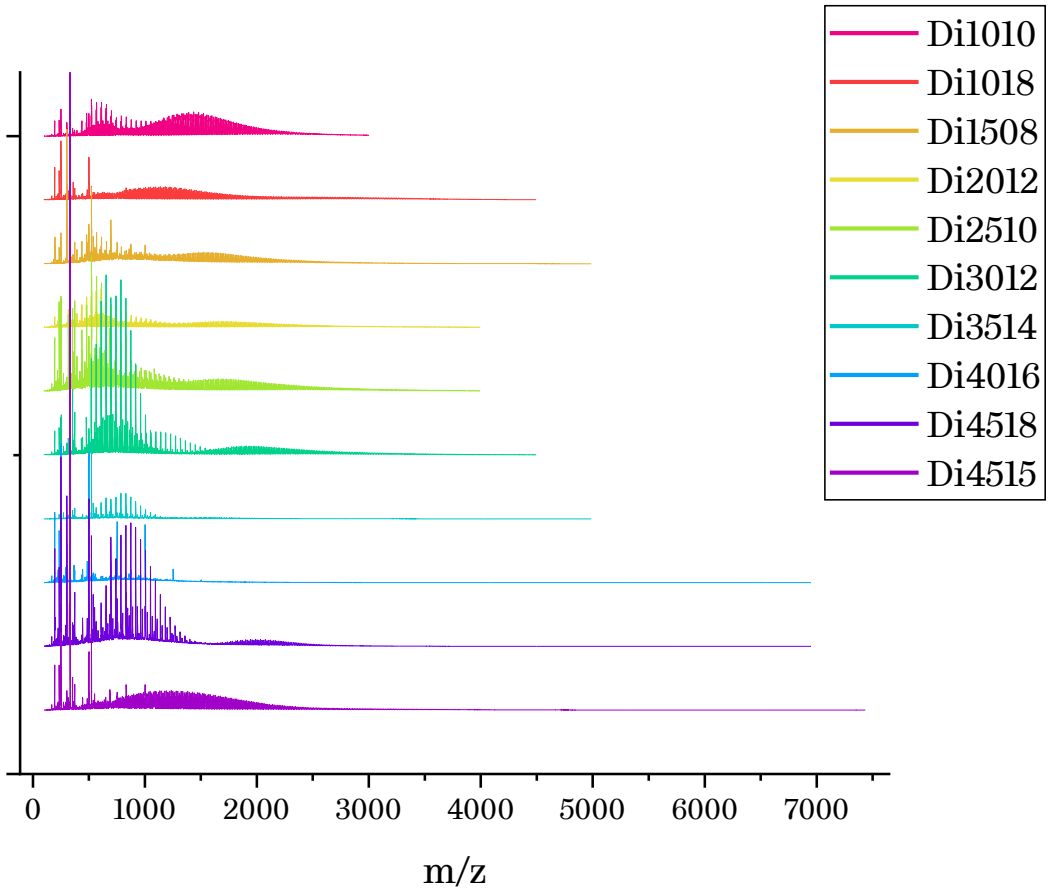

Figure 4. MALDI-TOF MS data obtained for a series of siloxane polyether surfactants. Most display two broad series of peaks. Surfactants with larger nominal masses displayed high-mass tails, but the resultant data was largely noise.

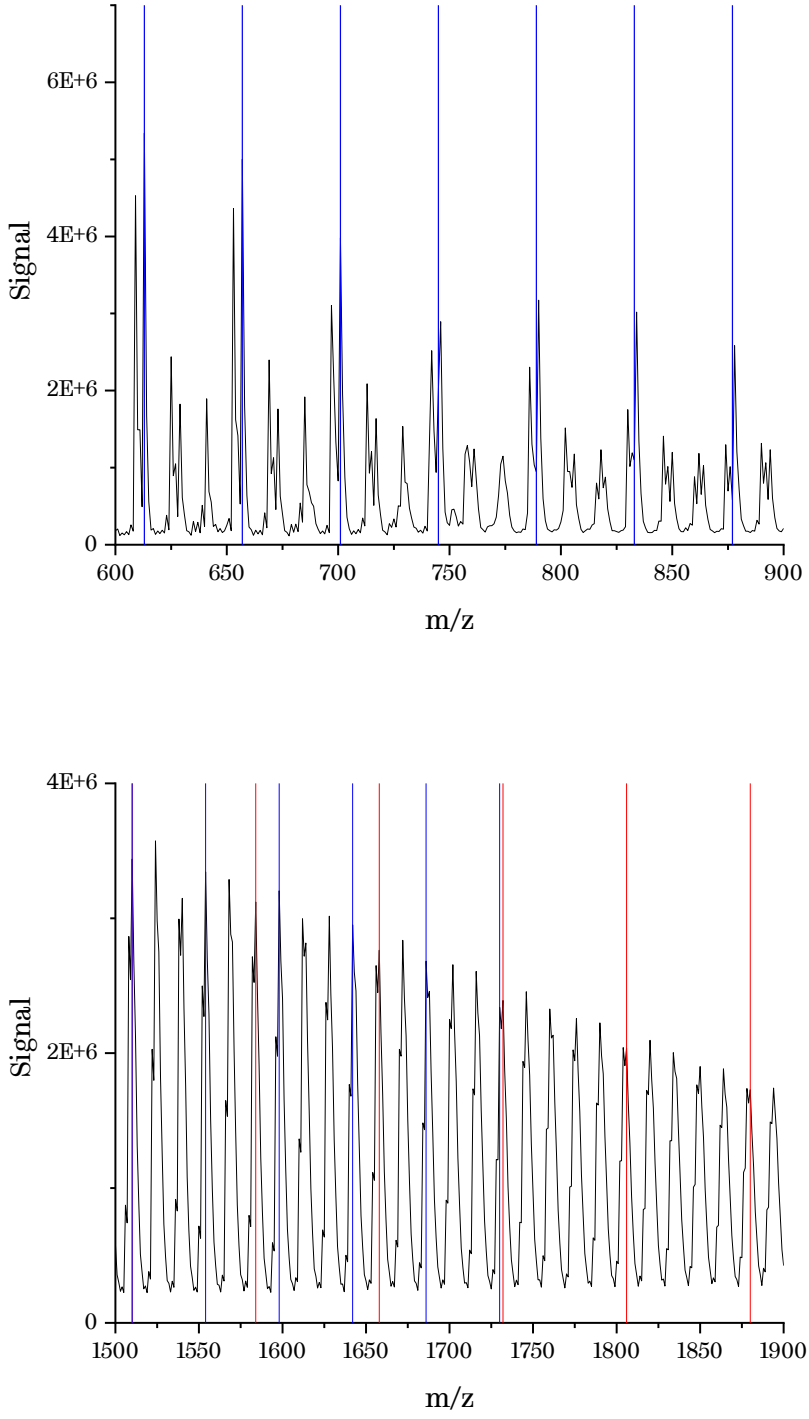

Figure 5. Top - A partial MALDI spectrum for Di1010. Peaks are spaced with a regular period of 44, suggesting a series of polymers each differing by one EO repeat unit. Bottom – A second partial MALDI spectrum for Di1010. Peaks show periodic spacings of both 44 (blue) and 76 (red) repeat units, suggesting the presence of a polydisperse range of siloxane polyethers.

In both MALDI and GPC, evidence can be observed for a lower-mass impurity in addition to a larger peak which likely corresponds to the target surfactant molecule. In MALDI, the peak in each trace with lower m/z values likely corresponds to EO-rich oligomers. These peaks can be identified by their characteristic 44 mass unit separation. In surfactants with mixed EO/PO peaks, these peak clusters show both 44- and 60-unit spacings, which is characteristic of mixed EO and PO polymers

Given the non-quantitative nature of matrix desorption, it is not valid to draw inferences about the relative abundances of the oligomers from peak intensities, but their presence gives valuable information.

Due to the lack of appropriate calibrants for siloxane polyethers, the analysis of GPC presented here is relative – that is, comparing the relationship between retention time and mass for the set of complete surfactants. GPC traces for many of the surfactants had clear secondary peaks, whose masses correlate closely with the estimated masses for their polyether side-arms (see Figure 6).

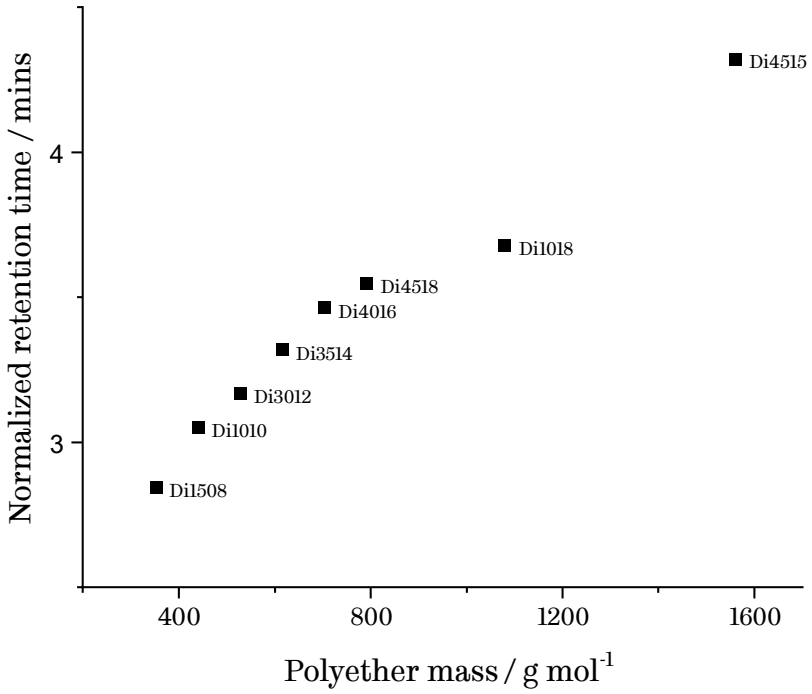

Figure 6. A plot displaying GPC retention times against the nominal mass for polyether end-chains. A close correlation is observed.

Taken together, the GPC and MALDI results suggest that the siloxane polyethers correspond well with their nominal nPDMS and nEO values. Their low purity and high polydispersity are typical of technical-grade surfactants.[71]

Di2510, Di3012, Di3514, Di4016 and Di4518 were also investigated by DSC. Surfactants demonstrated clear crystallization peaks over a range of temperatures, which correlated strongly with nominal nEO values– see Figure 7, below. Surfactants with larger nEO had crystallization peaks above room temperature – that is, their PEO chains were expected to be crystalline at room temperature. Some tested surfactants contained secondary peaks close to -80°C, whose origin is unclear.

While a 1H NMR spectrum of Di2510 indicated the presence of all expected chemical signals, the ratio between PEG and PDMS proton peak integrals was not as expected (measured: 1:1.74 *vs.* predicted: 1:1.88). This difference suggested an overabundance of PEG material, though it is not clear whether this additional PEG is present as a homopolymer as opposed to an EO-enriched triblock or diblock surfactant.

Solubility

While most siloxane polyethers tested were highly soluble in water-ethanol mixtures, Di4008 (see 4.3, below), Di4016 and Di4518 instead formed cloudy dispersions when dissolved in ethanol and ethanol-water mixtures.

While Di4008's lack of dissolution is likely due to its EO content being too low, it appears that Di4016 and Di4518 may be insoluble because nEO is too high, leading to formation of PEO lamella. DSC was used to investigate crystallization behaviour in the surfactant series: Di2510, Di3012, Di3514, Di4016, Di4518. DSC showed a smooth, progressive increase over the series in in T_m and T_c for a pair of peaks, which likely correspond to melting and crystallizing EO phases. As Figure 7 shows, Di4016 and Di4518 can have crystalline EO chains at 25°C, whereas those surfactants with smaller nEO cannot.

While these $T_m$values are measured for neat surfactants, they provide a good guide to those surfactants' behaviour in water/ethanol mixtures - those surfactants that had stable crystalline EO phases at room temperature did not dissolve in water-ethanol mixtures.

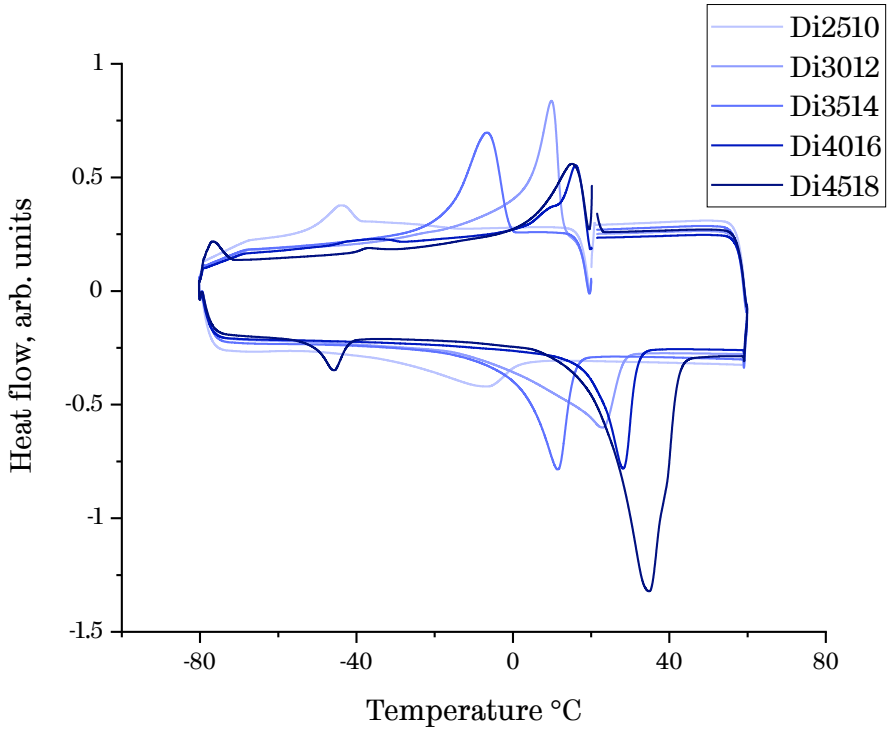

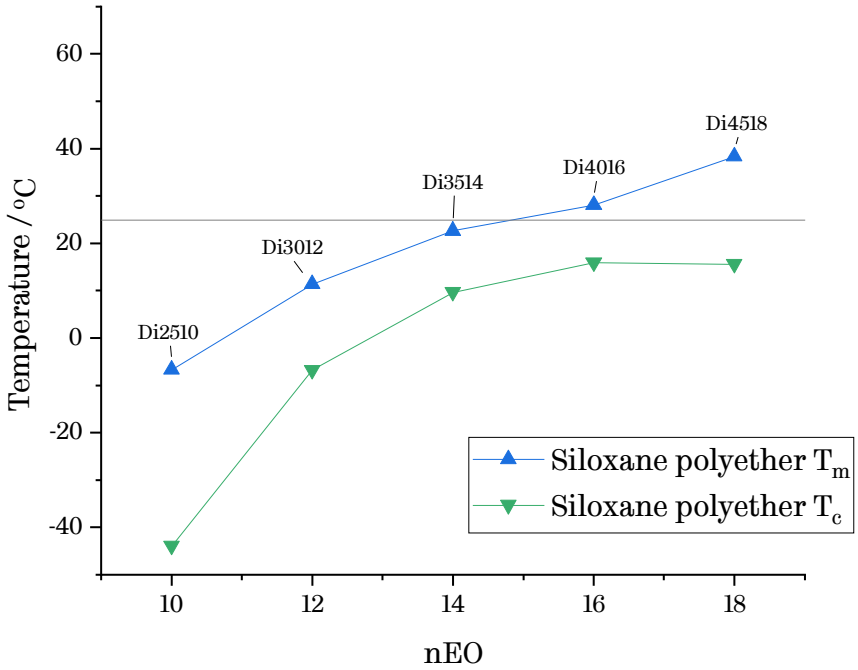

Figure 7. Above – DSC data for a series of siloxane polyethers, Di2510-Di4518. Below - Plot showing the measured melting and crystallization temperatures for nEO in a series of siloxane polyethers. Melting and crystallizing peaks for nEO end-blocks shift to higher temperatures as nEO increases. Data were gathered by DSC. 25°C is marked as a horizontal line.

These results are comparable with melting and crystallization temperatures for neat PEG homopolymer for a similar nEO range (see Figure 8, below).[72] This suggests that PDMS has little or no influence on the crystallization behaviour of the EO chains in neat surfactant.

Gently heating Di4016 and Di4518 gave transparent, viscous liquids, much like the dispersible surfactants described in this study. However, on addition to water-ethanol mixtures, both immediately crashed out of solution, forming white aggregates.

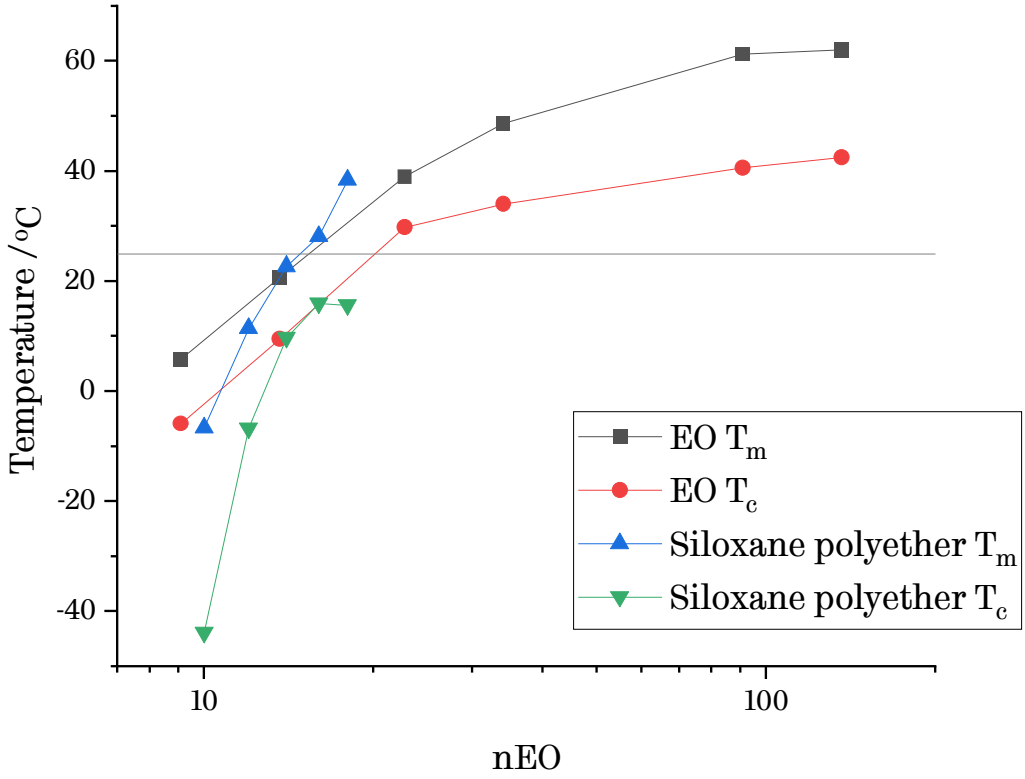

Figure 8. Comparison of melting and crystallization temperatures for nEO chains in siloxane polyethers with PEO homopolymer of similar n. Data for pure PEO chains reproduced from Johansson *et al.*[72] 25° C is marked as a horizontal line.

Below is a summary of the design rules that describe a zone of good solubility:

The lower boundary of EO for sufficient solubility must depend on both nEO and nPDMS – as Di1508 is a good surfactant, while Di4008 is not. A simple measure of nEO content is the %EO w/w - by that measure Di4008 is the most EO-poor surfactant in the dataset (19% EO). Di2510, the next-most EO-poor surfactant, is an effective surfactant in water-ethanol

mixtures and contains ~32% EO, so a lower bound on %EO to ensure good solubility may exist in the region $19\% \leq \%\mathrm{EO} \leq 32\%$.

A slightly more sophisticated approach accounts for the expected conformation of unimer surfactant in solution. If data for Pluronics also holds in siloxane polyethers, the latter are likely to adopt a 'mono-micelle' structure - a tightly coiled hydrophobic core, screened from solvent by the hydrophilic portion of the molecule.[46] We can use this model to develop a second solubility predictor.

It is assumed that the coiled core is a perfect sphere which completely excludes solvent. This pure micelle core would have volume V_{core}, approximately proportional to nPDMS. Its surface area, S_{core}, is given by:

$$S_{core} = 4\pi r_{core}^2 \quad (1)$$

r_{core} is the radius of the core, and can be given by:

$$r_{core} = \left(\frac{3}{4\,\pi} V_{core}\right)^{1/3} \quad (2)$$

Substituting for r_{core} and rearranging:

$$S_{core} = 36^{1/3}\pi^{1/3} V_{core}^{2/3} \quad (3)$$

$$\approx 4.836\, V_{core}^{2/3}$$

Here, both S_{core} and V_{core} are given in terms of arbitrary units which indicate the approximate scaling between the quantities.

$S_{core}/(2\ \mathrm{EO}_n)$ describes the relationship between the exposed area of the PDMS core and the number of EO units screening it from solvent. If this value is high, there may not be sufficient EO units to screen the PDMS core, and thus the surfactant will be insoluble. As nPDMS is increased, the divergence between solubility predictions based on $\%EO$ and $S_{core}/(2\ \mathrm{EO}_n)$ becomes larger.*

As discussed above, high nEO values can also lead to solubility issues through formation of an insoluble lamellar phase. As Figure 8 demonstrates, the melting and crystallization

* E.g. when nPDMS= 50, the criterion that $\%\mathrm{EO} \geq 30$ would require $\mathrm{EO}_n = 19$, but $S_{core}/(2\ \mathrm{EO}_n) \leq 2.1$ requires only that $\mathrm{EO}_n = 14$.

temperatures of EO chains appear to be quite unaffected by the presence of PDMS. Hence it appears that the upper bound on nEO before lamella formation occurs is essentially independent of nPDMS, and lies between 14-16. It should be noted that systematic study of other polymers – such as block copolymers of poly(ethylene oxide) and poly(butylene oxide) - has shown that the size of the non-crystallizing block can exert an influence on the onset of nEO crystallization.[73]

Both Di4515 and Di1018 exceed these apparent limits by using mixed EO/PO or pure PO side-chains, respectively, thus disrupting lamellar crystal formation.

In conclusion, there appears to be both an upper and lower bound on nEO for ethanol-dispersible siloxane polyether surfactants. The lower boundary is sensitive to nPDMS, but the upper boundary is not. Figure 9 summarises the predicted region for the block composition dispersible surfactants.

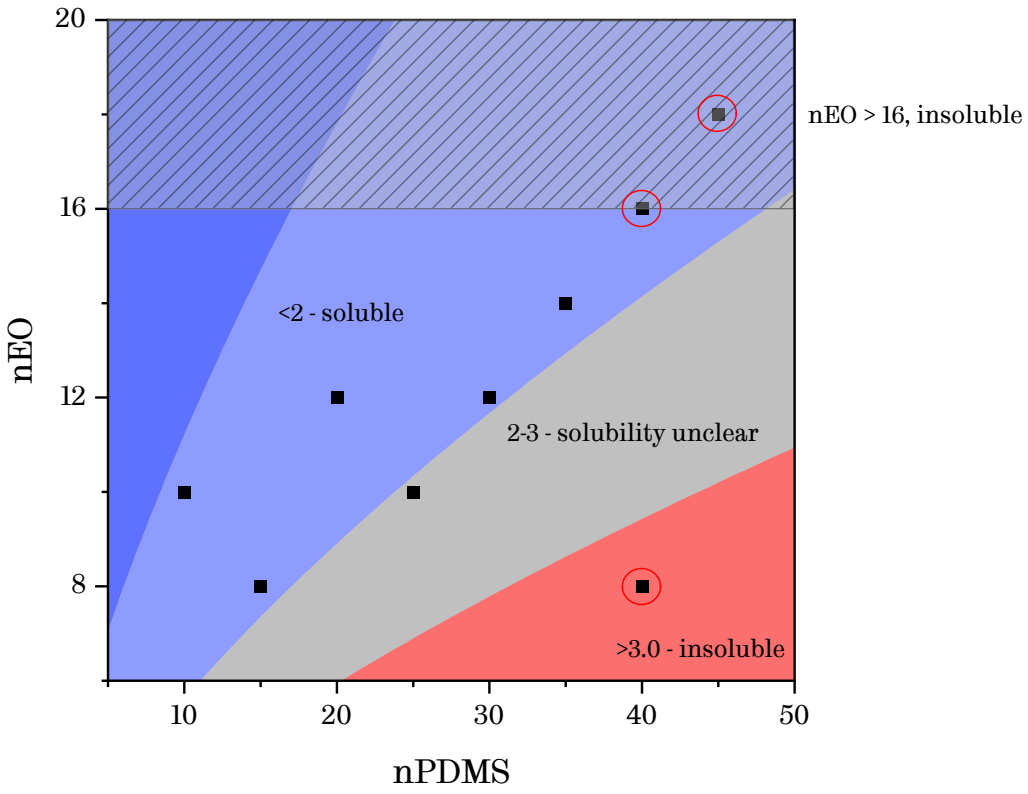

Figure 9. A contour plot summarising empirical rules for solubility of a range of siloxane polyethers in water-ethanol mixtures. Red or cross-hatched areas are predicted to be surfactants of low solubility. Tested surfactants are marked by squares. Solubility predictions for minimum and maximum EO values are based on the ratio

$S_{core}/(2\ EO_n)$ and a constraint imposed by EO lamella formation, respectively. Circled surfactants were either poorly soluble or insoluble in ethanol and water-ethanol mixtures.

4.2 Impurities and their influence on foaming

MALDI, GPC and NMR results from 4.1, above, strongly suggest that impurities are present in the surfactants used in this study. Solvent extraction and foam fractionation methods were used to isolate and quantify the presence of these impurities, before assessing their effect on foaming.

4.2.1 Methods

Solvent extraction

In the aqueous extraction, Di2510 (1 g) was dissolved in dichloromethane (DCM, 5 ml), before extraction into water (5 ml). Samples were vigorously shaken to mix them, before being allowed to separate over the course of 2 hours. Fractions were separated and dried by rotary evaporation for further analysis.

In the organic extraction, Di2510 (1 g) was dissolved in methanol (5 ml) and hexane was added (5 ml). Shaking produced a stable emulsion, which was destabilised by the addition of 0.5 ml water. The mixture was left to separate for 2 hours, before fractions were separated and dried for analysis.

In a scaled-up version of the organic extraction, Di2510 (10 g) was dissolved in methanol (100 ml) and hexane was added (100 ml). Shaking this mixture resulted in a thick, white emulsion which remained stable over several days. The emulsion was subjected to repeated centrifugation at 1200 RPM for 30-minute intervals, with an organic fraction being pipetted from the top as it formed. A persistent gel phase was removed and dried by rotary evaporation for further analysis.

The composition of these fractions was analysed by quantitative 1H NMR spectroscopy, as described above. Peak integrals were used to estimate the abundances of triblock copolymer surfactant, EO homopolymer and PDMS homopolymer in the crude surfactant. In these calculations, the mixture was assumed to contain only $EO_{10}PDMS_{25}EO_{10}$, PDMS homopolymer and PEG homopolymer, and the solvent extraction was assumed to have been 100% successful – that is, the hexane fraction contained only PDMS homopolymer and the triblock copolymer, and the water fraction contained only PEG and the triblock copolymer.

Foam fractionation

In foam fractionation, a solution is foamed, with the foam being constantly removed to separate surface-active impurities.

For quantitative separation, Di2510 (15 g) was dissolved in 500 ml water/ethanol mixture (90% ethanol, v/v%). Air was vigorously bubbled through for 2 hours, with the resulting foam overflowing the vessel and being collected in an overspill container.

Samples were periodically removed from the supernatant and dried for H1 NMR analysis. They were then resuspended and their foamability tested by the foam pump method (see 6.1).

Homopolymer doping experiment

Samples of Di2510 were prepared with differing levels of PDMS homopolymer contamination – some samples were purified by solvent extraction, giving a less contaminated sample than 'raw' Di2510. Other samples were intentionally doped with PDMS oligomers in varying quantities before dispersing in solvent. One surfactant sample was purified by solvent extraction, before re-doping with PDMS oligomer. All samples contained 3-4 mM crude or purified Di2510.

PDMS oligomer concentrations were estimated using NMR results from solvent extraction experiments, described above.

PDMS oligomers (M_n = 3000 g mol^{-1}) were used as purchased from Sigma-Aldrich.

At higher loadings, PDMS doping resulted in a turbid solution, suggesting that Di2510 was unable to solubilise the added oligomer. Prolonged stirring and shaking reduced this turbidity.

The foamability of these surfactant samples was compared using a foam pump-based testing rig (described in 6.1 below).

4.2.2 Purity results and discussion

As discussed in 4.1.2, preliminary characterisation of the surfactants used in this research suggested they contained homopolymer impurities. 1H NMR analysis of Di2510, also described above, showed that the ratio of PEG protons to PDMS protons in the surfactant was 1:1.74 – suggesting an over-abundance of PEG units. In addition, it was possible that PDMS homopolymer was present in the surfactant. Surface-active impurities are well-documented

in the surfactant literature, and can significantly change the interfacial behaviour of surfactants, even at low concentrations.[71]

PEG- and PDMS-rich impurities may be present in the form of unreacted homopolymer, or as PDMS-PEG copolymers that have undergone premature termination. The presence of very PDMS-rich impurities was a particular concern – PDMS homopolymer is well-studied as an antifoamer and its presence might be expected to suppress foam performance.[74]

I tested two methods for surfactant purification. The first, solvent extraction, exploited the divergent solubilities of PEG and PDMS homopolymer. In the 'aqueous' wash, Di2510 was dissolved in DCM, while PEG impurities were removed with distilled water – leaving a PDMS-enriched organic phase. In the 'organic' wash, Di2510 was dissolved in methanol, and PDMS impurities were removed by repeated extraction with hexane, leaving a PEG-enriched methanol phase.

the GPC traces of crude Di2510 and surfactant from the hexane phase shows the removal of a lower-molecular mass peak, retaining only the higher mass signal, which suggests PEG homopolymer has been removed – see Figure 12, below.

1H NMR analysis of the DCM and methanol phases showed remarkably divergent proton ratios. The methanol phase contained a PEG/PDMS proton ratio of 1:0.03, suggesting a large amount of PEG homopolymer was present. By contrast, the DCM phase had a PEG/PDMS proton ratio of 1:4.12, suggesting considerable enrichment of PDMS well above the predicted ratio for Di2510 (1:1.88). See Figure 10 and Figure 11.

By making some simplifying assumptions (see 4.2.1 above) regarding the composition of these fractions, it is possible to use mass balance to back-calculate the abundance of these components in the initial crude surfactant. This suggests the crude surfactant is ~10% PEG oligomer, 8% PDMS oligomer and 82% triblock surfactant by mass.

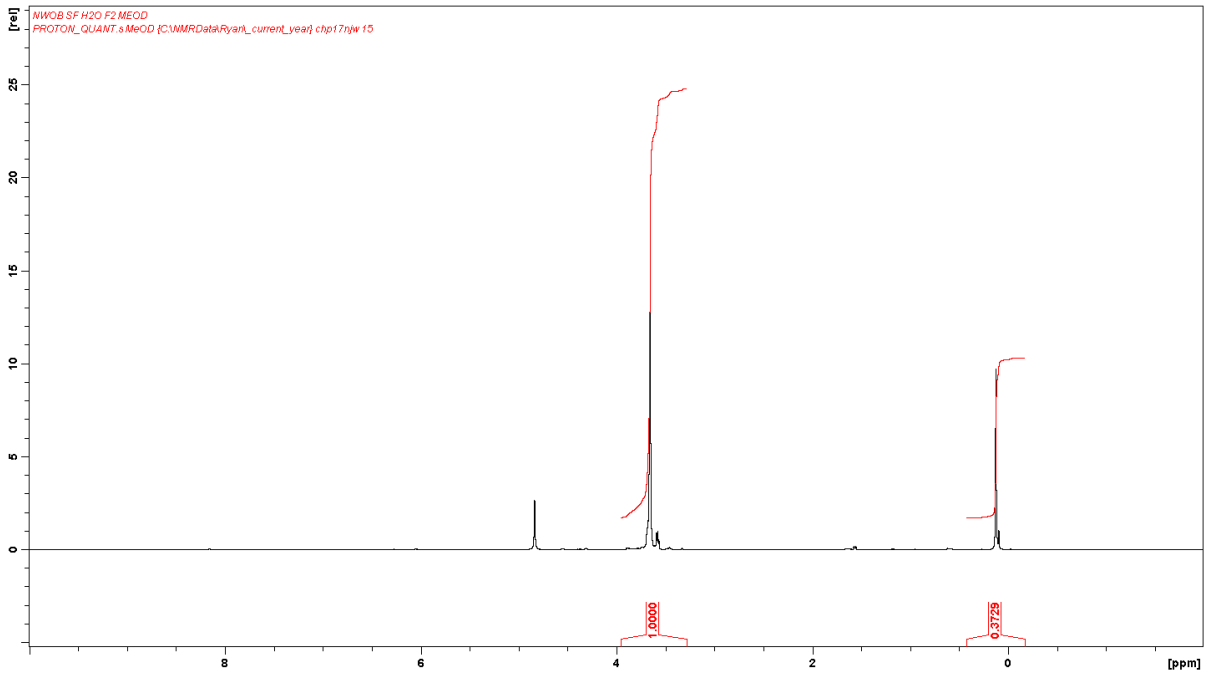

Figure 10. 1H NMR spectrum of the methanol phase produced by solvent extraction of Di2510. Integrals are scaled to the area of the PEG proton peak.

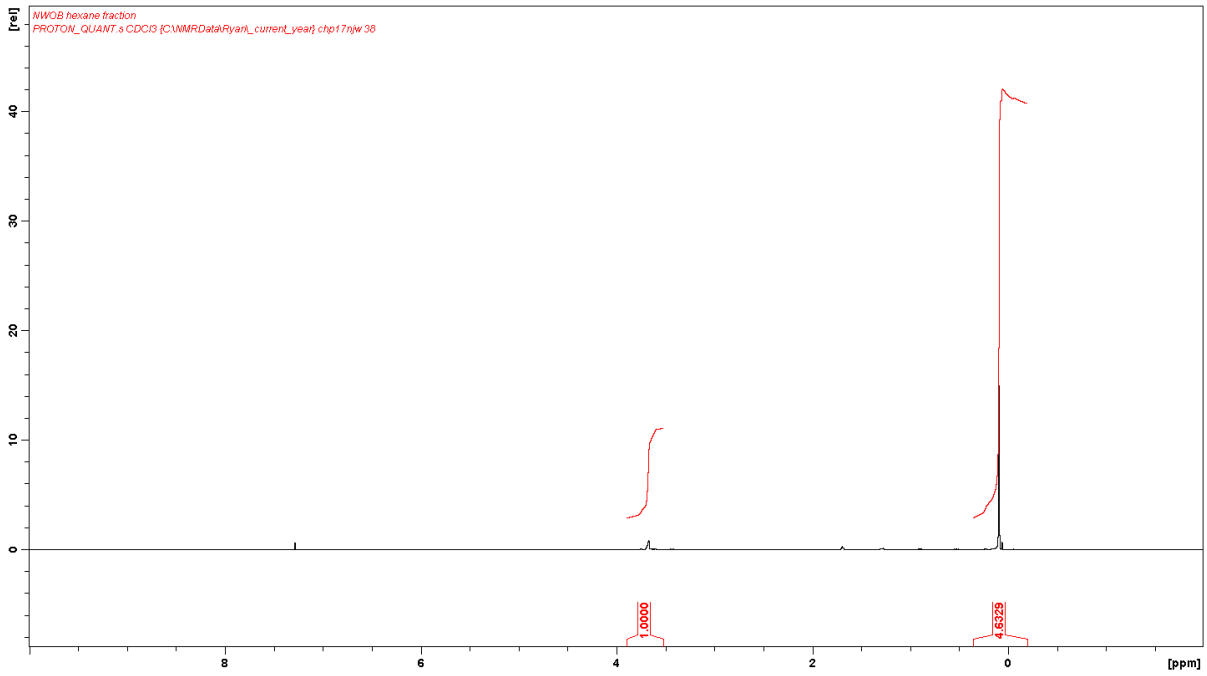

Figure 11. 1H NMR spectrum of the hexane phase produced by solvent extraction of Di2510. Integrals are scaled to the area of the PEG proton peak.

While this solvent extraction was effective in isolating and quantifying impurities, quantitative solvent extraction proved to be practically difficult. Di2510 is an effective emulsifier, producing very stable DCM/methanol emulsions that were resistant to separation, even by extensive centrifugation. In principle, it may be possible to optimise these conditions to minimise emulsion stability.

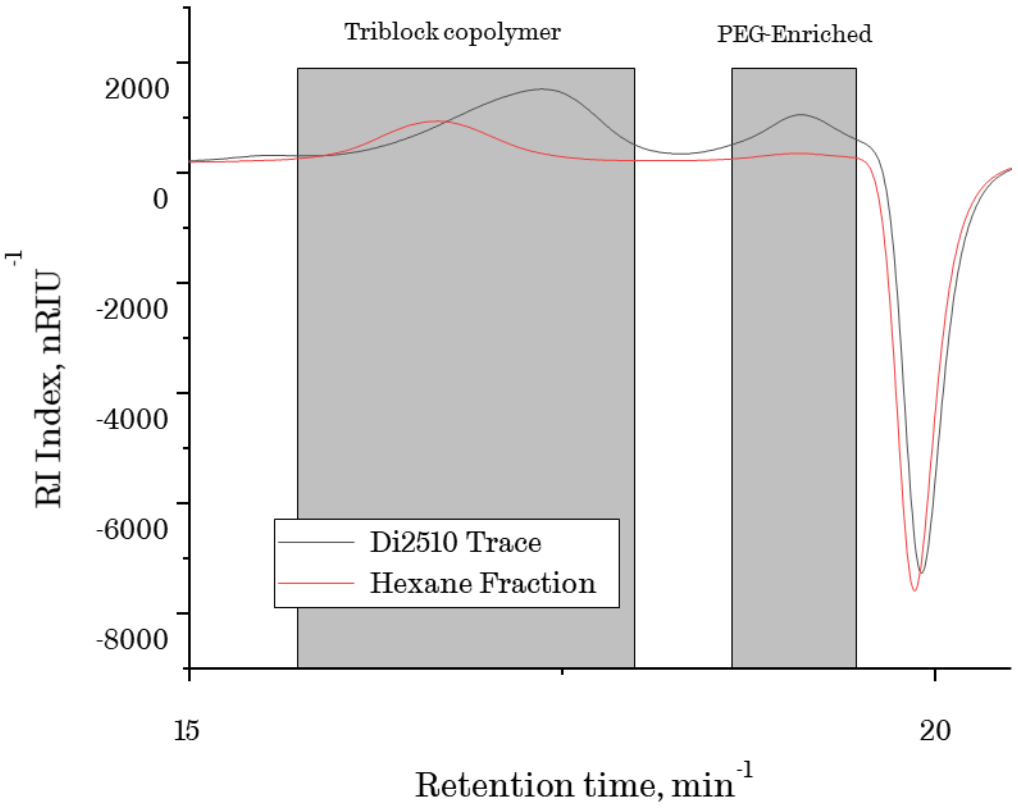

Figure 12. GPC trace of crude Di2510 (black) and the hexane fraction from a hexane-methanol solvent extraction.

The second approach explored was foam fractionation. During this process, a surfactant-containing solution is foamed by sparging. Surface-active impurities, such as PDMS homopolymer, are expected to preferentially adsorb at the interface in these foams, which are then removed. The remaining solution is thus purified.

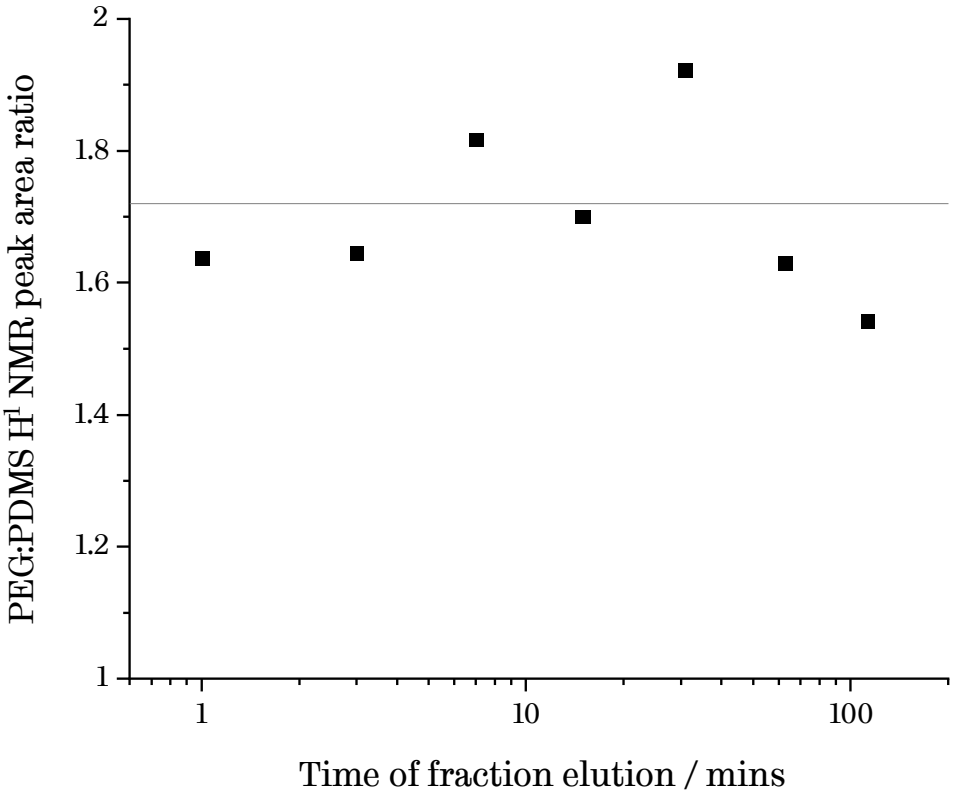

Figure 13. PEG:PDMS proton ratio by 1H NMR spectroscopy, versus foaming time in the process of foam fractionation. Fractions from foam fractionation of Di2510 become more enriched in PDMS over ~30 min, after which PDMS content begin to decline. The horizontal reference line indicates the peak area ratio observed for crude Di2510.

Fractions removed from the foamed solution showed generally increasing enrichment of PDMS, up to a peak after ~30 minutes of fractionation – suggesting that most PDMS-rich impurities had been removed at this time point – see Figure 13. Prior to fractionation, the surfactant had a peak ratio of 1:1.72. Post-fractionation, the surfactant remaining in solution had a peak ratio of 1:1.54, suggesting the foam phase was enriched with respect to PDMS-containing components of the surfactant. Several foam fractions had peak ratios above that expected for Di2510, suggesting they were enriched in PDMS-containing impurities.

Foam fractionation preferentially removes the surface-active components of the surfactant solution, resulting in a solution enriched in PEG homopolymer - hence over time, the PEG:PDMS proton ratio measured by NMR begins to decrease.

Fractions removed from the solution contained somewhat different levels of surfactant. Foamability comparisons were facilitated by interpolation using a simple quadratic model, fitted to results from crude Di2510 (see 6.3.3, particularly Figure 27, below). This allowed samples of different concentrations to be compared against an expected foam volume. The difference between the actual and predicted volume gives an indication of the fraction's performance against a comparable sample of crude Di2510.

These differences were initially negative – that is, the early fractions performed worse than a crude sample of the same mass. The residual generally increased through the course of the experiment. The final fraction, collected after 2 hrs, outperforms crude Di2510 by approximately 4 ml (see Figure 14) on a total foam volume of ~20 ml.

It is striking that fractions taken later performed significantly better than crude Di2510, despite containing more PEG-rich impurities per unit mass – as indicated by their lower peak ratios – see Figure 13. This corroborated concerns about the presence of PDMS-containing surface-active impurities adversely affecting the performance of Di2510. It is particularly striking that the sample collected at 30 minutes, a significant under-performer in terms of foaming, was also the most PDMS-rich fraction as measured by NMR.

It is not clear why, in the 3-30 min period, the supernatant apparently became enriched in PDMS-containing impurities, before declining again. This perhaps reflects complex solubilisation dynamics within the solution.

In summary, solvent extraction can be used to isolate either PEG-rich and PDMS-rich impurities present in crude Di2510. These two extractions could presumably be employed in series to provide a relatively pure sample of Di2510. Foam fractionation also appears to strip PDMS-rich components from the solution, resulting in a PEG-enriched copolymer that nevertheless produces larger foam volumes than would be expected for crude Di2510.

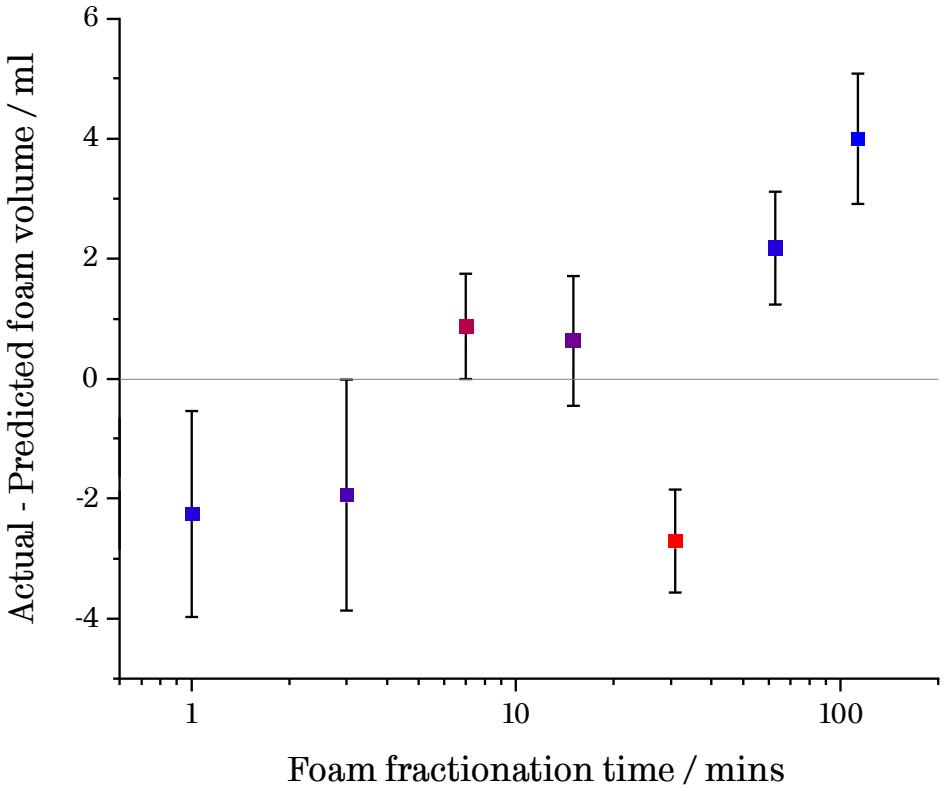

Figure 14. Foam volume of eluted fractions minus predicted foam volume for crude Di2510, as a function of foam fractionation time. Predictions were generated using simple quadratic fits as described in 6.3.3. Samples above $y = 0$ outperformed the predicted performance of an equivalent concentration of crude Di2510. Later foam fractions generally produced greater foam volumes than earlier ones. Error bars represent 95% confidence intervals. Symbol colour is scaled with copolymer composition as measured by 1H NMR peak ratio, where red is more PDMS-rich, and blue is more PEG-rich. The reference line indicates equivalent performance with crude Di2510.

A series of surfactant solutions with increased or reduced concentrations of surface-active impurities versus crude Di2510 were generated using solvent extraction and by the addition of known concentrations of PDMS oligomers. The foamabilities of this series of solutions were compared using the foam pump test rig. As with the foam fractionation result, these solutions' performance were compared to an equivalent concentration of crude Di2510 using interpolated data (see 6.3.3). In these measurements, Di2510 doped with PDMS oligomer performed significantly worse than crude Di2510, and purified Di2510 performed slightly better (see Figure 15). Crude Di2510 performed as predicted by the model.

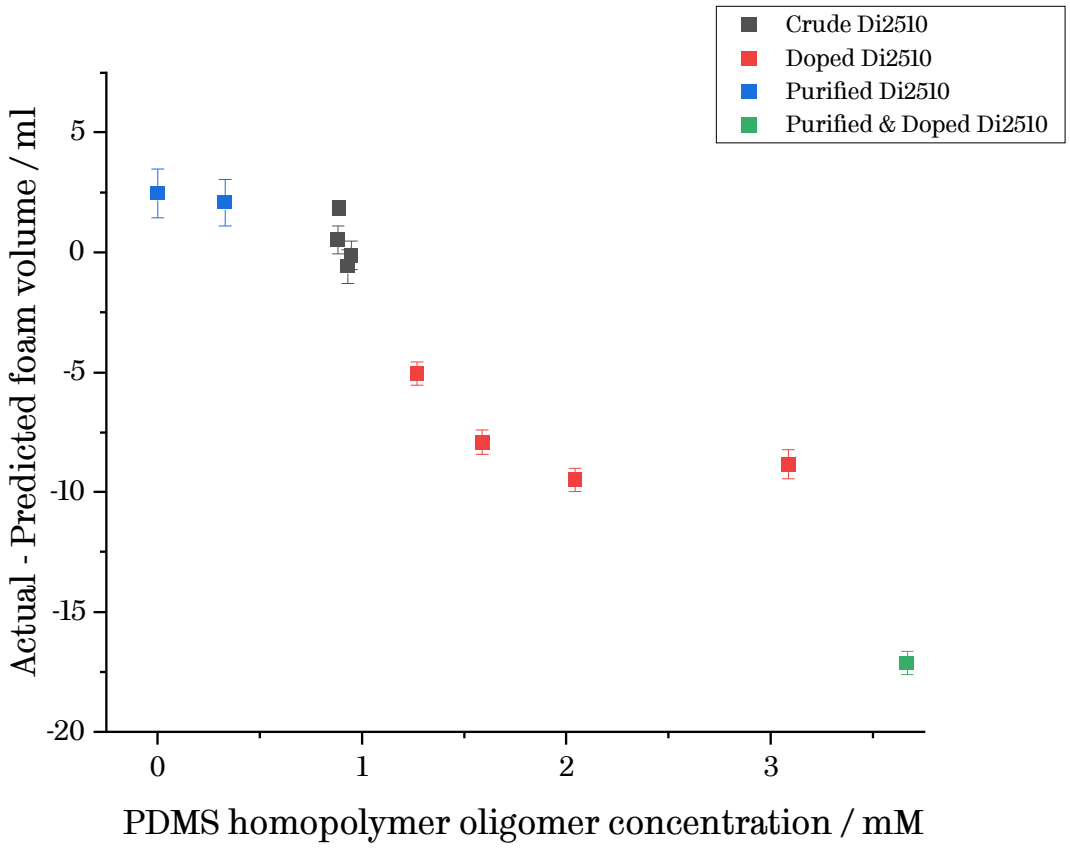

Figure 15. Actual minus predicted foaming performance of Di2510 samples against concentration of PDMS homopolymer. Predicted foam volumes were calculated using simple quadratic fits as described in 6.3.3. Samples above $y = 0$ out-performed the predicted performance of an equivalent concentration of crude Di2510. Higher PDMS homopolymer concentration is associated with reduced foam volumes in the foam pump test. Purification of surfactants appears to lead to improved foamability.

I ran a simple linear model to compare the effects of doped and 'natural' PDMS impurities (see Appendix 11.1). The model found strong evidence that addition of PDMS reduced foam volume – by approximately 9 ml / mM PDMS oligomer. The finding for 'natural' PDMS impurities was more ambiguous, with non-significant *p*-value of 0.132. The estimated effect of these homopolymer impurities was also smaller – with a 2-6 ml reduction in foam volume per mM oligomer added. This suggests that some of the improved performance of the purified surfactants in Figure 15 may simply reflect the higher concentrations of triblock surfactant in the purified samples rather than the impact of impurities on foamability.

In conclusion, there is good evidence that both PEG- and PDMS-rich impurities are present in the surfactant, and their combined mass fraction corresponds to around 18% of the crude Di2510. Both foam fractionation and solvent extraction have been shown to reduce the

concentration of surface-active impurities in these surfactants, leading to higher foam volumes. The mechanism of PDMS oligomers' negative effect on foam impurities is still unclear.

4.3 Surfactant synthesis

Methods

Novel surfactants were synthesised by *aza*-Michael addition of a mono-acrylate polyether (poly(ethylene glycol) monomethyl ether monoacrylate, Mn = 480) to bis(3-aminopropyl)-terminated PDMS (M_n = 2500) – see Figure 16. All reagents were purchased from Sigma-Aldrich and were used as received.

Reactions were carried out at 40°C in ethanol. Bis(3-aminopropyl)-terminated PDMS (5 g) was dissolved in 100 ml ethanol and stirred thoroughly. Mono-acrylate polyether (2 g, 2.1 mol. equiv.) was dissolved in 20 ml ethanol and added dropwise over six hours. The resulting turbid mixture was dried by rotary evaporation.

Products were characterised by 1H NMR spectroscopy and their foamabilities measured.

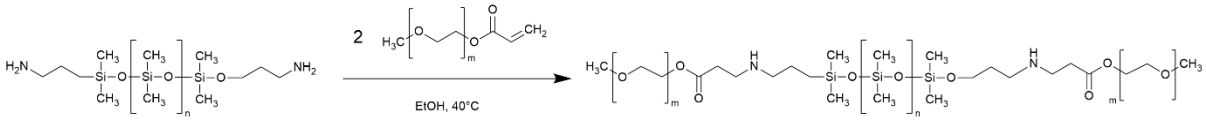

Figure 16. *aza*-Michael addition of poly(ethylene glycol) monomethyl ether monoacrylate to bis(3-aminopropyl)-terminated PDMS to form a triblock copolymer.

Discussion

Aza-Michael addition of amines to electron-deficient acrylates is a rapid reaction that proceeds rapidly at room temperature.[75] A "reservoir" approach to acrylate addition was adopted – it was added dropwise under vigorous stirring to minimise the potential for repeated addition at each amine – an effective method demonstrated by Genest *et al.* in a recent paper.[75]

NMR analysis showed that the reaction had been successful, with the distinctive acrylate splitting pattern at 6 ppm almost eliminated.

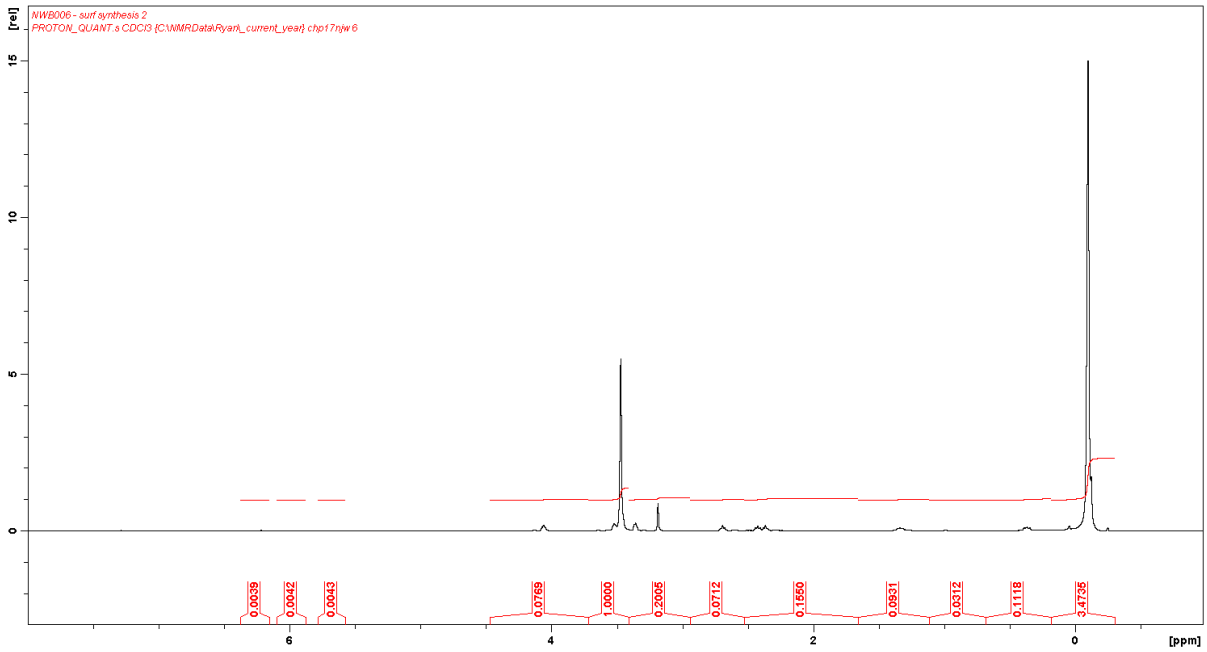

Figure 17. 1H NMR spectrum for Di4008, confirming near-disappearance of acrylate signals around 6 ppm. Integrals are scaled to the area of the PEG proton signal.

The resulting surfactant, named Di4008 in analogy with the nomenclature used for the other siloxane polyethers, was tested for foamability by simple vial test in a 90:10 ethanol to water mixture, and then using the foam pump method (see section 6.1, below). Its foamability was poor, possibly due to its low solubility. 3% w/w Di4008 generated ~15 ml foam, compared to ~27 ml for Di2510 in equivalent conditions.

5 Micelle investigation and characterisation

This chapter details several attempts to measure the CMCs of the surfactants used in this research and to characterise their micelles. Unsuccessful attempts to investigate the kinetic behaviour of micelles under non-equilibrium conditions are also described.

5.1 Materials and methods

5.1.1 Equilibrium surface tension

Six siloxane polyethers (Di1010, Di1018, Di1508, Di2012, Di2510, Di4515) were analysed by Du Noüy ring tensiometry using a Lauda T3 tensiometer. Sample concentrations for each surfactant ranged from approximately 0.001-3% (w/w). Samples were compared across three solvent mixtures (50%, 70% and 90% Ethanol/water, v/v).

The LAUDA T3 tensiometer was equipped with a 90:10 platinum-iridium ring of 6.283 cm circumference, 9.55 mm radius and 0.2 mm width. Surface tension of ultrapurified water was measured before use, with good agreement with a literature value of 72.8 mN m^{-1} being observed. Between each measurement, the ring was immersed in ethanol, flamed immersed in water and flamed again. The surface tensions of solutions were monitored until nine consecutive readings had a standard deviation of no more than 0.01 mN m^{-1}, or until 30 mins had elapsed. Densities of ethanol-water mixtures were calculated by interpolation of literature values.[76]

The solution temperature was controlled using a LAUDA thermostatic bath at 20 ºC.

Equilibrium surface tension was assessed by two methods. In the first, the final data point measured for the sample was taken to be the equilibrium value. In the second, dynamic surface tension, γ_t, was plotted as a function of $t^{-\frac{1}{2}}$, and a line of best fit generated. This line was extrapolated to the y-axis intercept, where $t^{-\frac{1}{2}} \rightarrow 0$ and $t \rightarrow \infty$.[77,18]

5.1.2 Dye solubilisation

Indigo, Nile Red and Sudan IV dyes were purchased from Sigma-Aldrich.

UV-visible spectrophotometry was carried out using glass cells of path length 10 mm and a Shimadzu 1800 spectrophotometer. Measurements were baselined against solvent mixture-only samples.

In initial experiments, indigo dye was dissolved in a range of solvents, including neat Di2510, where its solubility appeared much greater than either Ethanol or Ethanol-water mixtures.

Experiments were carried out to test the detection limit of indigo dye in water-ethanol mixtures. Indigo (1 mg) was (partially) dissolved in a 10:90 v/v water-ethanol solution (100 ml,), filtered, and its visible absorption spectrum recorded. The dye solution was then sequentially diluted by the removal of one third of its volume, to be replaced with 90:10 v/v water-ethanol solution. Dye detection was observed for 6-7 cycles of dilution, suggesting a minimum mass concentration of ~0.6 mg / L, or approximately 0.002 mM.

Research on non-ionic surfactants has suggested a surfactant/dye ratio, r, of 20 can be achieved without substantially changing the kinetic behaviour of the surfactant.[78] Thus, experiments with up to 0.04 mM copolymer surfactant should be possible.

Further experiments were carried out to establish whether indigo dye would be localised inside micelles. Solutions of indigo (1 mg / L, 0.038 mM) were made up in water-ethanol mixtures (90% v/v) and filtered. Di2510 was added at varying concentrations, and the resulting visible absorption spectra compared.

5.1.3 Small-angle X-ray scattering (SAXS)

SAXS samples were prepared at 1.5 CMCs (as measured by DLS – see below) in water-ethanol mixtures. They were held in open borosilicate glass capillaries (diameter = 2 mm) supplied by Capillary Tube Supplies Ltd, Cornwall, UK.

Scattering was measured using a Xeuss 2.0 beamline (Xenocs, Grenoble, France), with a 2D Pilatus 1M pixel detector (Dectris, Baden-Daettwil, Switzerland) and a MetalJet X-ray source (Excillum, Kista, Sweden). The x-rays were Ga Kα radiation with $\lambda = 1.34$ Å.

Each sample was scanned for 60 minutes, between ~0.004 $Å^{-1} < Q < 0.02$ $Å^{-1}$. Q values were calibrated to peak spacings observed for a sample of silver behenate.

Masking and azimuthal integration was carried out using FoxTrot. Data was processed using Igor Pro 8 and the Irena macro.[79] A core-shell model following Pederson and Gerstenberg (PG model) was used to fit the data up to the first minimum.[80] Electron scattering length densities for PDMS, EO, PO, H_2O and ethanol were calculated using literature density values and the chemical formulae of moieties in the system.

5.1.4 Dynamic light scattering (DLS)

DLS experiments were conducted using a Malvern Zetasizer instrument, operating in backscatter mode. Samples were passed through a 2.5 μm Whatman syringe filter prior to testing. Surfactant solutions (1.5 ml) were placed in a glass cuvette. At least three measurements, each consisting of 20 sub-measurements of 20 seconds, were recorded for each sample.

Samples were gradually diluted from an initial concentration by removing a fraction of the sample's initial volume and replacing that volume with solvent mixture. This process was repeated until the peak corresponding to micelles disappeared.

5.2 Results and discussion of micelle characterisation

Micellar properties have two key aspects of relevance to foamability. Firstly, unimer surfactant is significantly more able to quickly populate the gas-liquid interface when foam formation begins. As interfacial area grows, unimer surfactant can rapidly diffuse to and adsorb at the interface – whereas surfactant within micelles must pass over a (potentially large) energetic barrier in order to escape and then reach the interface.[46] Thus, a higher CMC implies that a larger reservoir of unimer surfactant is available for rapid adsorption.

The kinetics of micelle dissociation may also be highly consequential when a surfactant is present above its CMC. In this case, some or most of the surfactant will be located within micelles, and the rate at which unimers are released into bulk solution may thus govern the rate of surfactant adsorption. Patist *et al.* have emphasised the particular importance of micelle kinetics when foam formation is rapid.[31,81]

In the context of water-ethanol solutions, the question of micellar properties becomes more complex, as solvent quality plays an important role in determining both equilibrium and dynamic micelle behaviour.[46,82] Solvent quality can tune micelle-unimer exchange kinetics and the CMC, and thus influence foamability. As detailed in 2.2.1, the length of the solvophobic block also likely plays a significant role in controlling both static and dynamic micelle properties.

5.2.1 Equilibrium surface tension measurements

The equilibrium surface tension of pure surfactants has two distinct regimes – a region of rapid decline, whereby increasing surfactant concentration in the bulk drives greater surface

adsorption and reduces surface tension, and a second region in which surface adsorption is saturated and becomes uncoupled from the bulk concentration.

An abrupt change in the relationship of equilibrium surface tension with surfactant concentration is taken to indicate the onset of micelle formation and hence the CMC.

However, the case of impure 'technical-grade' surfactants makes such measurements problematic. Such surfactants typically include surface-active impurities (SAIs, see 4.2), which adsorb at the interface more quickly and strongly than complete surfactant molecules. Such molecules are typically largely insoluble in solution and can depress the surface tension below the 'true' equilibrium CMC value.[71] As micelles begin to form in solution, SAIs preferentially relocate to their (solvophobic) cores. This, in turn, increases the surface tension as it stabilises towards a 'true' equilibrium, formed by pure surfactant. Thus, the presence of SAIs leads to so-called 'hooking' in the surface tension/concentration graph, which disrupts attempts to find the 'true' CMC.[71]

Two methods are compared for their efficacy in finding the CMC for siloxane polyethers from Du Noüy ring tensiometry data: the simplest involves taking the final data point measured by the tensiometer. A second method involves fitting the dynamic surface tension γ_t as a function of time – specifically, $t^{-\frac{1}{2}}$. When this plot is linear, the surfactant adsorption process is diffusion-controlled. By extrapolating surface tension data to the y-axis, where $t \to \infty$ as $t^{-\frac{1}{2}} \to 0$, the equilibrium surface tension can be predicted from the y-intercept. These two methods gave slightly different CMC values, which converged as surfactant concentration was increased.

This method did not provide clear values of the CMC for the copolymer surfactants. Di1010 and Di4515 provide characteristic examples (see Figure 18, Figure 19). A clear CMC is obtained for Di1010 in 70% ethanol, but none is visible in 90% or 50% ethanol - likely because it falls outside the surfactant concentration range tested. By contrast, for Di4515, no kinks or discontinuities in the surface tension data are observed, and thus it is not possible to assess the CMC. Figure 19 also indicates hooking, described above, in the data obtained for 90% ethanol.

Where it could be determined, typically the CMC appeared to shift to higher concentrations as x_{eth} was increased.

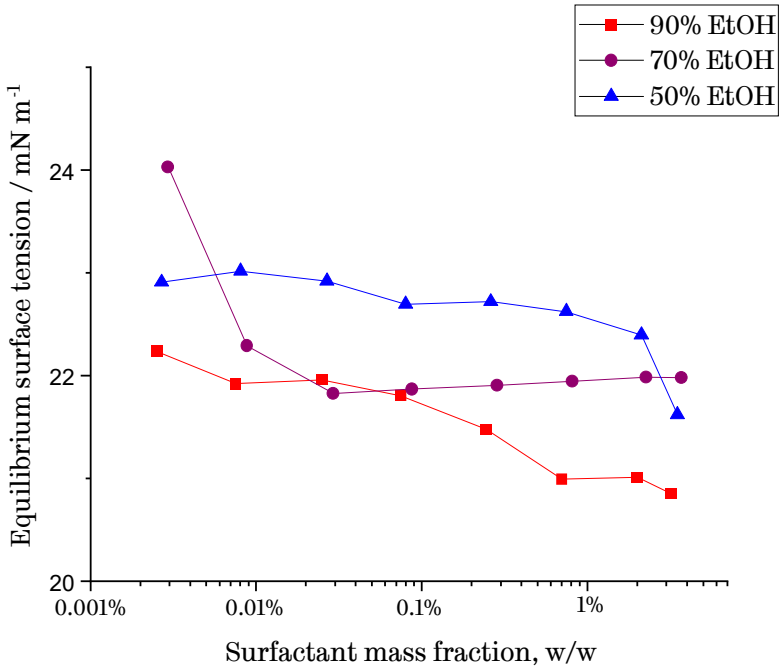

Figure 18. Equilibrium surface tension *vs.* surfactant concentration for Di1010 in 90, 70 and 50% Ethanol, measured after 30 mins, using Du Noüy ring tensiometry. CMCs are visible for 70 and 90% Ethanol, at approximately 0.0002% and 0.008% surfactant, respectively. Symbol colour is scaled with solvent composition, where red is 90% Ethanol and blue 50% Ethanol.

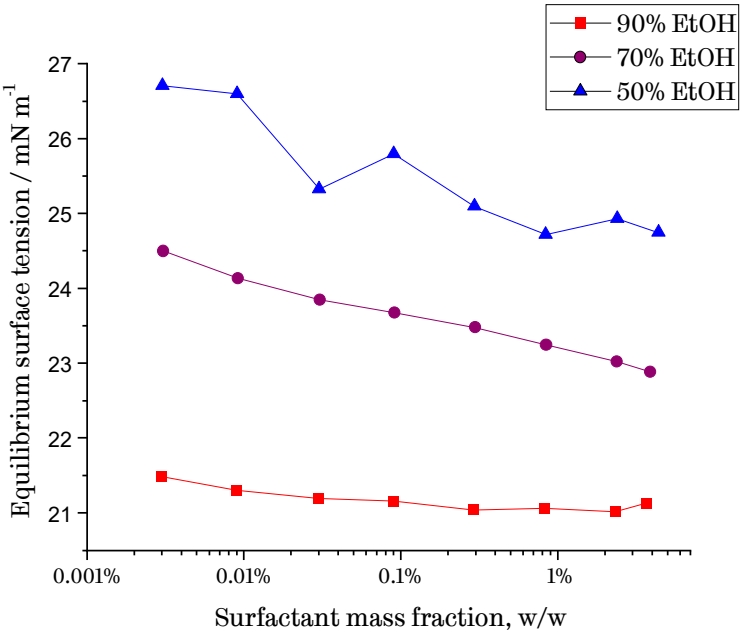

Figure 19. Equilibrium surface tension *vs.* surfactant concentration for Di4515 in 90, 70 and 50% Ethanol, measured after 30 min, using Du Noüy ring tensiometry. No CMC is visible. Symbol colour is scaled with solvent composition, where red is 90% Ethanol and blue 50% Ethanol.

5.2.2 Dye solubilisation measurements

Dye solubilisation methods were investigated for both static CMC determination and micellar dissociation measurements. Dye solubilisation methods exploit the solvatochromic effect, whereby the adsorption and emission characteristics of a dye molecule are influenced by its molecular environment. A highly hydrophobic dye dissolved in aqueous media, will become preferentially localised within the hydrophobic cores of micelles (if they are present), thus shifting its peak emission.[71,83,84] In the absence of micelles, surfactant has no effect on dye emission – but as the CMC is exceeded and micelles begin to form, dye partitions and the wavelength for maximum emission shifts.

As a method of detection that directly probes micellar structures, dye solubilisation avoids issues with surface-active impurities that produce 'hooking' in surface-tension-based CMC measurements.[71]

However, no dye exhibited a peak shift when dissolved in sub- and supra-CMC solutions of Di2510. In the case of Sudan IV and Nile Red, this is most likely a result of the relative solubility of these hydrophobic dyes in ethanol-water mixtures. Despite their hydrophobic nature, neither dye proved sufficiently insoluble in ethanol-water solutions to detectably partition into micelles.

Further experiments were carried out using indigo, a dye whose neutral form is essentially insoluble in both water and ethanol. In textile dying, indigo must be reduced to its *leuco*-form to dissolve, before being re-oxidised on contact with air to fix the stain.[85] Indigo also demonstrates a exhibits bathochromic shift, with a $\lambda_{max} = 608 \pm 2$ nm in ethanol, versus $\lambda_{max} = 595 \pm 5$ nm in benzene.[85] However, solutions of indigo dye also did not demonstrate any change in their visible adsorption behaviour in micellar solutions – see Figure 20 and Figure 21.

It is possible that the failure of hydrophobic dyes to localise in the cores of siloxane micelles is the result of PDMS having both hydrophobic and lipophobic character. To successfully carry out this experiment, it may be necessary to modify dyes with siloxane chains to give them sufficiently high affinity for siloxane-based micelle cores.[86]

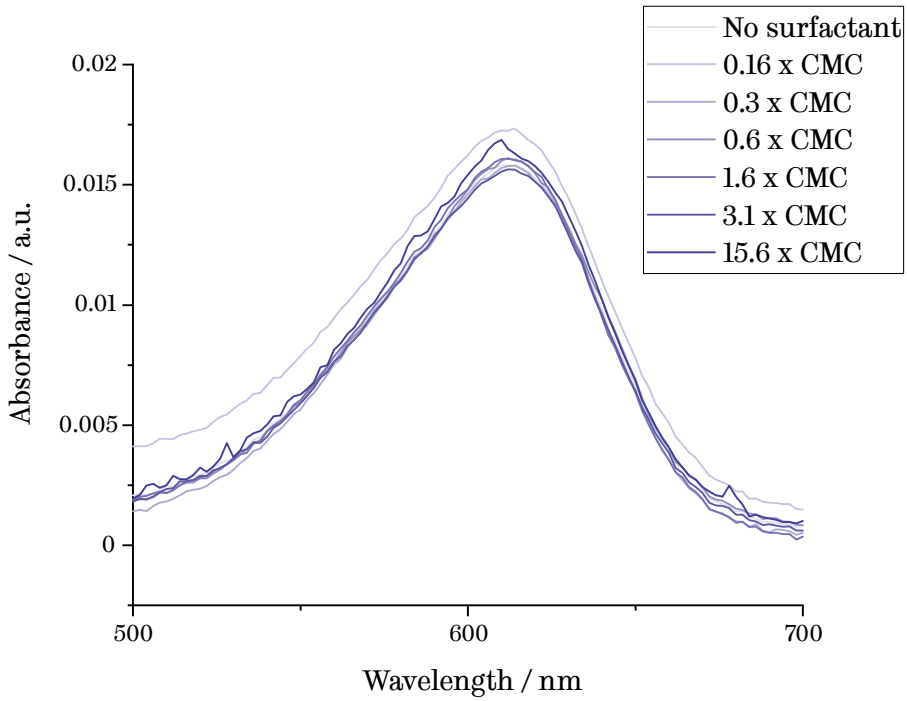

Figure 20. Visible absorbance spectra recorded for solutions of indigo dye and Di2510 at varying concentrations. No change in maximum absorbance is observed as the surfactant is diluted below its CMC.

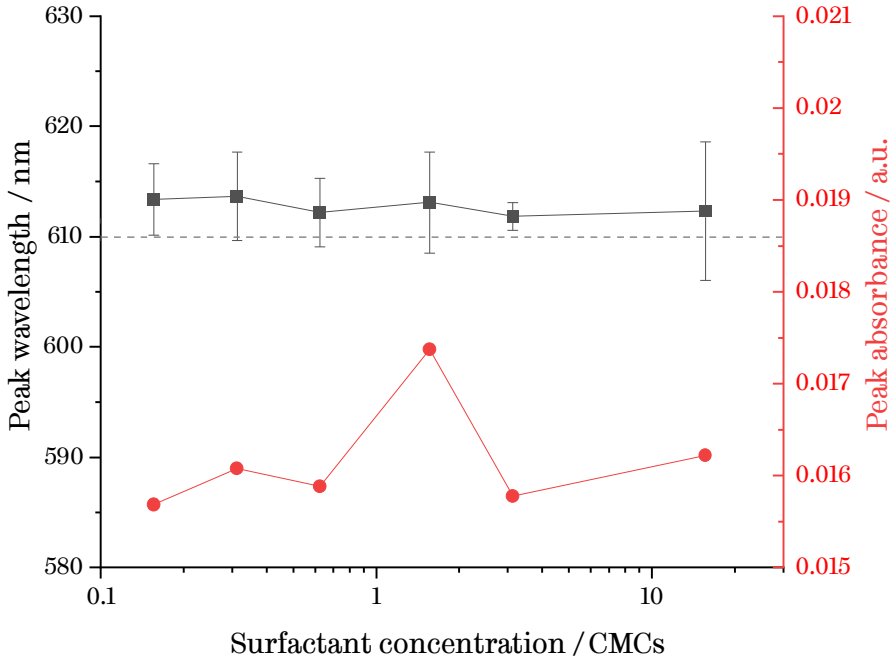

Figure 21. Maximum absorbance and λ_{max} versus surfactant concentration for a series of indigo-Di2510 solutions above and below the CMC. Neither parameter systematically changes as the concentration of Di2510 varies. The reference line indicates the λ_{max} value for indigo solution without surfactant.

5.2.3 Discussion of SAXS

SAXS did not prove to be an effective technique for either determining the CMC or following micelle dissociation. In both cases, the very low copolymer concentration involved, and the comparatively weak x-ray flux of the laboratory SAXS instrument made it difficult to collect sufficient data. At higher concentrations, however, it was possible to fit models describing micelles for three surfactants (Di4515, Di2510 and Di2012).

The Pederson-Gerstenberg model assumes a spherical micelle core composed entirely of PDMS. The soluble chains of the surfactant are assumed to be Gaussian in nature. Thus, the electron scattering length density of the shell blends from that of dissolved polyether to the solvent mixture. It is possible, therefore, to model both the shell and core thickness of the micelle. The resultant fits to the SAXS patterns are satisfactory (see Figure 22). Di1010, Di1508 and Di1018 did not produce scattering patterns that could be modelled – most likely because the detector was too close to the sample for the initial measurements.

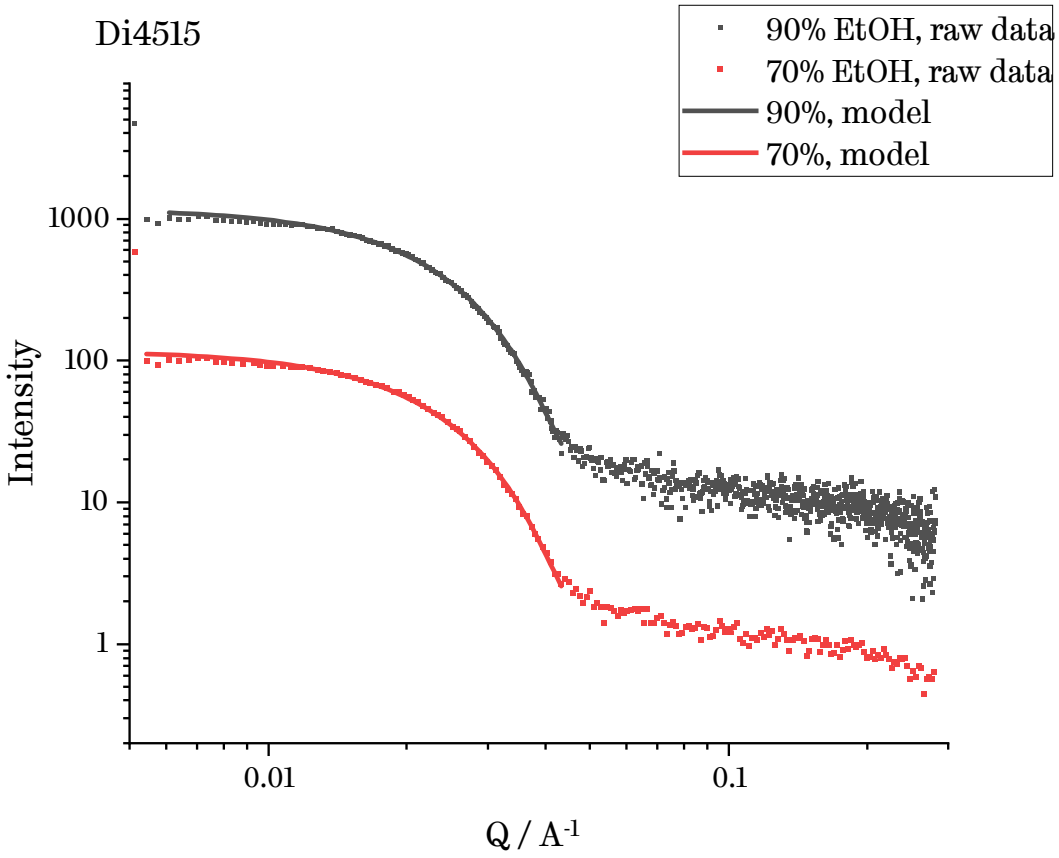

Figure 22. SAXS scattering patterns recorded for Di4515 in 90 and 70% ethanol. Lines show the Pederson-Gerstenberg model fit. 90% data is offset by a factor of 10, for clarity.

All models gave micelle radii between 50-90 Å, with Di2510 and Di2012 producing smaller micelles than Di4515. In all cases, the total radius of the micelle was smaller in 70% ethanol compared to 90% ethanol. On average, this reduction amounted to ~5% of the radius in 90% ethanol. In the case of Di2510 and Di2012, this contraction was driven by a reduction in both the shell and core radii. In Di4515, the core appeared to increase slightly in volume in 70% ethanol, versus 90%, but the shell shrank substantially.

It is possible to calculate an apparent aggregation number for these micelles by comparing the predicted core volume and the volume of a single siloxane chain. This calculation gives aggregation numbers of between 70 and 170, with Di2012 and Di4515 having larger aggregation numbers than Di2510. Di2012 and Di2510 had lower aggregation numbers in 70% ethanol, but the apparent aggregation number for Di4515 slightly increased.

Shell thickness roughly tracked the $nPolyether$ (i.e., nEO + nPO), with Di4515 having a substantially larger shell radius than Di2510 and Di2012.

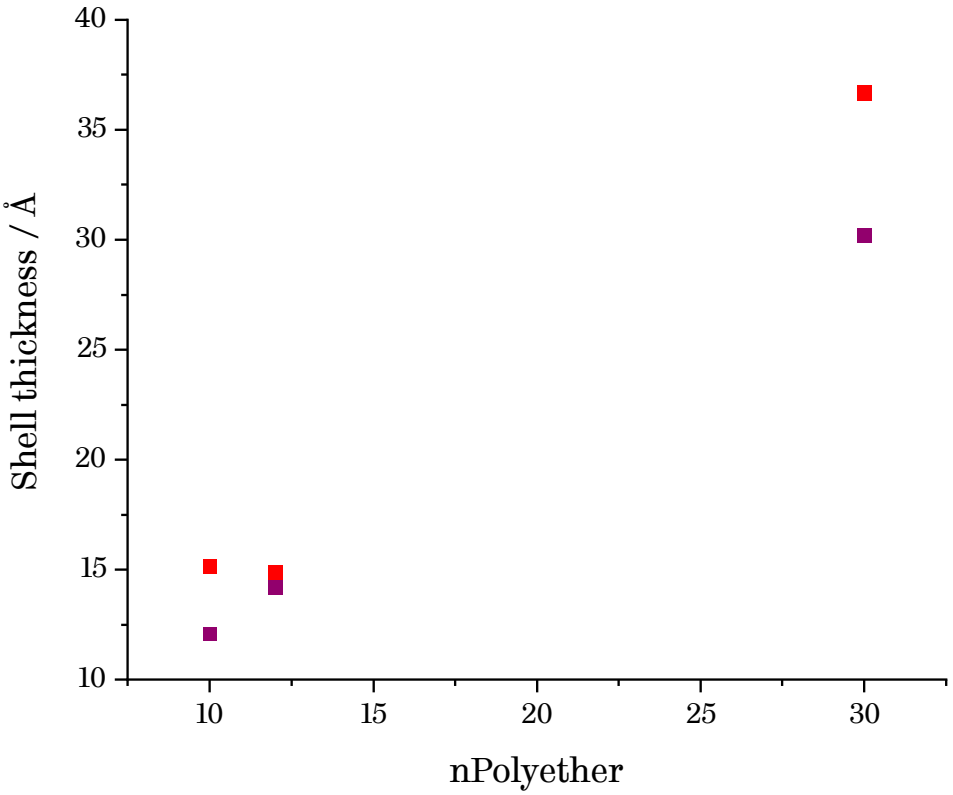

Figure 23. Micelle shell thickness versus nominal nPolyether. Micelle shell thickness grows with nPolyether. 90% ethanol samples are shown in red. 70% ethanol samples are shown in purple.

The SAXS study reported herein is limited due to timing, equipment availability and Covid working practices. Nevertheless, it is clear that the surfactants studied herein behave in a predictable manner with respect to micelle size, core and shell thickness and aggregation number.

5.2.4 Discussion of DLS

DLS is a technique that uses the Stokes-Einstein equation to predict the sizes of particles undergoing Brownian motion. A laser beam is focused on a solution, and the back-scattered light is monitored over time. This fluctuating signal can be used to fit an intensity auto-correlation function, which can be related to the particle diffusion coefficient and thus the particle radius.

DLS was used to determine the CMCs for surfactant in 90%, 70% and 50% (v/v) ethanol-water solutions.

In each case, when the surfactant concentration exceeded the CMC, z-average particle diameter between 5-20 nm was obtained for micelles in solution. This identification is supported by the SAXS studies, described above, which detected micelles with radii of 5-10 nm. As the concentration was reduced, this signal declined in intensity compared to those at > 200 nm, which were identified as either dust or other sub-micellar aggregates. Below the CMC, the micelle population, leaving only larger particles detectable in solution – see Figure 24.

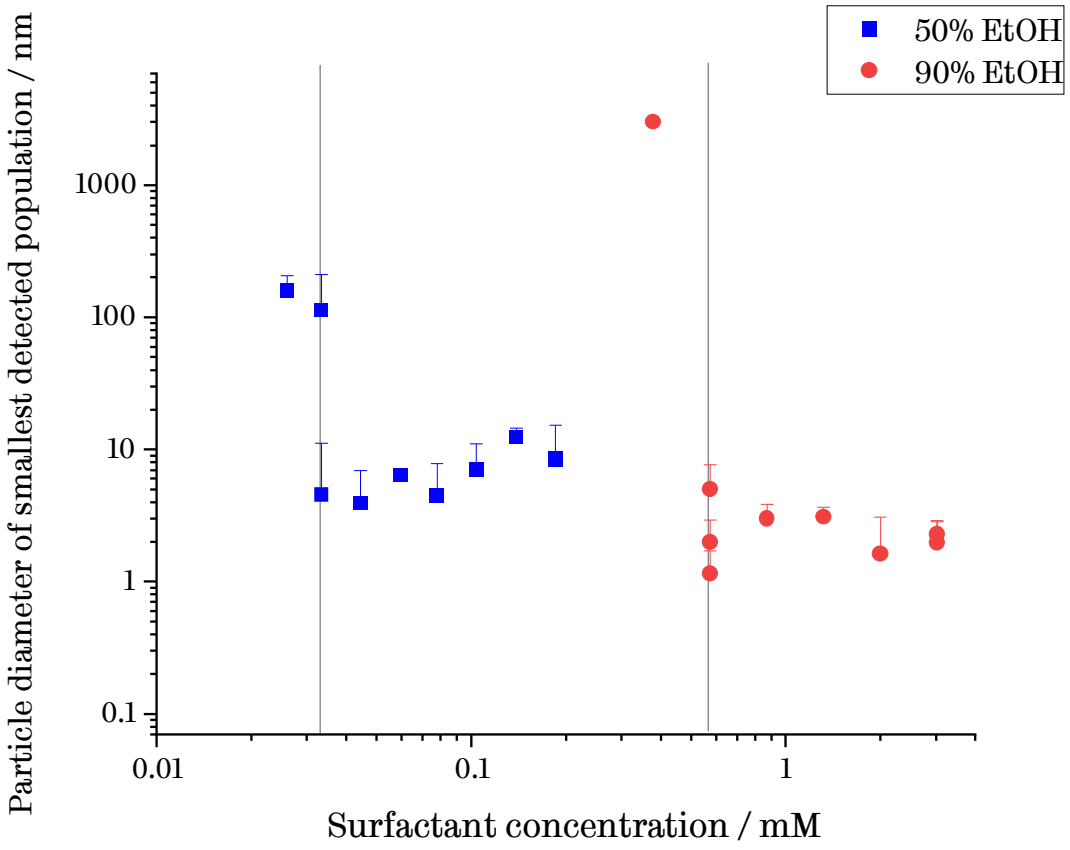

Figure 24. Particle diameter of the smallest detected population vs. surfactant concentration, determined by DLS measurements of Di1010 in water-ethanol mixtures. Confidence intervals indicate standard deviation calculated from three measurements. Lines indicate measured CMC.

This approach resulted in reproducible results for the CMC for all siloxane polyethers that were tested, across three solvent mixtures.

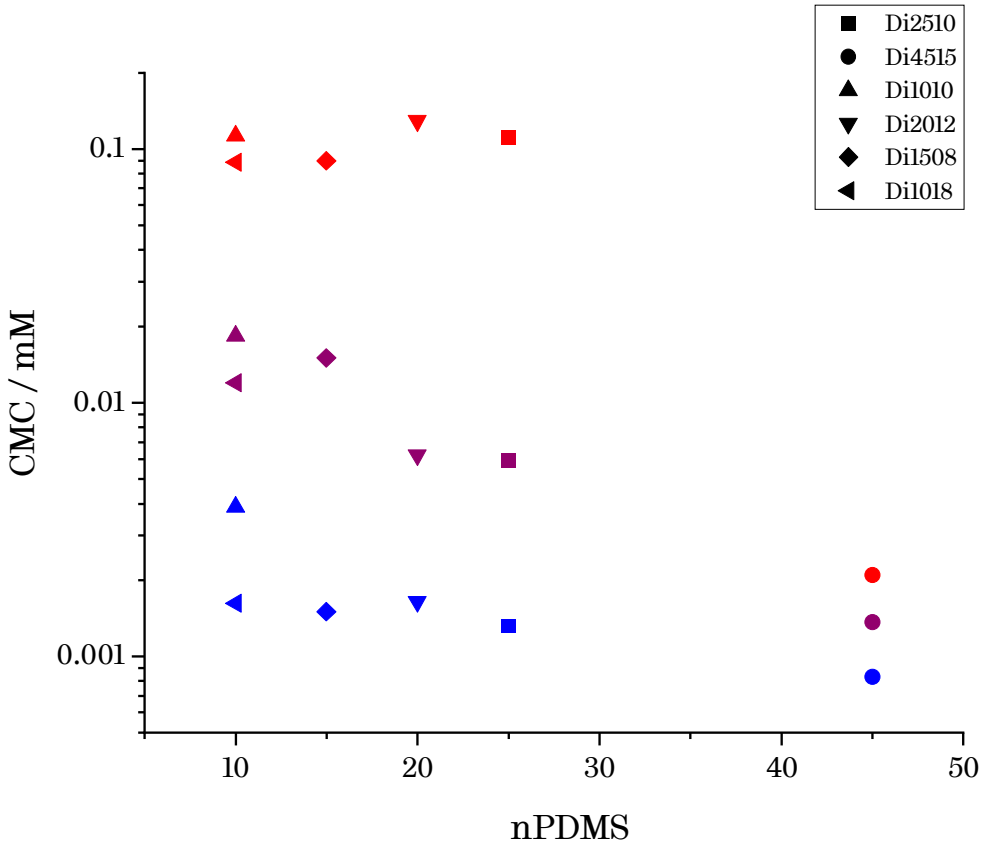

Figure 25. Variation in CMC vs nominal nPDMS for a range of siloxane polyethers. CMC values decline with both nPDMS and x_{eth}. Values measured by DLS. Colour is scaled to solvent mixture, with red representing 90% ethanol and blue representing 50% ethanol.

For the EO-only surfactants - Di1010, Di1508, Di2012 and Di2510 - a linear relationship is observed between log CMC of a surfactant with both the solvent composition and nPDMS. The CMC was lowered by approximately an order of magnitude for each 0.2 increase in water content in the solution (see Figure 25). For $x_{eth} = 50\%$ and $= 70\%$, increases in nPDMS had a similarly dramatic effect on the CMC. No effect of nEO was apparent.

Di4515 and Di1018 are included in Figure 25 but are not directly comparable to the other surfactants, as they contain either a mixture of EO and PO or pure PO side-chains. Di4515 exhibits a comparatively low CMC, likely as a result of its high nPDMS value. It is well-correlated for 50% and 70% ethanol, but its value for 90% ethanol is significantly lower than would be predicted on the basis of the smaller surfactants tested in this study.

These results are qualitatively consistent with theoretical predictions – reducing solvent quality and increasing hydrophobicity both increase the energetic benefit of micelle

formation and thus lower the critical concentration at which micelles form. This work is also largely consistent with data reported for Pluronics (see 2.3).[83]

Attempts were made to conduct 'time-resolved' DLS experiments to monitor micelle dissociation. In these experiments, rapid dilution was used to quickly reduce a supra-CMC solution to below its CMC. However, this approach failed due to the sudden emergence of large aggregates (~200 nm in diameter) that appeared as micellar solutions were diluted close to the CMC. These aggregates could be centrifuged out of solution, but rapidly reformed, leading us to conclude they were not contaminants but were in fact formed by copolymer surfactant in the sample.

Similar results have been recently reported by Shih *et al.* in the context of structurally analogous Pluronic surfactants.[87] These premicellar aggregates are likely weakly associated molecules - perhaps nucleated by homopolymer impurities in solution.

6 Foam research

This chapter describes several experiments aimed at exploring the foaming behaviour of siloxane polyether solutions, and the effect of ethanol, surfactant concentration, and rate of foam generation. Several foaming methods were examined, with the foam pump, sparging and vortexing methods eventually selected for further work.

Throughout this work, extensive use was made of Design of Experiments (DOE) approaches to efficiently collect data on the large number of input factors for testing – see 6.2, below. Regression modelling was also used to interpret data and to make predictions about foam performance.

6.1 Foam generation methods

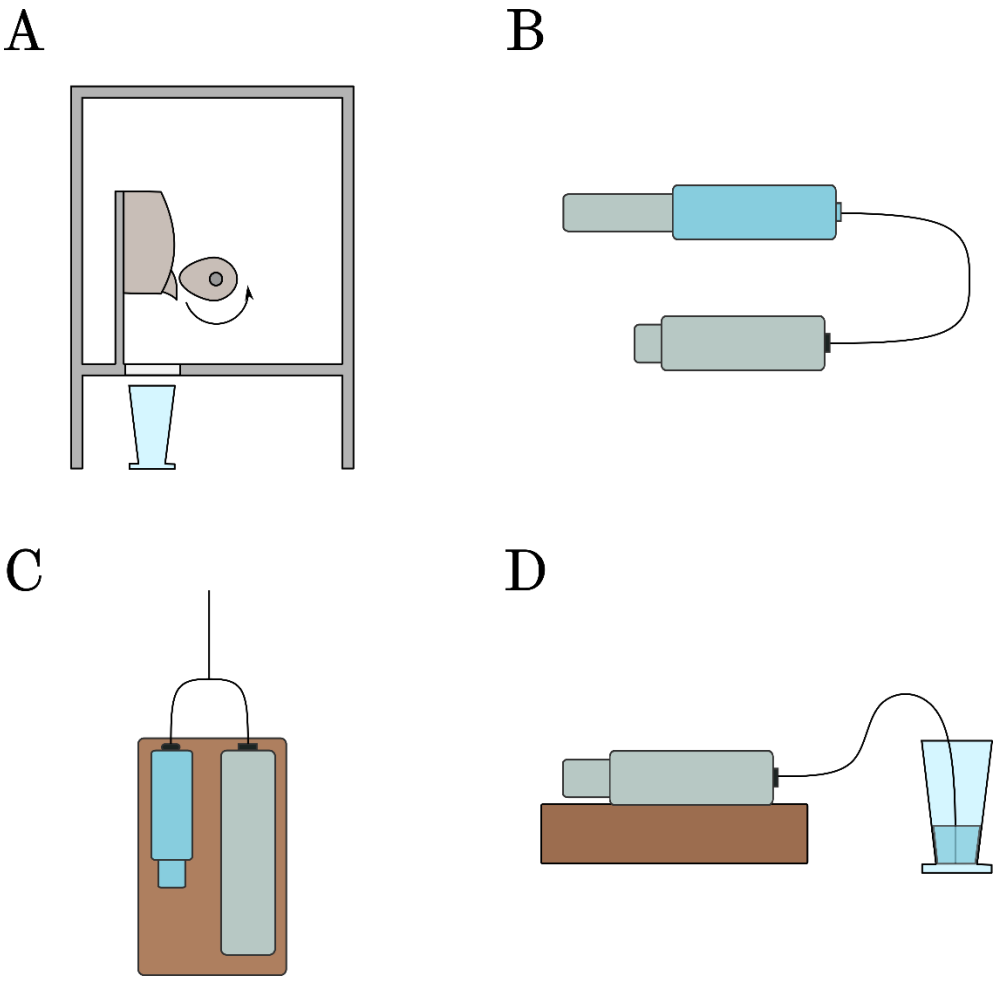

Figure 26. Illustration of four foaming methods. A - foam pump method (profile). B – double-syringe method. C - co-flow method (top). D - sparging method (profile). Blue colouration indicates syringes filled with surfactant solution, and grey-blue indicates syringes filled with air.

Pump-based approach

Foamability tests were carried out using a Deb Instant Foam™ pump, equipped with a modified solution cartridge to allow the use of custom solutions. The foam pump uses mechanical force (provided via a spring-loaded mechanism) to drive approximately 9 ml of air through 1.5 ml of liquid, pushing the two together down a short tube and through a series of gauze meshes. A custom rig was constructed to mechanically depress the lever of the pump via a rotating pear cam – see Figure 26A. The cam is attached to a shaft, which in turn was rotated by a Parvalux SD18 motor. The rate of this motor is controlled by a Mitsubishi D700-SC frequency inverter. The device is housed in a protective frame, with all moving parts limited by a safety toggle.

The speed of cam rotation was controlled by pulse width modulation using a custom controller. Generated foams emerge from the mechanism's protective housing and lands in a conical graduated vessel for immediate volume measurement. The combined volume of four dispenses were measured as one single foamability measurement.

The frequency of pulse width modulation was calibrated to obtain a time for total lever depression via observational measurements and simple geometric considerations.

Double-syringe approach

Foams for foam stability tests were generated using the double-syringe method. A 20 ml syringe was filled with surfactant solution and air at various volume ratios – see 6.2. It was then connected to a second 20 ml syringe via a short length of tubing of 5 mm internal diameter, see Figure 26B.

Foams were generated by alternately pumping the syringes, such that the foaming solution was forced from one to the other, for 30 complete cycles. The resulting foam was then injected into a measuring tube and a camera used to monitor the foam height over the course of 30 minutes. The measuring tubes were backlit to maximise contrast between the foam and liquid portions of the sample.

Initially, the foam heights were measured manually using the open-source software package ImageJ. An edge detection algorithm in LabView was later used to detect the top and bottom of the foams.

Co-flow approach

A prototype "co-flow" foamability device was constructed using a dual-barrel syringe pump. A large (100 ml) air syringe and smaller (10 ml) liquid syringe were attached by narrow PTFE tubing to a Kinesis T-junction fitting. On activating the syringe pump, air and liquid are simultaneously driven down the tube and mixed, prior to passing down a further section of tubing before being ejected into a measuring cylinder - see Figure 26C.

In some experiments, various meshes and gauzes were placed over the end of the tube in an attempt to enhance mixing of air and liquid, but these were ultimately ineffective due to low fluid velocities.

Sparging approach

A Harvard Apparatus PhD syringe pump was used in conjunction with two 50 ml Hamilton syringes. Neoprene tubing connected these syringes to the base of a conical measuring funnel, immersed in a small quantity (3 ml) of surfactant solution - see Figure 26D. Air (50 ml) was bubbled through the liquid at a controlled rate and the resulting volume of foam was measured. The half-life of the foam was also recorded – that is, the time taken for the foam to decay to half its maximum volume, immediately after the foam generation process.

All surfactant solutions were allowed to equilibrate for 1 hr at room temperature prior to use.

Vortexing approach

A 30 ml sample tube containing 4 ml surfactant solution was sealed and vortexed on a Cole-Palmer Vortex Mixer at 3400 rpm for 20 seconds. The resulting height was measured, and the foam allowed to decay before the process was repeated. Three measurements were carried out per solution, and the results were averaged.

6.2 Design of Experiments (DoE)

DOE is a field of applied statistics that seeks to maximise the efficiency of experiments seeking to uncover relationships between an observed variable and measurable parameters ('factors').[88]

A key difference between DOE and a typical single-factor experiment is the ability to test many variables efficiently. Rather than testing two factors, A and B, separately, it is possible to vary them simultaneously and model their effects, reducing the number of experiments that need to be carried out. Importantly, DOE methods allow for the measurement of interaction effects. These effects occur when the value of a variable affects the strength and/or direction of a second variable's relationship with the independent variable. Detecting and estimating the strength of such effects in single-factor experiments is cumbersome.

DOE offers several advantages relevant to the foam-based portions of this project. First, it maximises the efficiency with which limited surfactant samples could be used. Second, there are at least four variables of interest – the nature of the surfactant and its concentration, the water/ethanol composition of the solvent mixture and the rate of foam generation. This set of variables would be laborious to explore via a matrix of single-factor experiments. Finally, early scoping experiments suggested complex interactions between variables and foamability. It was important to be able to quantify these effects.

Double syringe design

An initial DOE experiment was carried out to investigate factors influencing the stability of foams formed from Di2510. Several control factors were also included in these experiments. The outcome variable for this test was $t_{1/2}$, the time taken for the foam to decay to half its initial volume, in seconds.

Table 3. Summary of the various factors and levels for the double-syringe foam stability experiment.

FACTOR	LEVELS
Container test size	Small vial, large vial
Sample size (ml)	2, 7
Surfactant concentration, % w/w	1%, 4%, 8%
Ethanol volume fraction (x_{eth})	60%, 75%, 90%

Foam pump design

A DOE experiment was designed to measure the factors influencing foamability as measured by the foam pump method.

For Di2510, Di4515 and Di2012, a more costly 'full factorial' approach was adopted - all combinations of several surfactant concentrations, push times and ethanol fractions were tested. For the final three surfactants, Di1010, Di1018 and Di1508, a more pared-back factorial approach was employed, allowing for efficient estimation of the sizes of various effects.

This was supplemented by a further 8 experiments positioned using a maximum projection approach, as implemented in JMP. For details of the maximum projection approach, see Joseph *et al.*[89] These experiments were intentionally placed in the largest areas of the experimental space that previously contained no data to ensure modelling was robust. The maximum projection approach begins by randomly positioning possible experiments in the experimental space. It then evaluates possible runs, seeking to maximise the product of the distances between proposed experiments, before selecting and proposing a set of experiments.

Factors and response limits were as described in Table 4:

Table 4. Summary of the factors and levels for the foam pump foamability experiment.

FACTOR	**LEVELS**
Surfactant identity	Di1010, Di1018, Di1508, Di2012, Di2510, Di4515
Surfactant concentration, % w/w	Varied (see text below) between 1-10%
Ethanol volume fraction (x_{eth})	50%, 70%, 90%
Push times (s)	0.3, 0.45, 0.6, 0.75

The concentrations of surfactants used in these experiments were initially measured in molar concentrations but limited surfactant supplies made such comparisons impractical. Thus Di4515, a particularly high molecular mass surfactant, was only tested at lower molar concentrations, while maintaining a similar mass fraction in the mixture to smaller surfactants.

Later, this design was extended to include Di3012, Di3514, Di4016 and Di4518. Factors and levels are presented below in Table 5.

Table 5. Summary of the factors and levels for the augmented foam pump experiment with additional surfactants.

FACTOR	LEVELS
Surfactant identity	Di3012, Di3514, Di4016 and Di4518
Surfactant concentration, % w/w	1%, 5%
Ethanol volume fraction (x_{eth})	50%, 70%, 90%
Push times (s)	0.5 (fixed)

In this experiment, the push time was fixed, as previous experiments had shown it to have only limited effect on foaming behaviour.

Di4008 (see 4.3) was also tested in several commercially relevant formulations. Its poor performance significantly changed the model predictions, and thus these data were included in the final dataset.

Syringe bubbling & vortexing design

In designing experiments for the syringe bubbling and vortexing approach, a short run of experiments employing only Di2510 were used initially. The resulting 2^3 factorial design had 16 experiments. The factors are listed below Table 6.

Table 6. Summary of the factors and levels for the syringe bubbling and vortexing designs.

FACTOR	LEVELS
Surfactant concentration, % w/w	0.1% – 5%
Ethanol volume fraction (x_{eth})	50%, 90%
Push speed, ml / s	25 - 100

I later expanded this experiment to cover all six Supplier A surfactants. The vortexing approach was carried out at a single mixing rate, and the setting of the push speed factor was therefore ignored for these tests.

6.3 Application of statistical methods

6.3.1 Regression

A multiple linear regression equation has the general form:

$$y = \beta_0 + \beta_1 x_1 + \beta_2 x_2 \ldots + \beta_n x_n + \epsilon$$

Here, y represents the dependent variable, β values represent various constant coefficients and x values represent independent variables. ϵ represents the effect of random noise which is not captured by the other terms in the equation.

Regression can also include higher-order terms – for instance, quadratic terms:

$$\ldots + \beta_{11}x_1^2 + \beta_{22}x_2^2 \ldots$$

They can also include interaction terms, which incorporate two or more dependent variables:

$$\ldots + \beta_{12}x_1x_2 \ldots$$

During regression modelling, β values for a given model are adjusted such that they maximise the fit of the model to the test data. Typically, this fit is measured by the sum of the squares of the distance between measured values of y and those predicted by the model. When this sum of squares has reached its minimum value, the model has achieved the best fit to the input data.

6.3.2 Modelling considerations

Overfitting

It was clear from previous experiments that both higher order (e.g., quadratic) and interaction terms would be required to predict the foamability and foam stability of surfactant solutions. Model fitting with a large selection of possible terms raises the potential issue of overfitting. A model is 'overfitted' when its quality of fit for the training dataset is improved at the expense of predictive power *outside* the training set, resulting in an ostensibly good model which has poor generalisability.[88]

Several metrics exist to quantify the degree of overfitting. One such approach is the adjusted R^2 - R^2_{adj}. The standard R^2 has the formula:

$$R^2 = 1 - \frac{SS_{res}}{SS_{tot}}$$

where SS_{res} is the residual sum of squares (a measure of model error) and SS_{tot} is the total sum of squares (a measure of variance within the dataset). As the model is made more complex, the residual sum of squares (model error) reduces and $R^2 \to 1$. However, it is almost always possible to reduce model error (and hence increase R^2) for a given model by adding more terms. R^2_{adj} addresses this problem by introducing a penalty term:

$$R^2_{adj} = 1 - (1 - R^2)\frac{n-1}{n-p-1}$$

where n is the sample size, and p is the number of terms in the model. Thus, as the number of model terms increases, the penalty increases. If the increase in R^2 is sufficiently small, R^2_{adj} will begin to decline, which indicates possible\ overfitting.

A second possible measure is the Akaike Information Criterion (AIC). The AIC estimates the amount of information lost by a given model from the underlying dataset, balancing goodness of fit and model simplicity.[88] The AIC is given by:

$$AIC = 2k - 2\ln(\hat{L})$$

where k is the number of model parameters, and $\hat{L}$ is the maximum value of the likelihood function for the model. The likelihood function describes the probability of generating the values in a dataset for a given set of model parameters. When $\hat{L}$ is high, there exists some set of parameter values which are likely to produce the true input dataset, and thus the model has a high goodness of fit. The AIC has been extended to better treat small sample sizes – this adjustment, the corrected AIC (AICc), is given by:

$$AICc = AIC + \frac{2k^2 + 2k}{n - k - 1}$$

where k is the number of model parameters and n is the sample size.[88]

The AICc is useful when explicitly comparing models generated in series – e.g., by elastic net regression, described below - whereas the adjusted R^2 provides a more general heuristic for overfitting, and was thus used as a check during ordinary least squares regression.

Model building

Model building refers to the process of selecting terms for, and refining, a statistical model to balance goodness of fit and simplicity – essentially, to avoid both over- and underfitting. Model building typically proceeds by a mixture of subject knowledge and model comparison. Several model building procedures are described below.

Some models – notably, the 'naïve' foam pump model described in 6.3.3 – did not require extensive model-building processes, as all their terms are highly statistically significant. In these cases, it was ensured that R^2_{adj} did not significantly diverge from R^2 to avoid overfitting. In other cases, more selection of model terms was required.

Initially stepwise regression, a model-building technique often used in conjunction with DOE, was applied. In stepwise regression, terms are sequentially added or removed from the model based on a *p*-value criterion – in forwards stepwise regression, for instance, the term with the lowest *p*-value below a threshold is added, followed by the next, and so on until no terms have a sufficiently low *p*-value to continue. Stepwise regression methods have been criticised by statisticians, as they violate several core statistical assumptions in linear regression by applying repeated significance tests to the same dataset. As a result, they produce biased *p*-values and can overemphasise goodness of fit.[90]

A more statistically robust approach is to use a penalised regression technique, such as elastic net regularisation, as described below.[91] Where elastic net regularisation was applied, the AICc (see above) was used as a stopping criterion to avoid overfitting.

All models were generated using JMP Pro 14, published by the SAS Institute.

Elastic net regularisation

Elastic net regularisation is a form of regularised or 'penalised' regression - a set of analytical methods developed to counteract overfitting, especially when using models with many potential inputs.

Elastic net regression combines two different regularisation approaches, blending them to maximise the model's predictive power. Each regularisation approach applies a penalty to the model fit – this desensitises the model fit to training data, but significantly improves its predictive power outside the training dataset. When both penalty strengths (denoted λ_1 and λ_2) are set to zero, elastic net regression is identical to ordinary least squares regression. As either λ value increases, the model is made less sensitive to changes in the model parameters.

The two penalties applied in elastic regression are taken from ridge and lasso regression – two simpler forms of regularisation. In ridge regression, the penalty has the form $\lambda_1\beta^2$, where β represents the coefficients present in the model. The lasso regression penalty, by contrast, has the form $\lambda_2|\beta|$. In practice, this difference means that increasing λ_2 can remove parameters from the model by reducing their coefficients to zero, whereas increasing λ_1 squeezes parameters down, such that they approach (but never reach) zero.[91]

Elastic net regression combines the lasso and ridge regression penalties, shrinking terms and/or removing them depending on which gives better predictive power. The strengths of

the penalties - λ_1 and λ_2 - are optimised to maximise a validation statistic – in my case, the AICc.

Generalised regression

Ordinary least squares regression assumes that data are drawn from a normally distributed population. This assumption holds well for the foamability data, but does not apply to foam stability, as measured by the half-life. This stability dataset is highly skewed towards low values and can be better modelled using a non-standard distribution.

Generalised regression is an extension of standard linear regression that adapts the method to a range of non-normal distributions. Half-life data fit a gamma distribution well and was used in combination with generalised regression to model foam stabilities.

Generalised regression can be used in combination with elastic net regularisation (described above) – this approach was used for both stability models.

6.3.3 Modelling methods

Table 7 summarises the modelling approaches and terms applied to each foaming method. The complete, fitted models are included in Appendices 11.2-11.7. In all models, interactions between continuous terms were mean-centred to aid interpretation.

Table 7. Summary of modelling approaches applied to different foam generation methods.

Model	Model type	Initial variables	Surfactants used
Double syringe half-life model	Generalised regression, elastic net	Sample size, container size, x_{eth}, surfactant mass concentration	Di2510 only
Foam pump naïve model	Standard least squares	Surfactant [categorical variable], x_{eth}, push time, surfactant mass concentration. All quadratic terms and first-order interactions between surfactant, x_{eth} and surfactant mass concentration	All surfactants except Di4008
Foam pump informed model	Elastic net	nPDMS, nEO, x_{eth}, push time, surfactant mass concentration. All quadratic terms and first-order interactions.	All EO-only surfactants (i.e., not Di1018 and Di4515)
Sparging foam volume model	Elastic net	Surfactant [categorical variable], x_{eth}, push speed, surfactant mass concentration. All quadratic terms and first-order interactions.	Di1010, Di1018, Di1508, Di2012, Di2510, Di4515
Sparging foam half-life model	Generalised regression, elastic net	Surfactant [categorical variable], x_{eth}, push speed, surfactant mass concentration. All quadratic terms and first-order interactions.	Di1010, Di1018, Di1508, Di2012, Di2510, Di4515
Vortexing foam volume model	Standard least squares	Surfactant [categorical variable], x_{eth}, surfactant mass concentration. All quadratic terms and first-order interactions.	Di1010, Di1018, Di1508, Di2012, Di2510, Di4515

Double syringe modelling

Half-lives of foams were modelled with elastic net regularisation regression and an AICc stopping criterion, as described above. The initial factors were sample volume, sample container, liquid fraction, x_{eth} and surfactant mass fraction. The stability data did not conform to a normal distribution and was modelled using a gamma distribution (see 'Generalised Regression').

Foam pump modelling

I developed two models for the foam pump.

The initial 'naïve' model did not contain any information about the nature of the surfactants used. Instead, it contained the surfactants as categorical variables only. Its input variables were the surfactant type, surfactant mass fraction, ethanol volume fraction and the pump push time. In addition, quadratic terms were tested for all continuous factors, and first-order interaction terms between surfactant type, surfactant mass fraction and ethanol volume fraction. The outcome variable was the foam volume, in ml, as measured by the foam pump test described in section 6.1. It was fitted using the standard least squares subtype in JMP.

This model excluded Di4008 as it was not tested across the full range of x_{eth} values and copolymer concentrations, and thus introduced singularities into the model.

A second 'informed' model replaced the categorical surfactant variable with two variables describing the nominal nPDMS and nEO for the surfactants. Where possible, quadratic terms for each of these variables were included, as well as interaction terms linking them with continuous terms in the model. Mixed EO/PO surfactants were excluded from this model, as they introduced significant multicollinearities (see 6.4 Foam pump modelling for further details).

This model was fitted using the 'generalised regression' subtype in JMP using elastic net regularization and an AICc stopping criterion.

Syringe pump & vortex modelling

Sparging foam volume and stability data were modelled using elastic net regularization and an AICc stopping criterion, as described above. The initial factors were surfactant (as a categorical variable), surfactant mass concentration, x_{eth} and the rate of syringe depression, with all interaction terms and quadratic terms for all numeric variables.

The stability data did not conform to a normal distribution and were therefore modelled using a gamma distribution (see 'Generalised regression' in 6.3.2).

Vortex foam volume data were modelled using a standard least squares approach. The initial factors were surfactant (as a categorical variable), surfactant mass concentration, and x_{eth} with all interaction terms and quadratic terms for all numeric variables.

Simple quadratic models

In some cases, when reliable predictions were required, and a unified model was not deemed necessary, simple quadratic models were used to fit the relationship between surfactant concentration and foam volume for a given surfactant/solvent combination (see Figure 27). These models were used to interpolate foam volume estimates with a high degree of fidelity for comparisons with purified surfactants (see 4.2.2, above) and for the relation of dynamic surface pressure to foamability (see 8.3.3, below). In each case, models were only used for the concentration range within which they had been originally fitted.

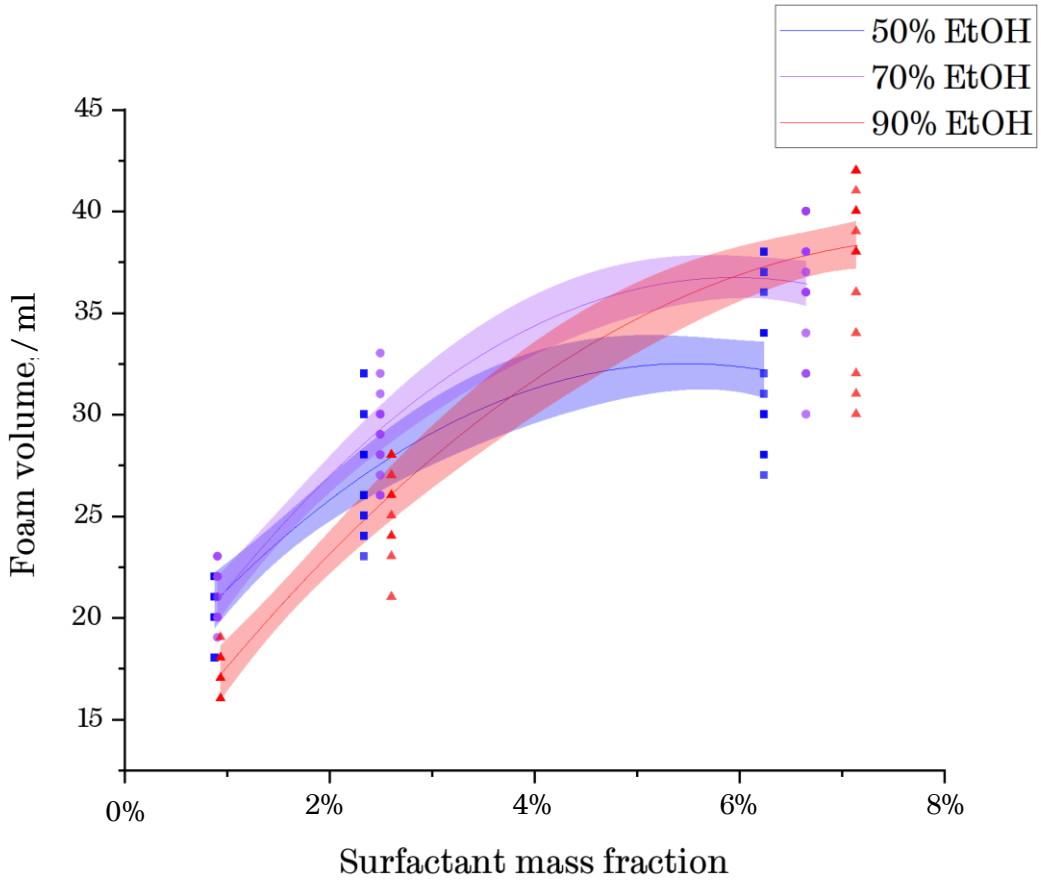

Figure 27. Foam volume versus surfactant concentration for Di2510 in three solvent mixtures - 50%, 70% and 90% ethanol. Simple quadratic equations provide robust interpolation for foam volume predictions. Shaded area represents 95% confidence interval for the quadratic fit.

Optimisation

Simulation and optimisation were carried out in JMP 14. JMP uses a constrained Newton's method optimiser, with step shortening.[92]

In general, the process of optimisation takes a function – in this case, the foam volume models described above – and finds the values of the function inputs which give the minimum or maximum output by some iterative process.

Newton's method optimisation proceeds by fitting a parabola to the function to be optimised at the trial value and finding the minimum or maximum of the parabola, as appropriate. That minimum or maximum is then set as the trial value for the next iteration of the procedure. This process continues until the value to be optimised converges and each successive step results in only trivial changes to the output value.

Unless otherwise specified, all simulations and optimisations were carried out at a constant surfactant content constant of 3% (w/w). Push time was held at 0.5 s for the foam pump method, and push speed at 85 ml / min for the sparging method.

6.4 Foamability results and discussion

Implementing foaming methods

High foamability is an important property in solutions intended for foaming ABHRs. As discussed in 1.7, high foamability has several beneficial effects on foam quality – a higher relative foamability implies a drier foam, which is easier and more pleasant to use, while reducing wastage and ensuring that a full measure of disinfectant is applied to a user's hands. These properties should increase compliance and therefore improve hand hygiene.

I tested several foaming methods throughout the project, described above in section 6.1 and illustrated in Figure 26. These methods ranged from relatively well-characterised and common approaches (e.g., sparging, or the double syringe method) to those with little use in the academic literature (e.g., foam pump and vortexing methods). These foaming methods were assessed according to their ease of use, sensitivity, repeatability, samples size requirements and verisimilitude to the context of ABHRs.

The double-syringe and co-flow methods were explored with the aim of maximising accuracy and repeatability, while using small samples. The double-syringe method, in particular, is noted for its ability to produce relatively narrow bubble size distributions, which in principle should have produce reproducible foam stability data.[93]

Sparging and vortexing were explored as foaming methods that could generate new interfaces on different timescales to the foam pump. Both proved straightforward to use and required only small amounts of surfactant.

In the **foam pump method**, air and gas are driven together by the depression of a spring-loaded lever. The two are forced down a short tube, through a series of narrow meshes, before being ejected. A motor-driven cam was used to ensure that the lever of the foam pump was depressed in a repeatable fashion – see Figure 28. The use of a commercial foam pump in my implementation of this method ensured that it was as close to 'realistic' ABHR use as possible. Using this equipment had several associated disadvantages – repeatability was somewhat lower than other foaming methods, and large surfactant solution volumes were required. To counteract issues with repeatability and to enable more accurate visual measurement of foam volumes, the combined volume of four foam dispenser cycles were measured per test.

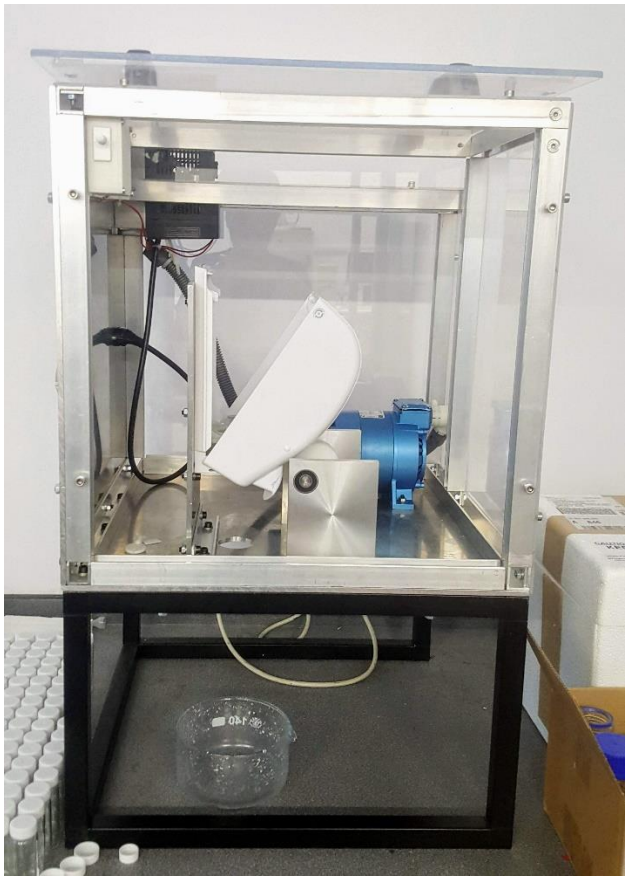

Figure 28. A photograph of the custom-designed foam pump testing rig.

In the **double-syringe method**, two syringes – each containing air and surfactant solution - are connected by a length of tube. The plungers on each syringe are alternately depressed to drive the solution through the tube and back again. The narrow neck of tubing produces high shear forces which drive air into the solution and break up bubbles passing through, thus generating foam.[93] A number of issues with the double syringe method were identified. For the setup described in 6.1, the method could not generate foams with liquid fractions below

50%, which is well above the liquid fraction of interest in the context of ABHRs. Further, the double syringe method imposes a maximum foam volume, which is set by the syringe volume and the ratio of liquid to air selected during setup. It was, therefore, not capable of generating foams across a range of foamabilities. Nevertheless, the results of early work on foam stability using the double syringe method are described below.

In the **co-flow method**, two syringes – one containing air and the other surfactant solution - are connected by tubing at a T-junction, before being simultaneously depressed by a syringe driver. The two phases are driven together, mixing in the junction before flowing down an exit tube. The co-flow method can generate foams, is quite straightforward to use and bears at least some resemblance to a simplified commercial foam pump. Its key weakness is a lack of sensitivity – it could not effectively discriminate between solutions which, measured by the pump test, generated significantly different foam volumes. This is most likely the result of an insufficiently aggressive foaming process, providing too much time for interfaces to form and stabilise. This remained the case even when experimental conditions were adjusted to maximise foam generation speed.

In the **sparging method**, a syringe driver was used to bubble a fixed volume of gas through a conical measuring cylinder containing surfactant solution via a short neoprene tube. The sparging method frequently produced highly voluminous foams, but could still discriminate between some surfactant solutions. The use of a syringe driver enabled very precise control over the rate of gas injection into the system.

In the **vortexing method**, a benchtop vortexer was used to mix a sealed tube containing air and surfactant solution. This method bore some resemblance to the double-syringe method, in that it involved a significant period of bubble shear and breakup before measurement.

I conducted most of my research using the foam pump, but also carried out relatively small-scale factorial experiments using the double-syringe, sparging and vortexing methods.

A factorial experiment measuring foam stability was carried out for both the double-syringe method and the sparging method. These experiments confirmed the chaotic and path-dependent nature of foam structure. Large bubbles, for example, tend to coarsen foam quickly (see 1.5.2) – hence the presence of a single large bubble could quickly destabilise the foam. Further, rupture events in foams tend to occur in clusters – with the collapse of one film triggering a cascade of films rupturing elsewhere – but the timing of these cascades is

essentially random.[1] Hence, summary measures (such as the time required for a foam to reach half its initial volume, $t^{1/2}$) were used to compare foam stabilities.

Foaming methods and foamability

Figure 29 shows the degree of correlation between foam volumes achieved by sparging, the foam pump and vortexing. While the results obtained by the vortexing method were strongly correlated to those produced by the foam pump, the sparging method produced a different distribution of results. Below a low threshold (~12 ml in the foam pump test), samples performed very poorly in the sparging test. Above that, all samples achieved near the maximum volume possible for the sparging test.

The divergence of these results highlights to the importance of the choice of foaming method, particularly in determining whether foaming is dependent on the equilibrium or dynamic properties of surfactants. These findings will be related to dynamic surface section 8.3.3.

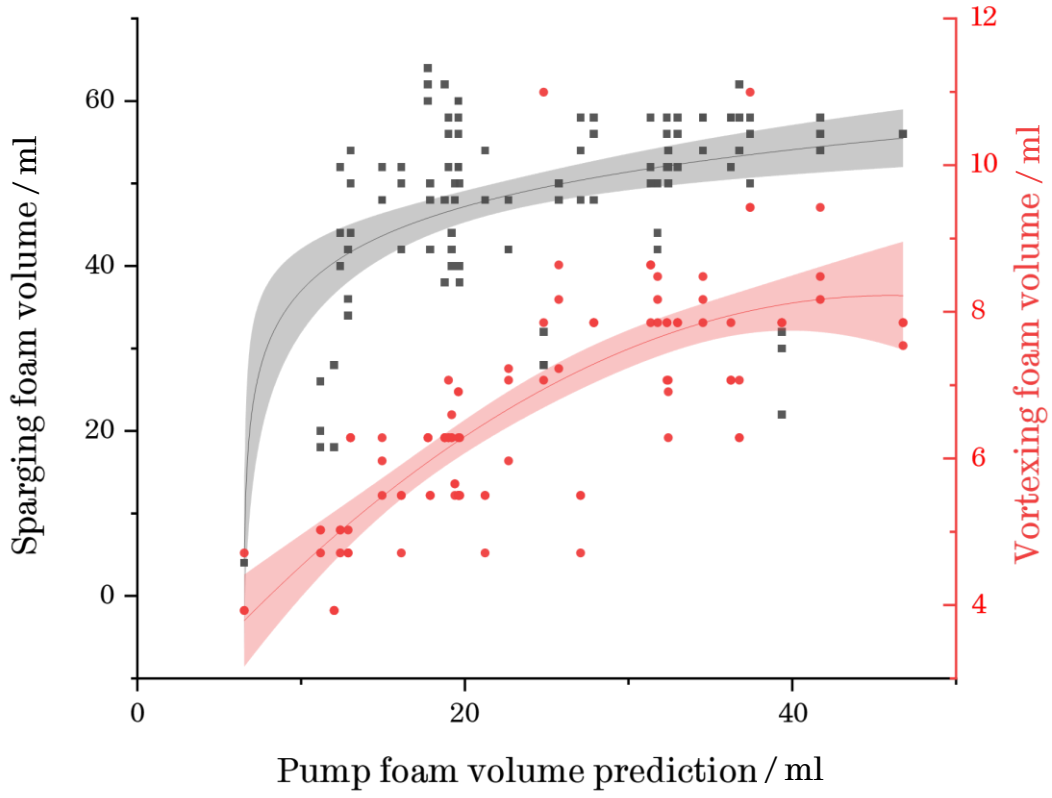

Figure 29. Relationship between sparging and vortexing foam volumes and predicted foam pump volume, generated using the 'naïve' foam pump model. The vortexing data is fit to a quadratic function, and the sparging data to a logarithmic function. 95% confidence intervals are shaded.

Foaming by the sparging method was, under some test conditions, sufficiently slow that stability-foamability coupling was clearly visible. That is, the foam began to collapse before generation was complete, meaning that the final foam volume was a product of both foamability and stability.

Foamability modelling

In general, the modelling of foam volumes by the foam pump, sparging and vortexing methods were quite successful, and achieved reasonably good fit – see Figure 30 shows a graphical comparison between these three models ($R^2(sparging) = 0.84$, $R^2(vortexing) = 0.85$, $R^2(pump, naive) = 0.92$). In addition, R^2_{adj} was close to the standard R^2 and therefore showed no sign of overfitting.

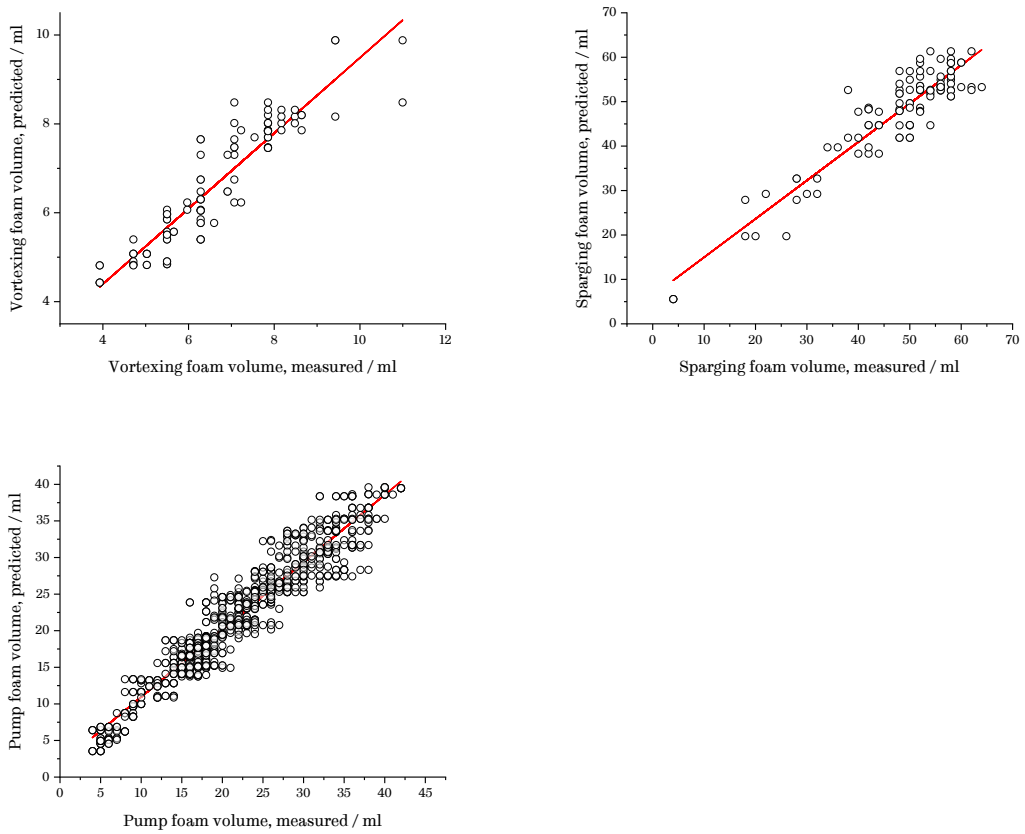

Figure 30. Comparison of the measured and predicted foam volume for the vortexing (top left), sparging (top right) and naive foam pump (bottom) volume models. ($R^2(sparging) = 0.84$, $R^2(vortexing) = 0.85$, $R^2(pump, naive) = 0.92$).

The naïve pump model and vortexing model were fitted using a standard least squares regression, as all terms tested in the initial models were significant. The sparging and

informed pump models both had a number of non-significant terms and were therefore fitted using an elastic net approach (described above).

Qualitatively, the models produced by these fitting procedures had many similarities, and formulations which performed well or poorly in one tended to perform similarly in the others – see Figure 29. For all three models, higher surfactant concentrations lead to larger foam volumes, whereas higher x_{eth} was associated with smaller foam volumes. There was also a persistent interaction between x_{eth} and surfactant, with the performance of smaller surfactants generally suffering much more from high x_{eth} values than larger ones. In the vortexing method, Di1508 was found to have a large, positive interaction with x_{eth}, in contrast to data obtained from the other two methods. However, given the sparse nature of the experimental design adopted for the vortexing method, this may simply be an outlier.

The rate of foam generation was varied for both the foam pump and sparging methods. In the case of the foam pump, push time had only a small impact on the foam volume and did not have any strong interactions with other parameters in the model. By contrast, the speed of foam generation interacted very strongly with x_{eth} in the sparging model – such that high push speeds were predicted to result in lower foam volumes when x_{eth} was high. Based on experimental observations, this may be due to poorer stability of foam films in high-ethanol foams, which were more prone to rupture during high-speed foam generation.

Both the vortex and foam pump models showed a positive interaction between surfactant mass concentration and x_{eth}, with higher x_{eth} values increasing the effect of surfactant mass concentration on foam volume. This may be the result of micelles being 'unlocked' due to changes in solvent quality, allowing micelles to dissociate more quickly – an effect which should be stronger when more micelles are present in solution. This hypothesis also explains why such an interaction was not evident in the sparging test, which generates foams on a much slower timescale and is thus unlikely to be sensitive to changes in micellar kinetics.

Foam stability modelling

I modelled foam stability for foams generated by the double-syringe method and by sparging. The sparging model produced a significantly better fit ($R^2 = 0.88$) than the double-syringe model ($R^2 = 0.75$). In both cases, foam half-life data did not conform to a normal distribution, instead showing a significant negative skew and long positive tail. This is a common feature of lifetime data, which is often modelled using an exponential or gamma distribution.[88]

In both models, higher ethanol contents and lower surfactant concentrations reduced $t_{1/2}$. In the sparging model the effect of ethanol was much stronger for smaller surfactants such as Di1010 and Di1508, which exhibited very low $t_{1/2}$ at higher x_{eth} values.

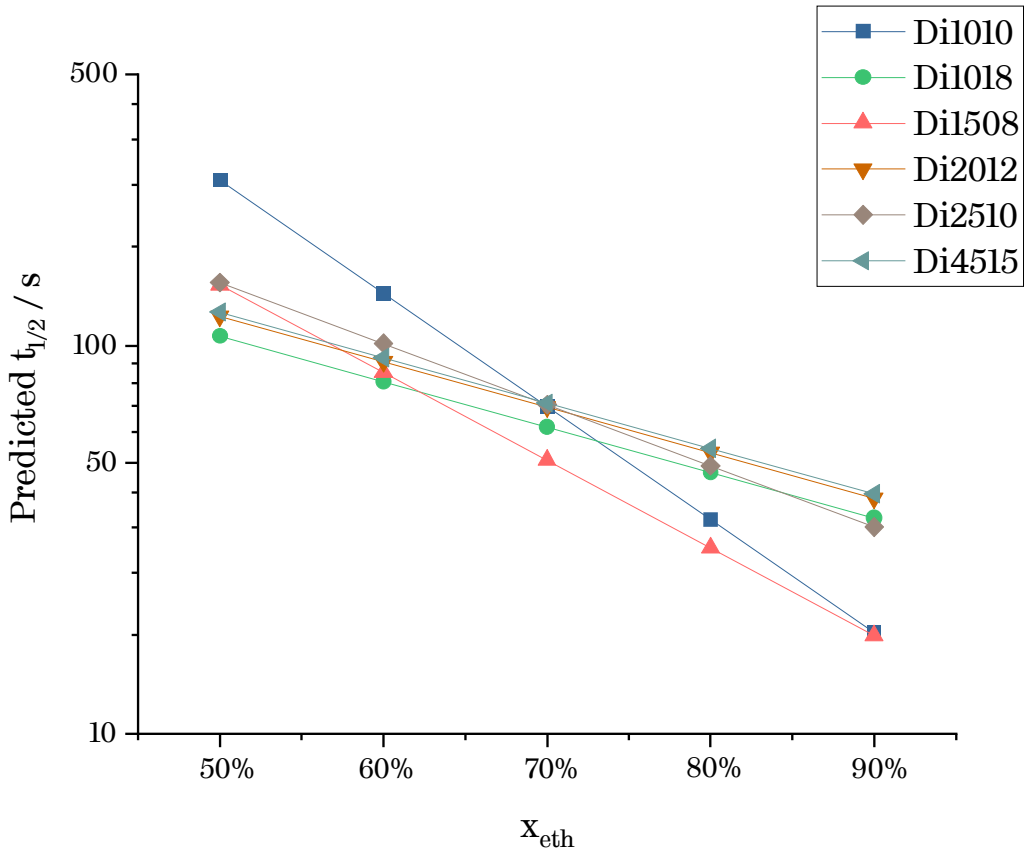

Figure 31. Predicted foam half-life, $t_{1/2}$, generated by sparging for a range of ethanol contents in water-ethanol mixtures. Predicted foam half-life decreases rapidly as x_{eth} increases. Changes are particularly pronounced for Di1010 and Di1508. Values were simulated using the sparging stability model.

Foam pump modelling

Two models were fitted for the foam pump - the 'naïve' model included the surfactant as a categorical variable and the 'informed' model decomposed the surfactant into two further variables: nPDMS and nEO. When fitting this second model, multi-collinearity problems arose between nPDMS and nPO. Di4515 and Di1018, the PO-based surfactants, are also structurally extreme compared to the other surfactants in the dataset. Di4515, for instance, has both the highest nPDMS and the largest number of polyether units. It was therefore impossible for a statistical model to separate the effect of this extreme structure from the

effect of nPO. Thus, both PO-containing surfactants were removed when fitting the 'informed' model.

Both models produced directionally similar results and achieved similar goodness of fit (naïve $R^2 = 0.92$, AICc = 4263. Informed $R^2 = 0.88$, AICc = 3984). This similarity attests to the robustness of the models and the surfactant samples, as blinding the model to the chemical structures of the surfactants should not have provided significant additional information.*

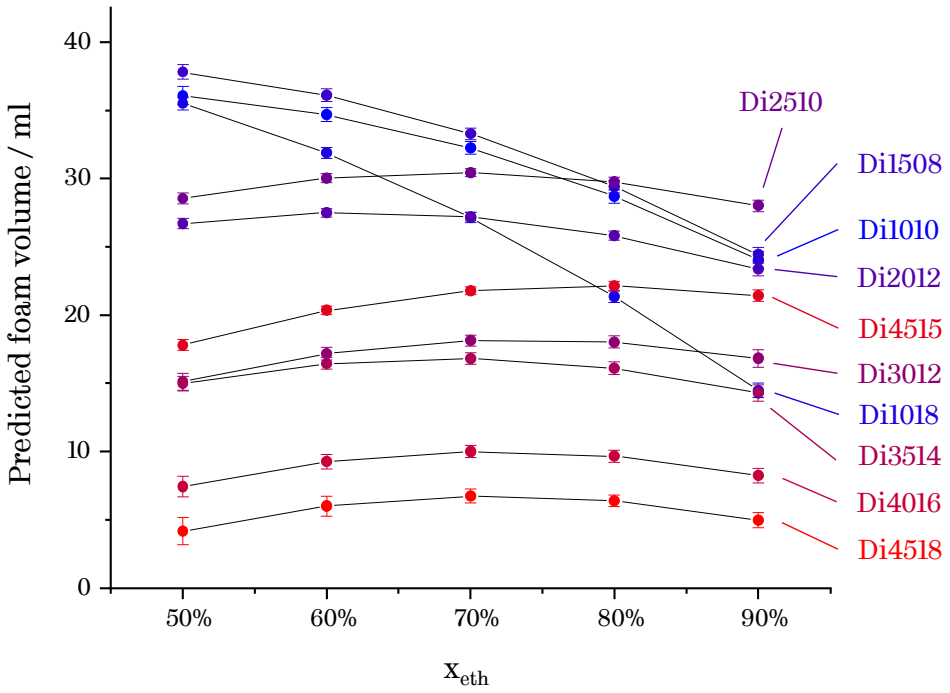

Figure 32. Predicted foam volumes for all surfactants, versus ethanol content of water-ethanol mixtures. Smaller surfactants have a negative interaction with ethanol contet, whereas larger surfactants have a positive interaction. Data was generated using the 'naïve' foam pump model. Symbol colour is scaled to nPDMS, with blue indicating low nPDMS and red indicating high.

As described above, a key result when using these models was the discovery of a strong interaction between x_{eth} and the surfactant. Some surfactants, particularly those with low

* If one particular surfactant had contained significantly higher amounts of impurities, for example, then the naïve model should have been able to identify this sample and thus produce a significantly better fit than the informed model.

nPDMS values, experienced much more significant declines in performance as x_{eth} was increased. By contrast, the performance of larger surfactants' was predicted to improve as x_{eth} was increased (see Figure 32).

A clear relationship exists between the ethanol content at which a surfactant generates the most foam, $opt(x_{\mathrm{eth}})$, and nPDMS - see Figure 33. As nPDMS increases, the surfactant's ideal ethanol fraction also tends to increase, towards a maximum value around 75% ethanol.

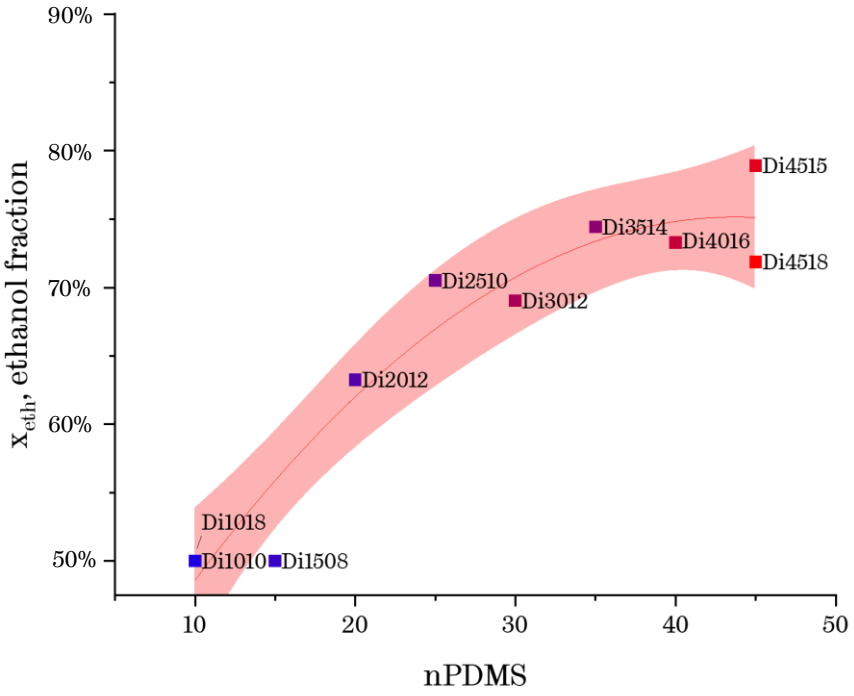

Figure 33. A plot of the surfactants' optimum water-ethanol solution mixture (x_{eth}) versus nPDMS. A clear correlation is visible. Data was generated from optimisation of the 'naïve' foam pump model. Symbol colour is scaled to nPDMS, with blue indicating low values and red indicating high. The data is fitted to a quadratic function, with 95% confidence intervals shaded.

This relationship is particularly striking given that the naïve model did not have access to nPDMS during the fitting procedure – the correlation instead emerges naturally from the underlying results. To test its effect, nPolyether was incorporated into a regression model alongside nPDMS and $(\mathrm{nPDMS})^2$. In this model, nPolyether had a p-value of 0.115 – not yet statistically significant but possibly warranting further investigation.

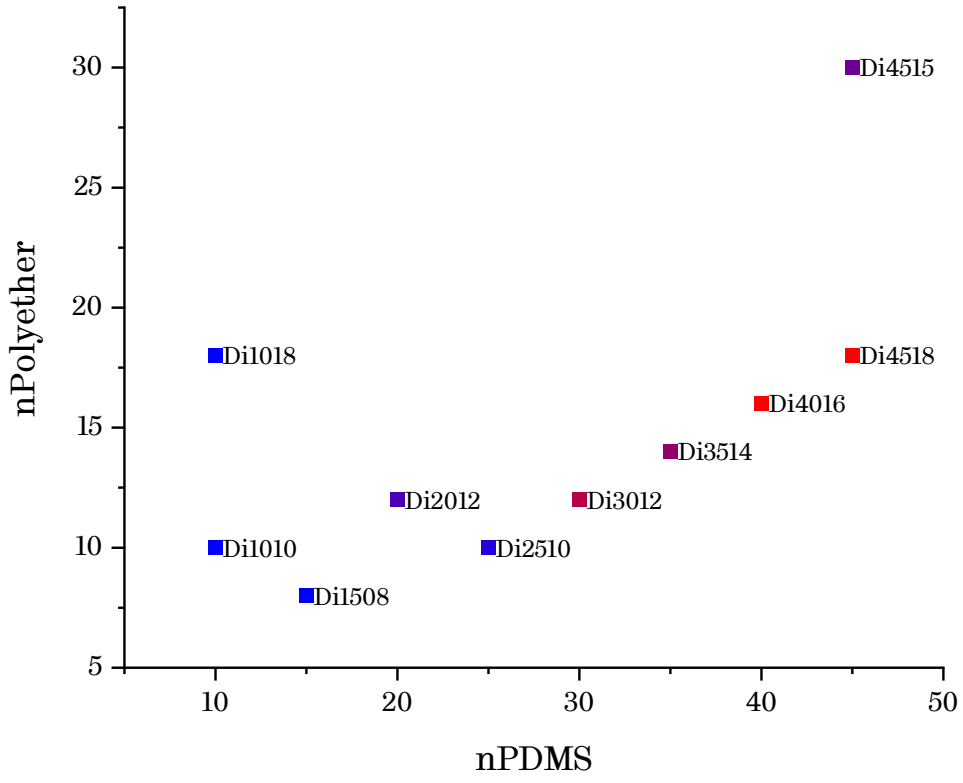

Figure 34. nPolyether versus nPDMS plot, where the symbol colour is scaled to predicted foam volume. Blue indicates high performance and red indicates poor performance. Maximum foam volume is negatively correlated with nPolyether and nPDMS. Predicted foam volumes were generated by optimisation of the 'naïve' foam pump model.

A second clear correlation in the naïve model is between surfactant size and optimum performance. As nPDMS and nEO increase, the performance of the surfactant in its optimum solvent mixture declines (see Figure 34). Di4515 and Di1018 are included here for context but are not directly comparable to the EO-only surfactants.

The 'informed' model identifies similar trends. nPDMS and nEO have an overall negative effect on foam volume, but nPDMS interacts strongly with x_{eth}. High x_{eth} values make the effect of nPDMS on foam volume less negative. This significantly changes the relationship between surfactant structure and foam volume as x_{eth} is increased from 50% to 90% – see Figure 35 and Figure 36.

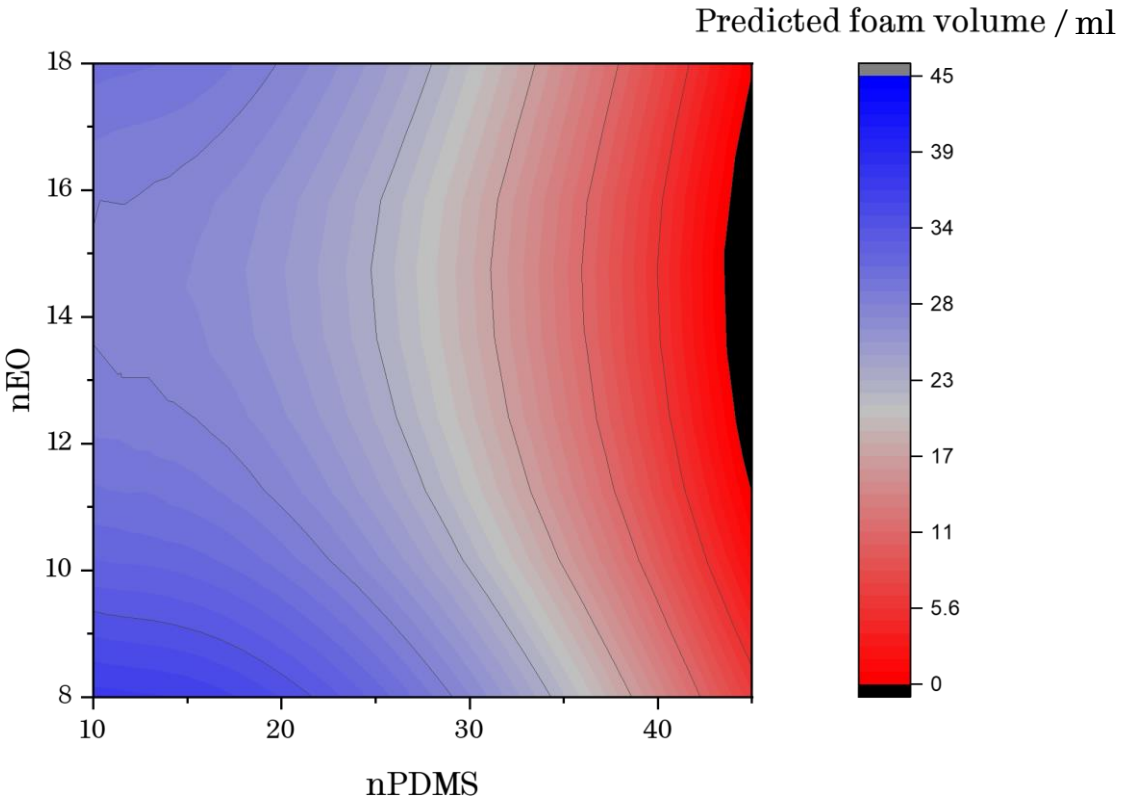

Figure 35. Contour plot showing predicted performance for a range of siloxane polyethers in 50% ethanol. When $x_{eth} = 50\%$, Di1008 has the maximum predicted performance. Predicted foam volumes were generated using the 'informed' model. Colour is correlated with foam volume, where blue indicates high predicted volume and red indicates low predicted volume.

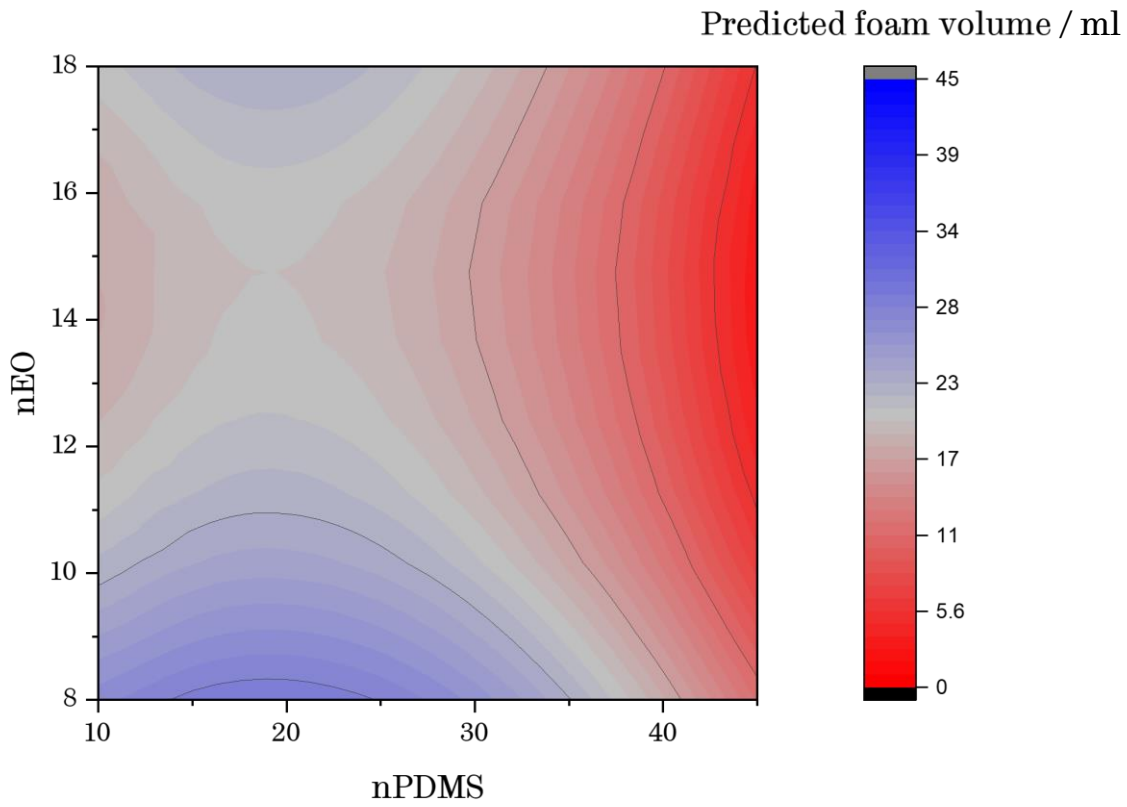

Figure 36 Contour plot showing predicted performance for a range of siloxane polyethers in 90% ethanol. When x_{eth} = 90%, Di1908 has the maximum performance. Predicted foam volumes were generated using the 'informed' model. Colour is correlated with foam volume, where blue indicates high predicted volume and red indicates low predicted volume.

When $x_{eth} = 50\%$, the optimum surfactant is predicted to be Di1008, with smaller, EO-poor surfactants performing well. When $x_{eth} = 90\%$, the optimum surfactant is predicted to be Di1908, with a wider range of EO-poor, PDMS-rich surfactants predicted to perform best. There are substantial differences between the expected performance of these optimum surfactants – Di1008 is predicted to generate 35.8-38.1 ml (95% CI) foam in 50% ethanol, whereas Di1908 is predicted to produce 27.7-30.1 ml foam in 90% ethanol.

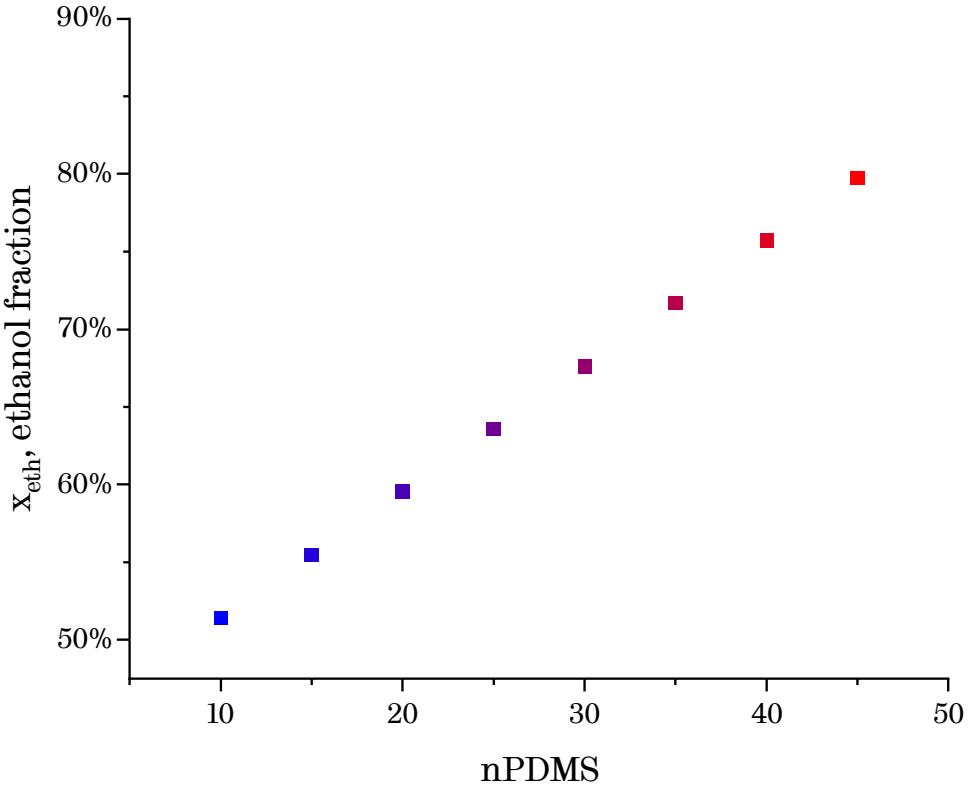

Figure 37. Surfactants' optimum water-ethanol solution mixture (x_{eth}) versus nPDMS. The optimum water-ethanol solution mixture for foam pump performance is strongly correlated with nPDMS. Data was generated from optimisation of the 'informed' foam pump model. Symbol colour is scaled to nPDMS, with blue indicating low nPDMS and red indicating high.

Figure 37 represents an analogous output to Figure 33 using the 'informed model'. Due to the nature of the nPDMS $\times x_{\mathrm{eth}}$ interaction term, this plot was constrained to linear behaviour and is consistent with the non-linear function obtained from the output from the naïve model.

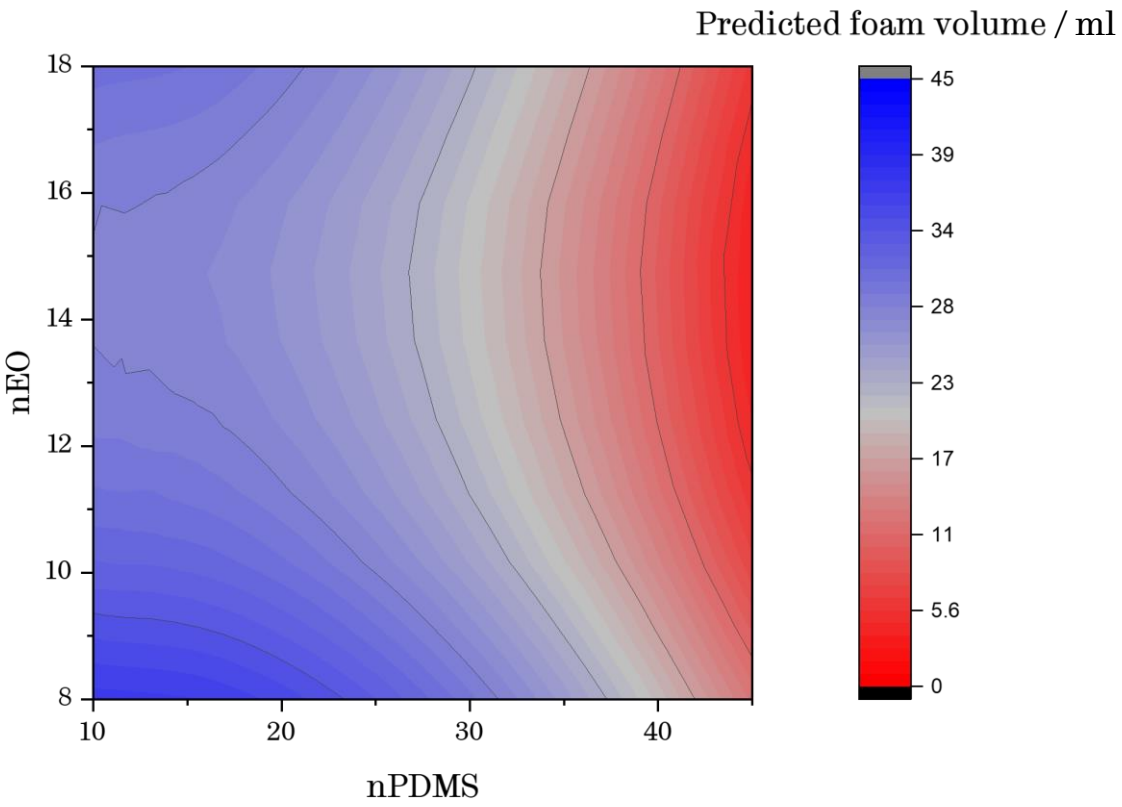

Figure 38. Contour plot showing maximum predicted foam volume for a range of siloxane polyethers. Maximum foam performance is negatively correlated with nPolyether and nPDMS. Colour is scaled to predicted foam volume, with blue indicating high and red indicating low. Predicted foam volumes were generated by optimisation of the 'informed' foam pump model.

Likewise, Figure 38 represents the 'informed' model's version of Figure 34. As in the naïve model, the 'informed' model predicts that surfactants with greater nEO and nPDMS values will generate lower foam volumes under their optimum solvent conditions.

Model interpretation

The naïve model suggests that it is not possible to tailor a siloxane polyether surfactant that combines both strong performance *and* a preference for ethanol-rich solutions. Increasing nPDMS simultaneously increases ethanol preference *and* reduces performance - increasing nEO, by contrast, only appears to reduce performance.

As discussed in 2.4, the introduction of ethanol cosolvent significantly changes the behaviour of surfactant solutions. Increasing x_{eth} has two principal effects on surfactant behaviour. The first is to make the hydrophobic segments of the surfactant more soluble. This has the raises the CMC and most likely reduces micelle stability, allowing unimer surfactant to arrive

at the interface more quickly during foaming. The second effect is to reduce the 'headroom' for surface tension, making it more difficult for surfactants to generate the surface tension gradients required to stabilise nascent foams.

Surfactants must occupy an intermediate zone of solubility to be effective: if solubility is too low, the surfactant will form stable structures in solution and reach interfaces relatively slowly, if at all. However, if it is too high, the surfactant will no longer be sufficiently surface-active. Typically, it is only possible to find the 'Goldilocks zone' of optimal solubility by changing the hydrophobicity of the surfactant, but x_{eth} provides a second degree of freedom that can be altered, adjusting the solubility of the PDMS chain. Figure 33 shows the combinations of nPDMS and x_{eth} values within this optimal zone of solubility.

In addition, the findings in Figure 3425-33 show that the overall surfactant performance declines as nEO and nPDMS grow. This is because surfactants with larger hydrophobic groups are exhibit slower micellar dissociation, and both larger hydrophilic and hydrophobic groups may lower surface activities by reducing interfacial packing efficiency.[40,95] The interaction between surfactant structure, adsorption kinetics and surface activities will be discussed further in Chapter 8.

The presence of Di1018 and Di4515 in the dataset raises this question: what effect does replacing EO chains with mixed EO/PO or pure PO have on foaming? This modification has a significant effect on the behaviour of these two surfactants. As discussed in 4.1.2 above, a surfactant with nEO $= 18$ or 30 would most likely be insoluble in water-ethanol mixtures. Di4515 *is* soluble, and therefore much more effective than Di4518, the all-EO surfactant that is most similar in molar mass. However, both Di1018 and Di4515 are outperformed by smaller, pure-EO surfactants within the dataset.

It is unclear whether a surfactant with mixed EO/PO side-chains would perform better or worse than a comparable all-EO surfactant in the case where both were soluble, as neither this work nor the literature on siloxane surfactants contains any direct comparisons between such surfactants.

Design rules and optimisation results

The design rules below aim to summarise the relationships established in this chapter between nPDMS, nEO, x_{eth} and foam volume, for the purpose of designing surfactant solutions for foam pump-based ABHRs:

nEO has a largely negative effect on foam volume and should therefore be minimised. However, the value of nEO must be such that the surfactant can still be effectively dissolved. Solubility issues tend to arise when nEO is small (≤ 8) and nPDMS is large (≥ 40) – hence Di1508 is sufficiently soluble, while Di4008 is not. In addition, when nEO ≥ 16, solubility issues caused by EO crystallisation may emerge (see 4.1.2 for further details).

nPDMS's effect on foam volume depends on solvent composition. When x_{eth} is low, smaller nPDMS values give superior foam volumes, but as x_{eth} increases, larger nPDMS values are required.

Figure 39 shows the relationship between the predicted optimum nPDMS for a range of x_{eth} values. The optimum nPDMS increases by ~2.2 units per 0.1 increase in x_{eth}, while the predicted foam volume declines. In all cases, the predicted optimum nEO $= 8$, but lower values may improve performance further. When $x_{eth} = 50\%$, the optimum nPDMS is 10, but given that this is the smallest surfactant tested, further improvements might be made by setting nPDMS < 10. When $x_{eth} = 90\%$, by contrast, the optimum nPDMS $= 19$.

The naïve model suggests Di1508 is the superior surfactant when $50\% \leq x_{eth} \leq 80\%$, while Di2510 is superior when $80\% < x_{eth} \leq 90\%$. Figure 40 compares the predicted foam volumes for the optimum surfactant, as predicted by the 'naïve' and 'informed' models. As would be expected, the informed model generally outperforms the naïve model, which is constrained to surfactants within the dataset original dataset.

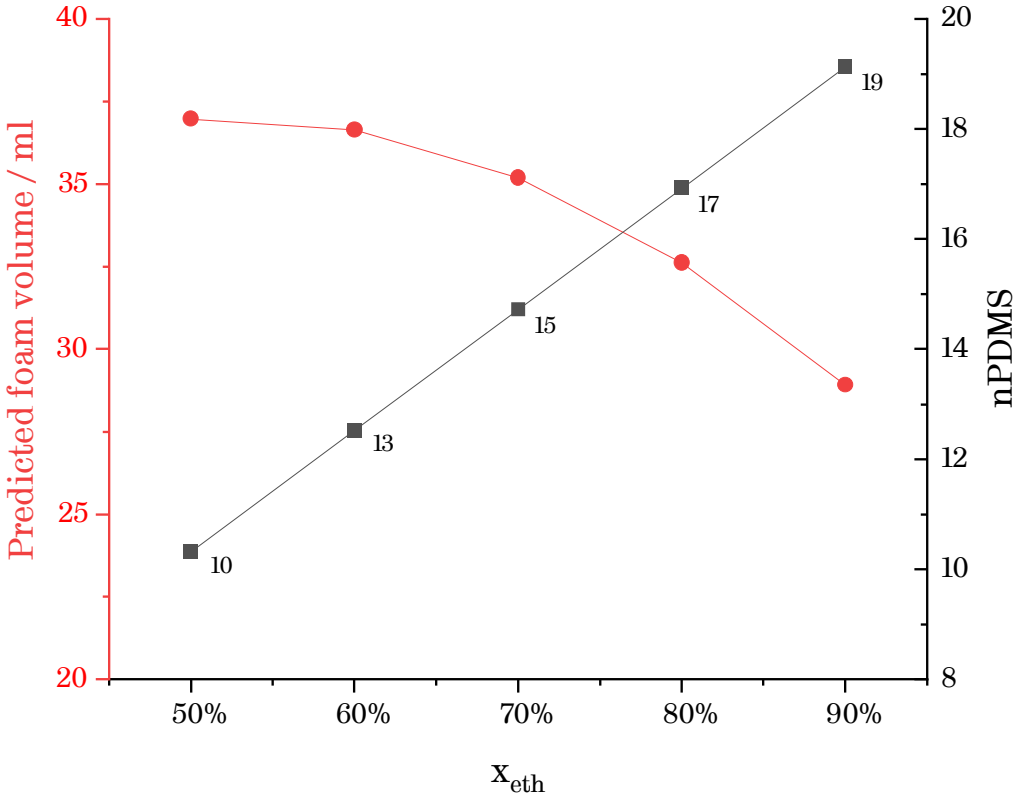

Figure 39. Predicted foam volume and optimum nPDMS versus ethanol content for a series of siloxane polyethers. As x_{eth} increases, the optimum surfactant for foam pump performance has an increased nPDMS and the predicted foam volume declines. For all optimised surfactants, nEO = 8. Predictions were generated by optimising the 'informed' foam pump model. Labels indicating nPDMS values were rounded to the nearest integers.

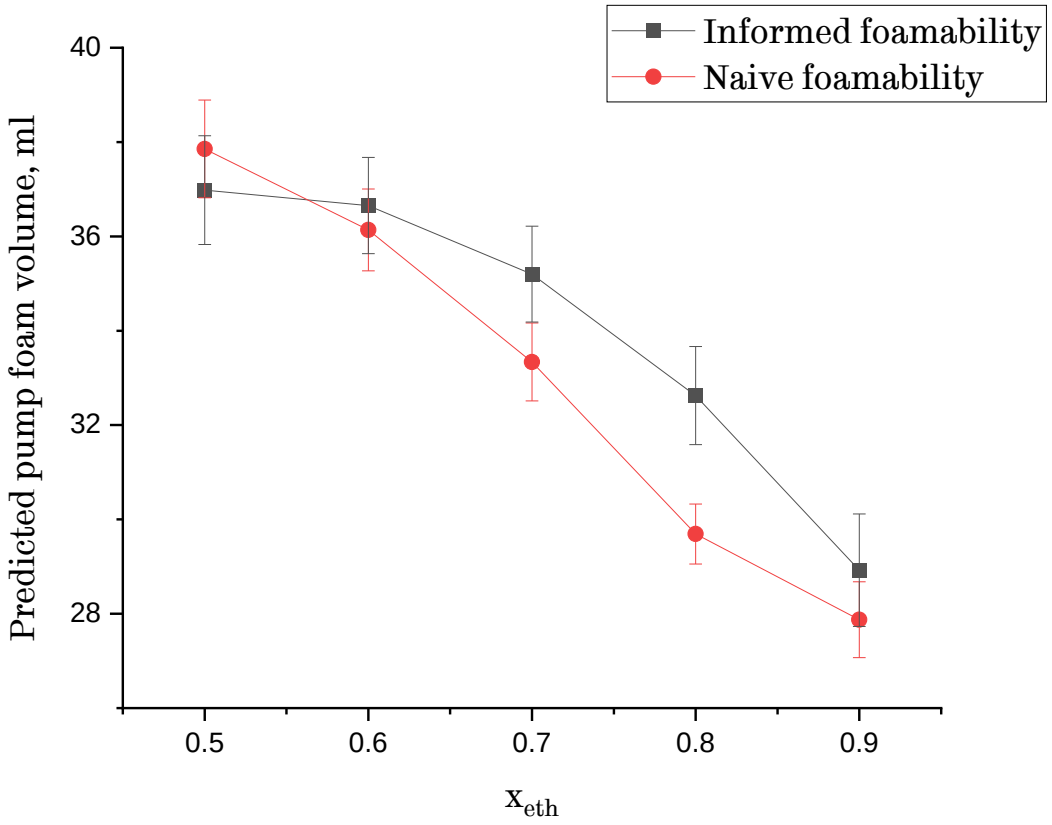

Figure 40. Predicted pump foam volume vs ethanol content. 'Informed' and 'naïve' foam volumes for the optimum surfactant declines as x_{eth} increases, but the naïve prediction reduces more quickly. Optimum surfactants were generated by optimising both the informed and naïve foam pump models. Error bars indicate 95% confidence intervals.

7 Development of pendant drop tensiometer

This chapter covers the development a pendant drop tensiometer, including both instrument and software capabilities. It had been hoped that it would be possible to use this device to measure dynamic surface tension from ~1 s to 120 s, and the Gibbs elasticities of surfactant-laden interfaces. While the instrument could measure dynamic surface tensions, a number of persistent issues relating to the low surface energy of siloxane surfactants meant that this instrument did not ultimately contribute data to my project (as it was superseded by the purchase of the bubble pressure tensiometer described in 8.2.2).

7.1 Theory

Pendant drop tensiometry is a well-established technique for the measurement of surface tension of liquids. A drop of analyte is suspended from the tip of a needle, where its shape is determined by the interplay between two sets of forces – gravity on the one hand, and capillary forces on the other. The former is easily calculated using the density difference of the fluids being measured, and the latter varies primarily with the radius of the needle in use, and the liquid's surface tension. Axisymmetric Drop Shape Analysis (ADSA) is the most widely-used family of methods for imputing surface tension from the shape of the drop.[96,97]

ADSA typically requires the measurement or fitting of several values – an x and y coordinate pair that describe the apex of the drop (typically denoted X_0, Y_0), a radius of curvature R_0 at that same point, and finally an adjustment factor ω to account for deviations from perfect vertical alignment. These values are combined in a set of differential equations involving the Bond number, Bo, which is defined as:

$$Bo \equiv \frac{\Delta\rho g R_0^2}{\gamma}$$

From these values, and given the Young-Laplace equation, it is possible to derive a set of differential equations whose solution gives the shape of a drop:

$$\frac{d\varphi}{d\bar{s}} = 2 - Bo\bar{z} - \frac{\sin\varphi}{\bar{r}}$$

$$\frac{d\bar{r}}{d\bar{s}} = \cos\varphi$$

$$\frac{d\bar{z}}{d\bar{s}} = \sin\varphi$$

Here φ represents the tangent angle of the drop to the vertical, $\bar{s}$ is an arc length measured from the drop apex, and $\bar{z}$ and $\bar{r}$ are the vertical and radial elements of a cylindrical coordinate system, centred on the drop apex. Here, a bar indicates that these quantities have been scaled by the radius of curvature at the drop apex, R_0.

ADSA begins with some guess for the numerical values of relevant parameters (typically X_0, Y_0, R_0, ω and Bo) based on a simple model, after which the set of differential equations given above can be solved to predict the drop outline. By comparing the expected and actual outlines, the initial values are optimised until satisfactory convergence has been achieved. The surface tension can then be calculated *via* the Bond number.

Recently Berry *et al.* have investigated the sensitivity of an ADSA procedure to the Bond number of the system. They found that low Bond-order systems (typically meaning smaller pendant drops) result in higher error in the apparent surface tension. They also create a dimensionless ratio, the Worthington number (Wo) which describes the balance of gravity and capillary forces acting upon the drop.[96]

$$Wo = \frac{\Delta\rho g V_d}{\pi\gamma D_n}$$

Here, $\Delta\rho$ describes the density difference between the fluid phase, g is the gravitational constant, V_d is the drop volume, γ is the surface tension and D_n is the diameter of the needle.

The Worthington number is derived from earlier work by Tate who derived ab equation for the maximum volume of an 'ideal' drop. For such a drop, when $Wo = 1$, gravity overwhelms surface forces and the drop detaches from the needle. Berry shows that as $Wo \to 1$, the accuracy of PDT methods significantly improves, whereas lower Wo values give rise to greater error in γ predictions.

7.2 Instrument design and construction

I designed and constructed a Pendant Drop setup using an optical rail on which a vertical platform containing a syringe could be moved. Two-axis dovetailed stages enabled precise movement of the needle/drop towards and away from the camera, and vertically.

An LED light source, diffuser, and green filter were located close to the sample stage. A LUMIX Infinity 2-1R camera, equipped with a high magnification zoom lens, was located at the opposite end of the rail, to capture images of the drop (see Figure 41). The instrument was contained in a blackout box to reduce ambient light.

A diffuser and green filter were applied to ensure that the light source produced diffuse, monochromatic light. Previous iterations of the setup had proved less accurate due to chromatic dispersion at the edges of the drop.

A Hamilton gastight syringe was positioned such that its tip entered a cuvette, which was sealed with parafilm. This minimised the effect of air currents moving the drop and provided a controllable atmosphere which could be saturated with solvent vapour in order to reduce the rate of surface evaporation.

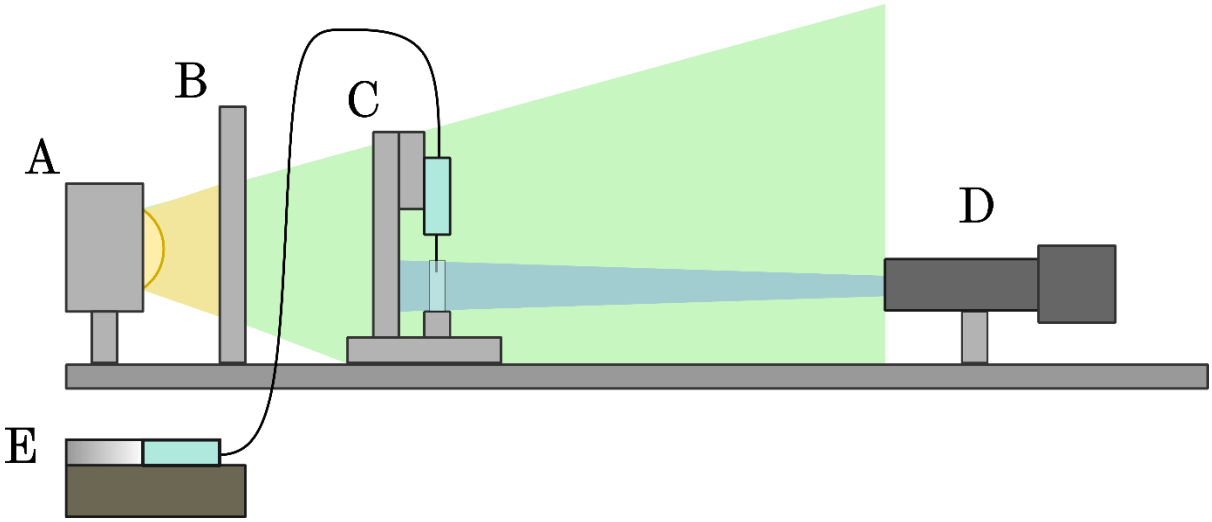

Figure 41. Schematic representation of the pendant drop tensiometer. An LED light source (A) illuminates the drop via a green monochromatic filter (B). The syringe and needle are held in a sample stage (C), which can be translated vertically and along the rail via dovetail stages. A camera and lens (D) capture high-magnification images of the needle tip and drop. A syringe driver (E), connected by gas-tight tubing, generates drops at the needle tip.

Initially, drops were generated by rotating a screw to depress the syringe plunger. Later, this setup was replaced with a syringe driver, linked to a short section of tubing, which could generate droplets of controlled volume in a repeatable fashion.

The relatively low surface tensions of surfactant solutions used in these experiments made conventional needles difficult to use – as drops emerged from the needle's tip, they frequently wet the side of the needle. To counter this issue, PTFE-lined needles were employed. The flexible nature of the PTFE linings made calibration of the diameter somewhat difficult. For this reason, the width of the needle was measured and used to calibrate the image scale. While the PTFE lining was more effective, it still suffered from persistent wetting when using even low concentration surfactant solutions.

7.3 Code interface & algorithmic development

7.3.1 In-line calculation

Initially, the software component of the PDT was designed to carry out real-time calculations of surface tension. This was achieved by applying an ADSA-type algorithm in LabView, exporting this dataset as a text file and thus removing the need to store footage. A script was designed to implement this process.

First, the script connected to and controlled the camera, importing images and processing them to grayscale, and applying a suitable rotation to ensure proper orientation of the drop. An algorithm which quantified the degree of noise at the edge of the needle was also implemented to facilitate focus adjustment. Edge detection was performed via a wheel-and-spoke method to generate a set of drop edge coordinates, which formed the basis of further calculations.

The drop's volume and surface area were measured via a simple rake edge-detection procedure, which divided the drop into a set of 1 px-tall cylinders of varying widths and summing their volumes or exposed surface areas.

Finally, a simple edge detection algorithm was employed to measure the width of the needle sheath in pixels, thereby calibrating the image against a known width. The needle width was measured with a micrometre gauge before use.

Next, an ADSA algorithm, combining elements from the work of Berry and Touhami, was developed.[96,98] As discussed above, an important first step in such an algorithm is to develop an initial prediction for the values of X_0, Y_0, R_0 and Bo. More accurate initial predictions reduce the number of optimisation cycles required in later steps, which are computer-time intensive.

These values were predicted by fitting a circle to the bottom 10% of coordinates in the drop edge using a standard least squares algorithm, as suggested by Berry *et al*.[96] This enabled calculation of X_0, Y_0 and R_0 via its radius and centre point. A prediction algorithm for Bo was not implemented – instead, the user supplied a predicted value.

The values of X_0, Y_0 and R_0, once optimised, could be recalled from previous frames as the new initial value in order to save computational resources and minimise optimisation cycles.

Once these required values had been calculated or recalled, the drop profile was predicted using fourth order Runge-Kutta integration. The predicted drop profile and the measured drop profile were then compared. For each point on the measured drop profile, the nearest predicted drop profile coordinate was found, and the distance squared. The sum of these squares was a measure of the goodness of fit.

A downhill simplex method was implemented to search the parameter space to maximise fit. More efficient algorithms, such as Quasi-Newton or Conjugate gradient optimisation were explored to accelerate fit, but the parameter space proved to be too highly nonlinear – very small differences in Bo resulted in relatively large changes in the predicted drop profile, and thus these methods were not useful.

With more robust optimisation approaches, it was possible to achieve a good fit – for example, using an evolutionary search algorithm – but the computation required was too intensive to apply in real time.

The final optimised values and diagnostic data was saved as a .csv file for later processing.

7.3.2 Offline calculation

While the inline calculation approach, outlined above, could calculate dynamic surface tension with some accuracy, it was not possible to achieve both real-time data collection *and* to iterate the optimisation procedure sufficiently to achieve a stable fit. A schematic comparison of the in-line and offline calculation methods is provided in Figure 43.

The recording and data processing steps of the algorithm were separated, such that a more intensive optimisation procedures could be used. The LabView code was adapted to focus on image handling and storage, and limited processing was limited to crucial steps – noise quantification, volume calculation and needle width calibration – with these values being stored in a .csv file alongside the image frame to which they corresponded. An approximate Worthington number, Wo, was also calculated. This could be used to calibrate the size of drop required for robust data based on values inputted by the user, the predicted surface tension and the measured drop volume/width.

This second setup had the disadvantage of requiring storage of data in image format for analysis. To mitigate this, several space-saving changes were made – first, images were heavily cropped before saving. More importantly, a tool was developed which enabled more

flexible camera timing, allowing the user to distribute captured images nonlinearly through time.

The equation for calculating the time gap Δt at which the next image would be collected is given below:

$$\Delta t = \Delta t_{prev} + b$$

Where b can be set by the user. $b = 0$ results in a linear distribution of images through time. When $b > 0$, the resulting images are distributed quadratically through time (see Figure 42). For each run of the program's main loop, the program checks whether $t_{current} \geq t_{prev} + \Delta t$. If so, the image would be saved, and a new Δt calculated.

With a low initial Δt and $b > 0$, the program captures many images in the first ~30 seconds, during which change is rapid, and then significantly reduces the density of images at longer times, as the drop approached equilibrium.

A)

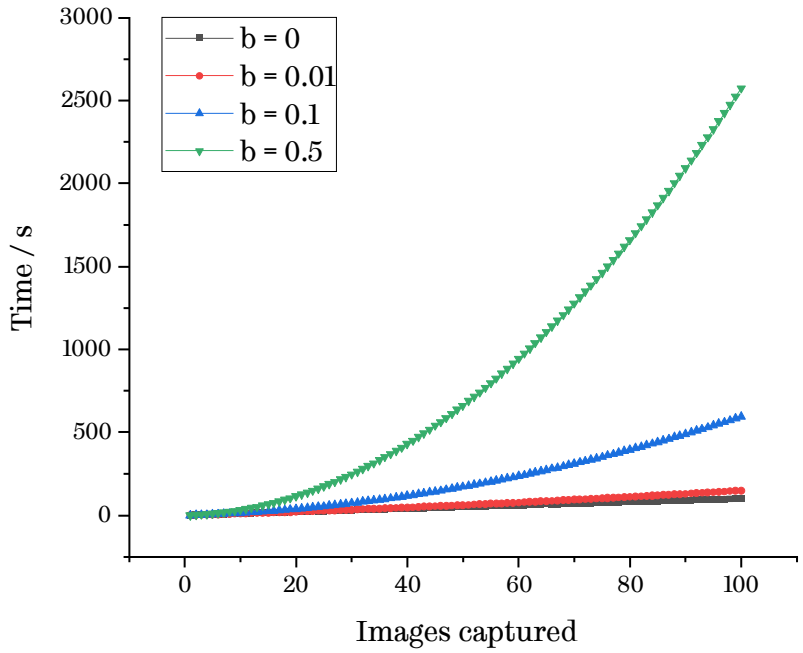

B)

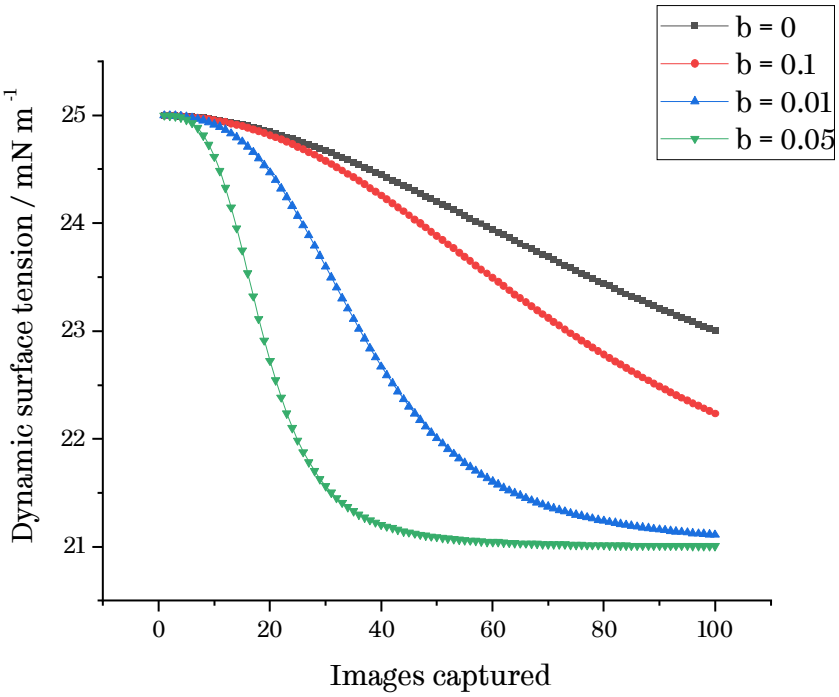

Figure 42. Plots comparing image capture using a standard approach and the time gap algorithm. The time gap algorithm enables more efficient collection of surface tension data. A) higher values of *b* give rise to non-linearly spaced images. B) example data from a typical surface tension decay over 100 images, given different values of *b*. Higher values of *b* capture the process more efficiently.

After capturing image data, dynamic surface tension data were calculated using an open-source ImageJ plugin, PendantDrop, developed by Daerr *et al.*[99]

To adjust for potential drift in the position of the needle, PendantDrop was run in pixel units. A frame-by-frame calibration into distance units was applied using the width of the needle sheath.

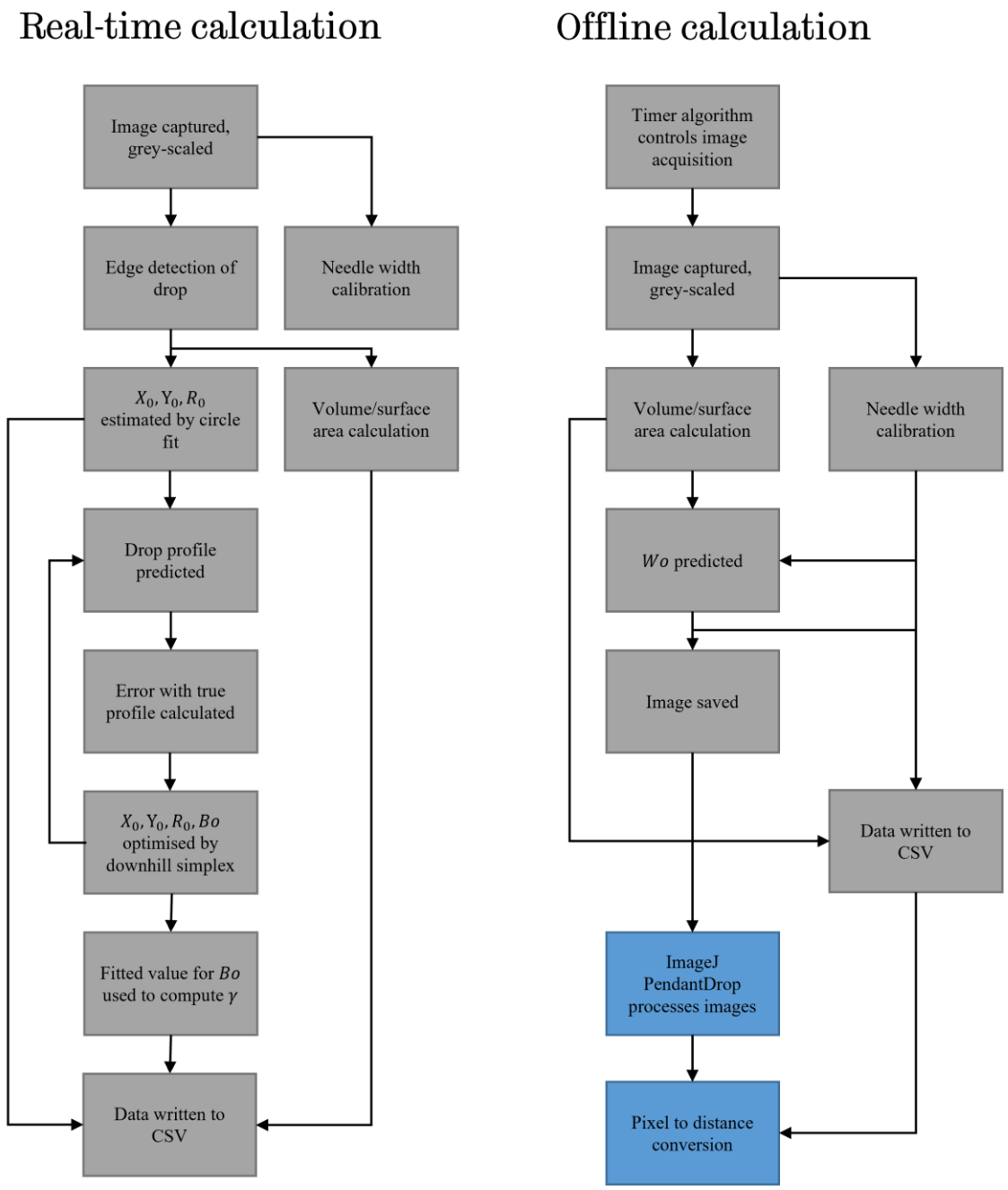

Figure 43. Schematic differences between real-time and offline pendant drop tensiometry algorithms. Grey components were carried out in real-time, whereas blue components were carried out separately.

7.4 Sample results

The pendant drop setup described above generally produced high-resolution drop images with sharp edges, which could be processed to measure surface tension data (see Figure 44 and Figure 45).

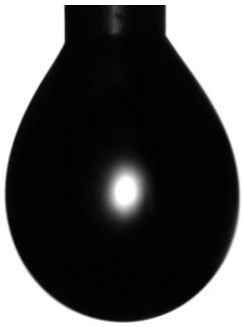

Figure 44. An image captured by the pendant drop tensiometer. The solution is 0.1 mM Di2510 in 90% ethanol.

The setup was most effective at intermediate copolymer concentrations where surface tension decay was relatively rapid. When the surface tension was static, significantly noisier data was obtained. This is likely due to the effect of air currents, thermal fluctuations and changes in drop volume.

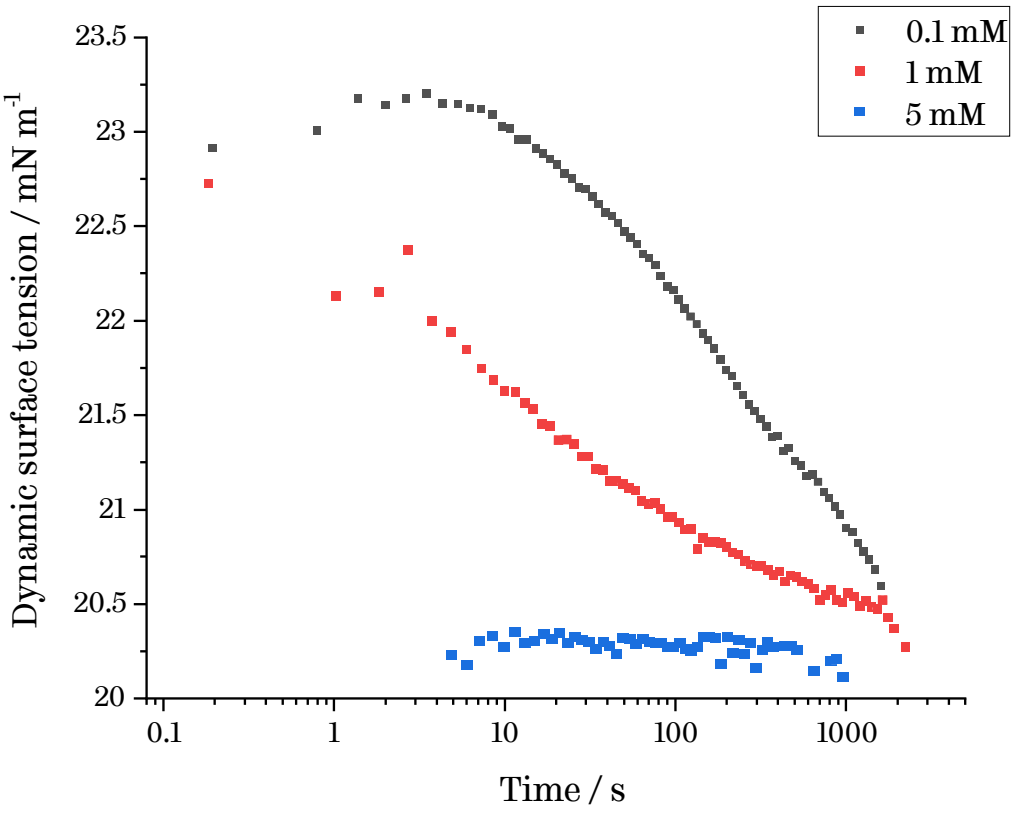

Figure 45. Variation in dynamic surface tension over time for three concentrations of Di2510 solutions in 90% ethanol, as measured by pendant drop tensiometry, using a custom-built instrument and analysed using OpenDrop.

Especially at higher copolymer concentrations, siloxane solutions would frequently wet the needle's PTFE sheath, disrupting the drop shape and making ADSA analysis impossible. Further, despite being located in an enclosed, solvent-saturated atmosphere, drop volumes significantly reduced over the course of the measurement, most likely as a result of evaporation (see Figure 46). Evaporation of ethanol at the drop surface increases the surfactant concentration and (depending on the composition of the vapour phase) results in a drop enriched in water. Evaporation is particularly problematic for small drops, which have higher surface/volume ratios.

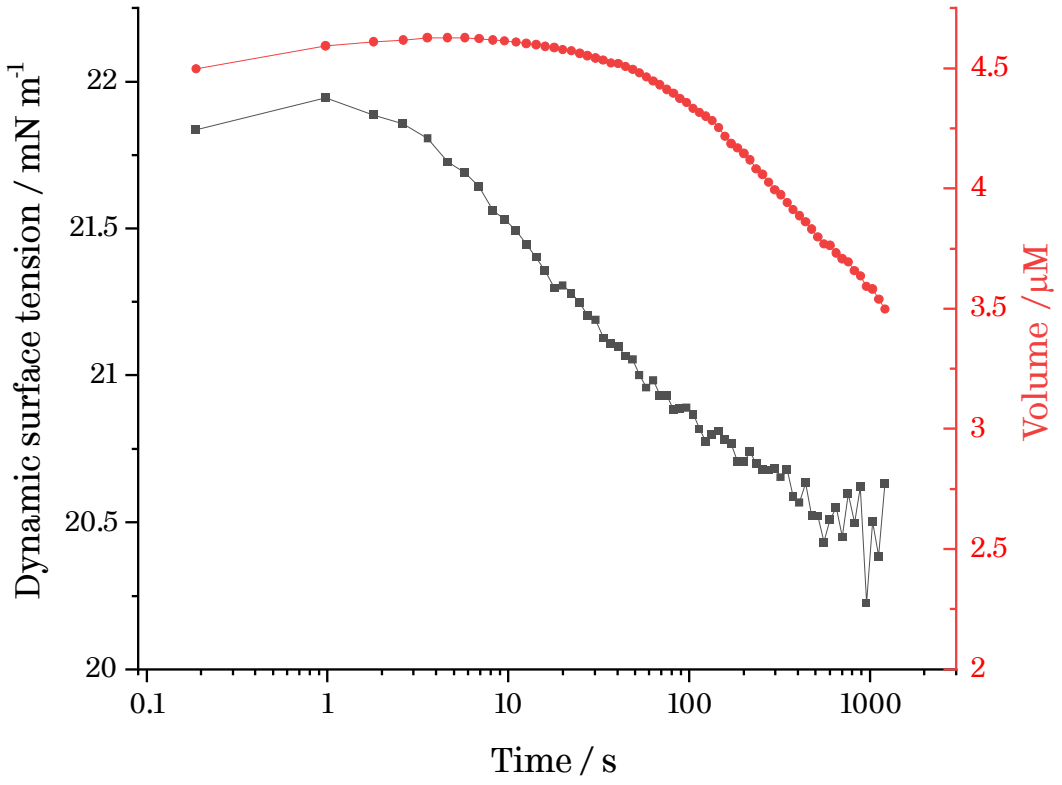

Figure 46. Dynamic surface tension and drop volumes as a function of time in the example case of 1 mM Di2510 in 90% ethanol. Drop volumes significantly reduce over the course of such measurements.

Finally, as a result of needle wetting and time taken to reach mechanical equilibrium, the pendant drop tensiometer could not determine dynamic surface tensions accurately for surface ages below ~10 s. This did not enable me to probe surface tensions around 0.1 – 1 s, which is the relevant timeframe for the foam pumps commonly used in hand foam applications.

These issues lead me to seek an alternative approach to measuring surface tension at early surface ages, culminating in the use of the maximum bubble pressure method (see 8.3.2).

8 Dynamic surface tension

8.1 Theory

Dynamic surface tension is the measure of surface tension with respect to time, typically through the generation of 'bare' interfacial area by some method. Common approaches to these measurements include the maximum bubble pressure method, ring or plate tensiometry and pendant drop tensiometry. The key difference between these approaches is in terms of surface ages – in other words, the minimum and maximum time after surface generation that a given surface tension method can resolve.[91]

Surface adsorption is a dynamic process – thus the creation of new interfacial area disturbs the equilibrium between desorption and adsorption, leading to net flux of monomer towards the surface. Depending on the surfactant system, this process has been assumed to be either diffusion-controlled or mixed kinetic-diffusion models, depending on whether there is a significant kinetic barrier to adsorption. Such barriers might include saturation of the interface, molecular rearrangement of some kind, or relatively slow micellar dissolution.[77]

The Rosen-Hua equation is an empirical equation which accurately describes surface tension decay for most surfactants over a range of timescales. It is a sigmoidal decay of the form:

$$\gamma_t = \gamma_{eq} - \frac{\gamma_0 - \gamma_{eq}}{1 + \left(\frac{t}{t^*}\right)^n}$$

t^* controls the onset of rapid surface tension decay after an induction period, and n determines the steepness of that decay.[77]

8.2 Methods

8.2.1 Du Noüy ring tensiometry

Du Noüy ring tensiometry was carried out using an automated LAUDA TD3 tensiometer, equipped with a 90:10 platinum-iridium ring of 6.283 cm circumference, 9.55 mm radius and 0.2 mm width. Surface tension of ultrapurified water was measured before use, with good agreement with literature values of 72.8 mN m^{-1} being observed.

Between each measurement, the ring was immersed in ethanol, flamed immersed in water and flamed again. The surface tensions of solutions were monitored until nine consecutive readings had a standard deviation of no more than 0.01 mN m^{-1}, or until 30 mins had elapsed. Densities of ethanol-water mixtures were calculated by interpolation of literature values.[76]

For dynamic measurements, the surface of the sample was disrupted using a Pasteur pipette prior to measurement, following the protocol reported by Muñoz *et al.*[100]

The temperature of samples was controlled using a LAUDA thermostatic bath at 20 ºC.

Samples were made up by the addition of concentrated aliquots of surfactant solution to a larger volume, initially comprising pure water & ethanol. As further aliquots were added, the surfactant concentration was gradually increased. A range of concentrations, from weight fractions 2 x 10^{-7} (~2 x 10^{-5} %) to 0.03 (~3%), were achieved by this method.

The Rosen-Hua equation was used to interpolate data to generate datasets with comparable times.

8.2.2 Maximum bubble pressure method (MBPM)

MBPM was carried out on a Krüss BP100 instrument, using disposable polypropylene capillaries. Capillary radius was calibrated against ultrapure water. Surface tensions were measured between 10 ms and 1000 ms. At each time point, 10 measurements were made and averaged.

Surfactant samples were prepared as for Du Noüy ring tensiometry, as described above. An initially pure solvent solution (75 ml) was repeatedly mixed with aliquots of concentrated surfactant solution (20 ml, 10% w/w surfactant) to produce a series of solutions of gradually increasing surfactant concentrations. The resulting set of measurements typically ranged from 0.005% to 3% w/w.

8.3 Dynamic surface tension results

This chapter will refer throughout to the surface pressure, π, which is a measure of the degree of surface tension depression versus the expected surface tension of a pure solvent solution:

$$\pi = \gamma_{sol} - \gamma$$

This parameter facilitates comparison between surface pressures in different solvent mixtures. While surface pressures are normally calculated at equilibrium, this thesis will frequently refer to 'dynamic surface pressures' – which is the value of π at some specific surface age.

8.3.1 Du Noüy ring tensiometry

Du Noüy ring tensiometry is a comparatively slow method of surface tension measurement, requiring 10-30 seconds for the ring to locate the surface and measure surface forces. This restricts Du Noüy ring tensiometry to measuring surface tension behaviour at long times.

Figure 47 shows that for all samples except 0.002%, almost all the decay from γ_{sol} to γ_{eq} has already occurred.

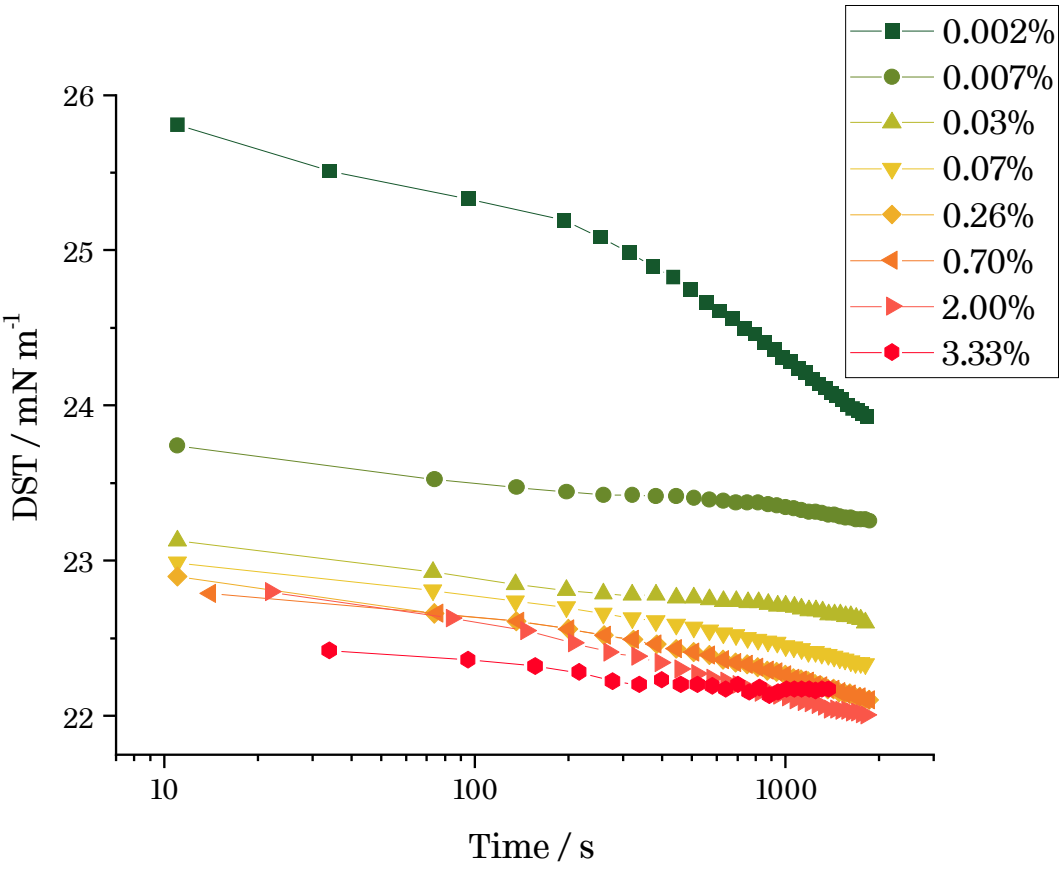

Figure 47. Dynamic surface tension (DST) for Di1508 in 50% ethanol over a range of surfactant concentrations. Surface tension declines more quickly at higher surfactant concentrations.

In general, surface tension decays were much more pronounced in 50% ethanol mixtures than in 90%. As shown in Figure 48, surface pressure increased much more rapidly with respect to concentration in more water-rich mixtures, and reached higher levels – the maximum measured surface pressure for Di1508 is ~7.5 mN m^{-1} in 50% ethanol, *vs.* ~2.1 mN m^{-1} in 90% ethanol.

For all surfactants, γ did not fall below 20.6 mN m^{-1}. This is approximately the surface tension of neat PDMS, ~21 mN m^{-1}, which the air-liquid interface closely resembles as it

becomes more densely packed with siloxane moieties. This limit was particularly evident for 90% ethanol solutions.

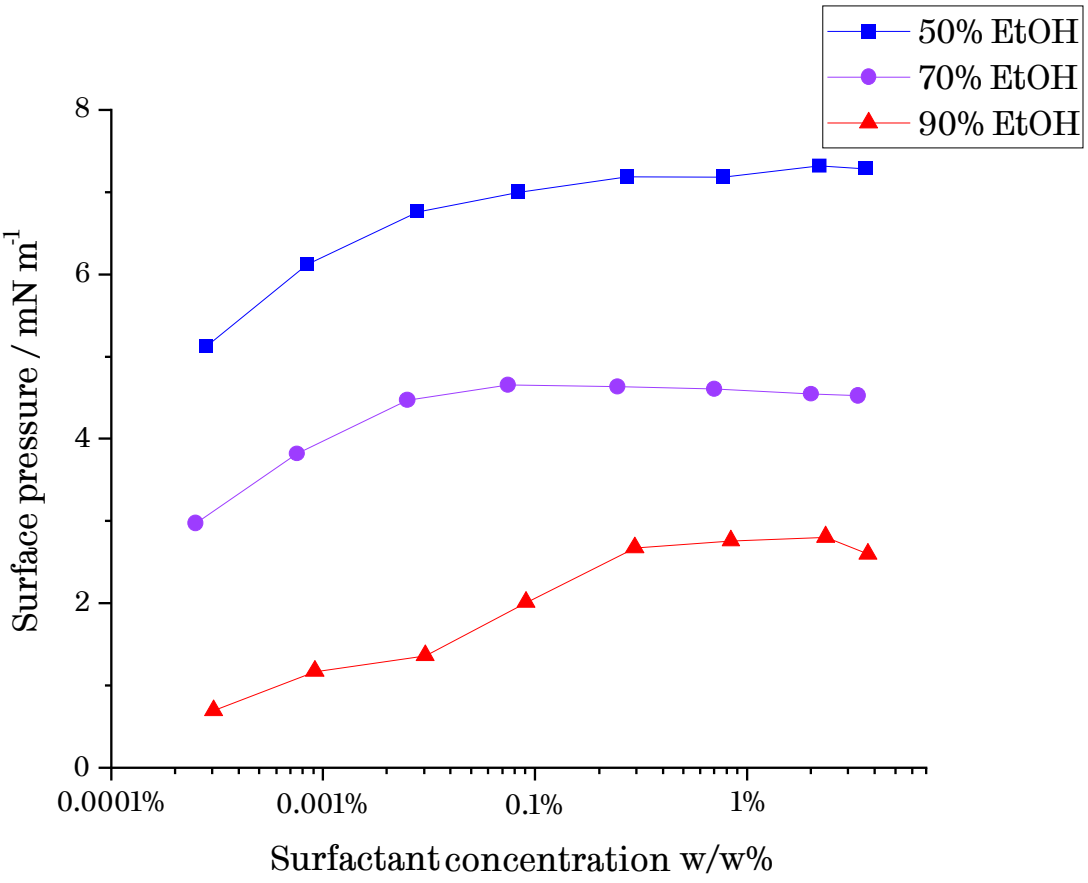

Figure 48. Surface pressure (at 1000 s) versus concentration for Di1508 for three solvent compositions, as measured by Du Noüy ring tensiometry. Surface pressure increases with surfactant concentration, but does so more rapidly in more water-rich solutions.

Surface pressure could also be related to surfactant structure. As Figure 49 shows, maximum surface pressure declines markedly as nPolyether is increased, especially in 50% ethanol. By contrast, surface pressure appears to reach a maximum with respect to nPDMS between 10-20, before declining – see Figure 50. The nature of the surfactants in this dataset means that the independence of these two effects cannot be readily assessed.

A multiple linear regression was fitted to assess the relative effects of nPolyether, nPDMS and ethanol content. Achieving good fit ($R^2 = 0.94$), the model suggests that nPDMS does not have a significant effect on surface pressure. Both the ethanol content and nPolyether terms are statistically significant and predicted to be negatively correlated with surface pressure. See Appendix 0 for full model results.

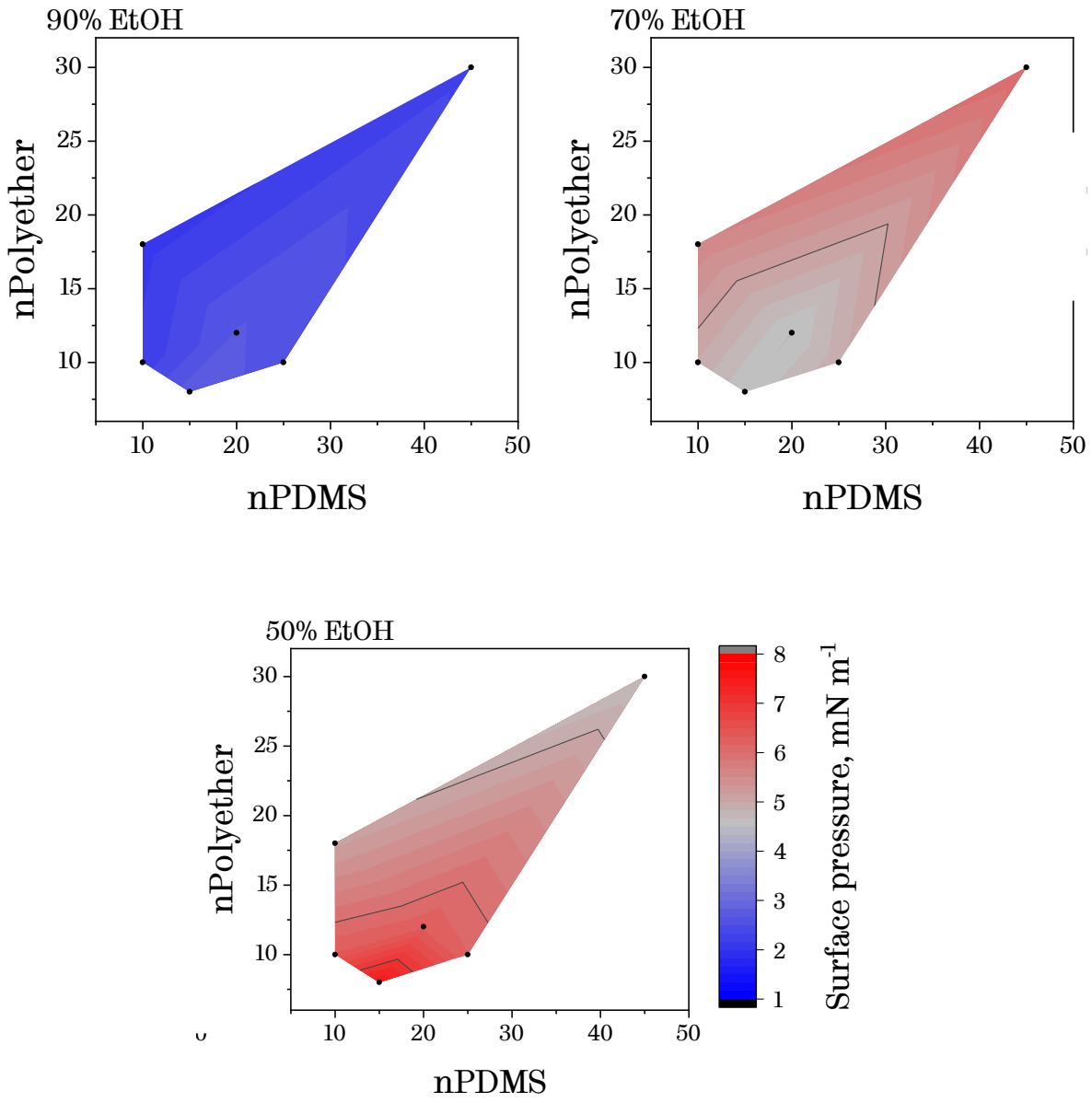

Figure 49. Above - contour plots of surface pressure versus nPolyether and nPDMS. Below – plots showing the relationship of nPolyether and nPDMS to surface pressure. Surface activities decline markedly as the ethanol concentration is increased. Maximum surface pressures (and thus surface activities) decline with nPolyether and are largest when nPDMS is in the range n = 15-25. Surface activities are compared for 1% w/w solutions, after aging for 3000 s. Colour is scaled with surface pressure, with red indicating high surface pressure and blue indicating low.

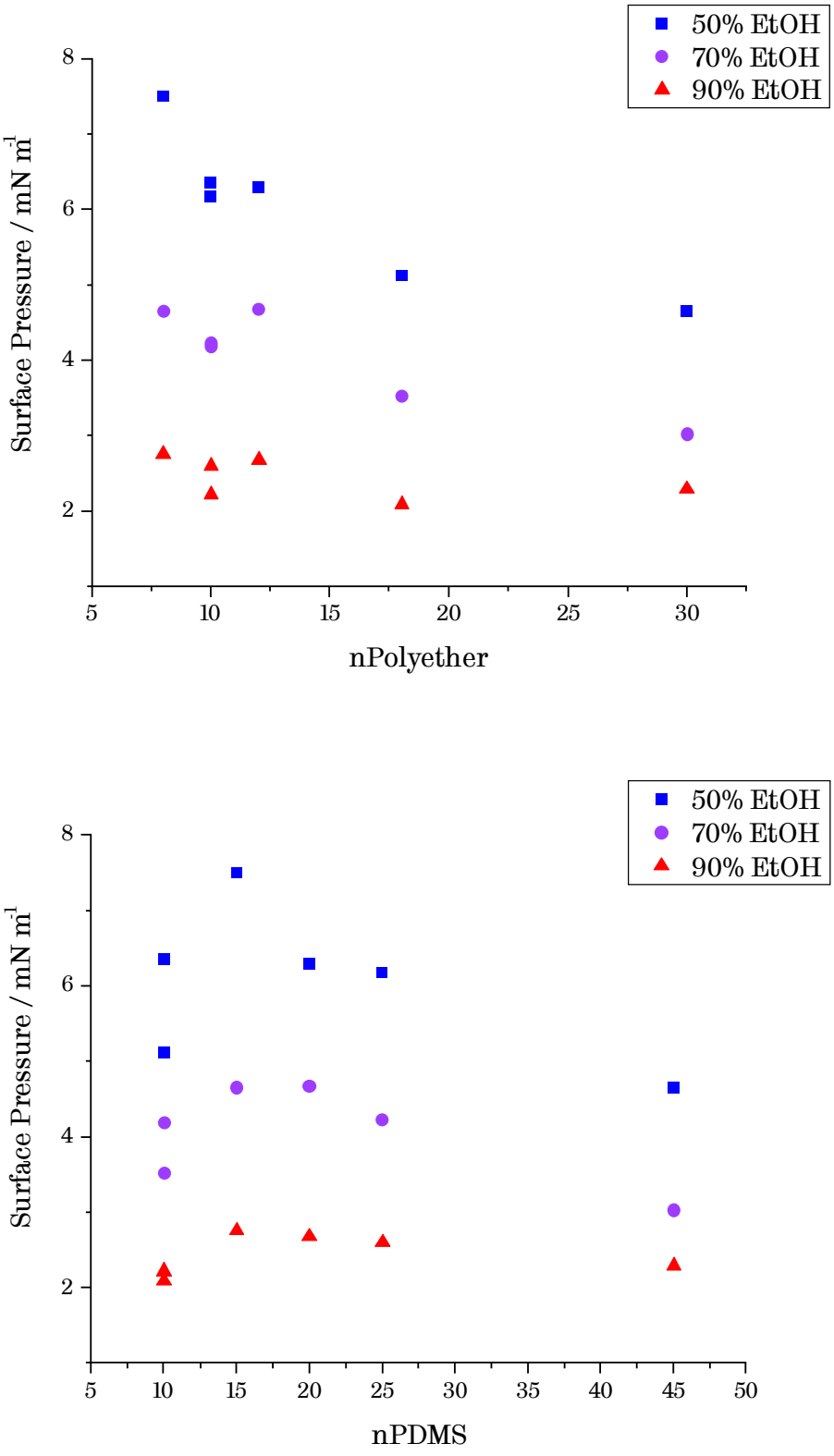

Figure 50. Plots showing the relationship of nPolyether (top) and nPDMS (bottom) to surface pressure. Surface activities decline markedly as ethanol concentration is increased. Maximum surface pressures (and thus surface activities) decline with nPolyether and are largest when nPDMS is in the range n = 15-25. Surface activities are compared across 1% w/w solutions, after aging for 3000 s. Colour is scaled with ethanol content, with red indicating high and blue indicating low.

For Pluronics, the highest surface activities are achieved by surfactants with high nPO values and low nEO values (see 2.3). This structure allows for dense packing of PO units at the air-water interface. Section 2.6 discussed the lack of literature consensus on the relationship between surface activity and surfactant structure in siloxane polyethers. My work supports the established view that higher nEO values are correlated with lower surface pressures. This analysis does not find any effect of nPDMS on equilibrium surface activity.

8.3.2 Maximum bubble pressure method

Bubble pressure tensiometry, or the maximum bubble pressure method, is a well-documented method for measuring surface tension at early surface ages. A number of issues relating to the very low surface energies of siloxane surfactants were encountered, in particular relating to the instability of bubbles at the tips of glass capillaries, which caused sharp jumps in surface tension. Better results were achieved using polypropylene disposable capillaries but measurements of surface ages over 1000 ms proved infeasible. These capillaries occasionally gave anomalously high surface tension data at early surface ages, before returning to expected levels.

All surfactants produced rapid decays in surface tension within 10-1000 ms, with decays becoming more pronounced as surfactant concentration was increased. No evidence of surface saturation was obtained in this period, even at high concentrations. As with Du Noüy ring tensiometry, surface tension decays were faster and more extreme for 50% ethanol mixtures than in 70 or 90% ethanol. For Di1010, Di1018 and Di1508 in particular, dynamic surface tension decays were markedly slower in alcohol-rich mixtures (see Figure 51).

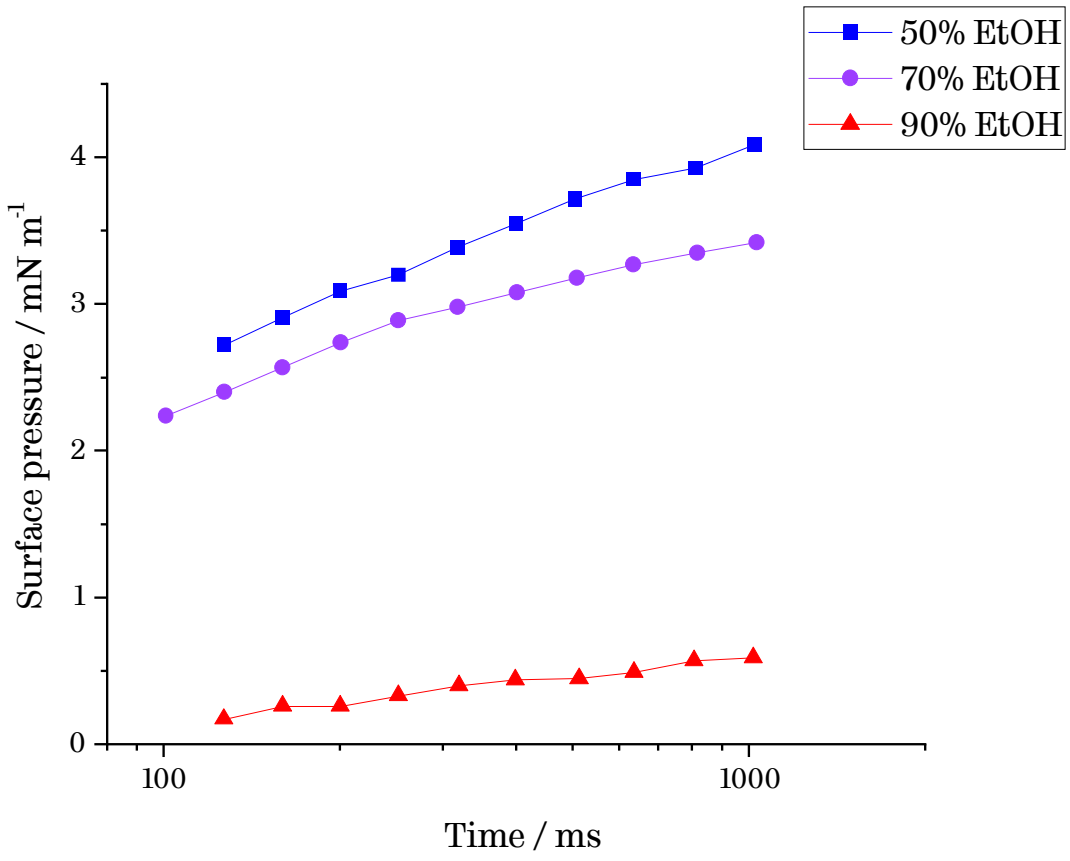

Figure 51. Surface pressure versus time plot for Di1010 at 3 solvent compositions. Surface pressure increases more slowly in 90% ethanol for Di1010. Data is measured by bubble pressure tensiometry. Surfactant concentration is ~1.5% w/w.

This is in contrast to the behaviour observed at longer times, using Du Noüy ring tensiometry, where sharp changes in behaviour from 70% to 90% ethanol were not observed. The surface pressures for Di2012, Di2510 and Di4515 were progressively less sensitive to ethanol content. For Di4515, surface pressure vs surface age for all three solvent mixtures converge into essentially a single curve.

Comparing the surface pressure data obtained from Du Noüy ring tensiometry and bubble pressure tensiometry, it is possible to produce a 'map' of surfactant behaviour in water-ethanol mixtures. Here, surfactants are arranged vertically according to their surface pressure at 1 s, and horizontally according to the difference between the surface tension at 1 s and that of (quasi)equilibrium at 3000 s (see Figure 52). The x-axis thus represents the kinetic 'gap' between the rapidly attained surface tension and its equilibrium value.

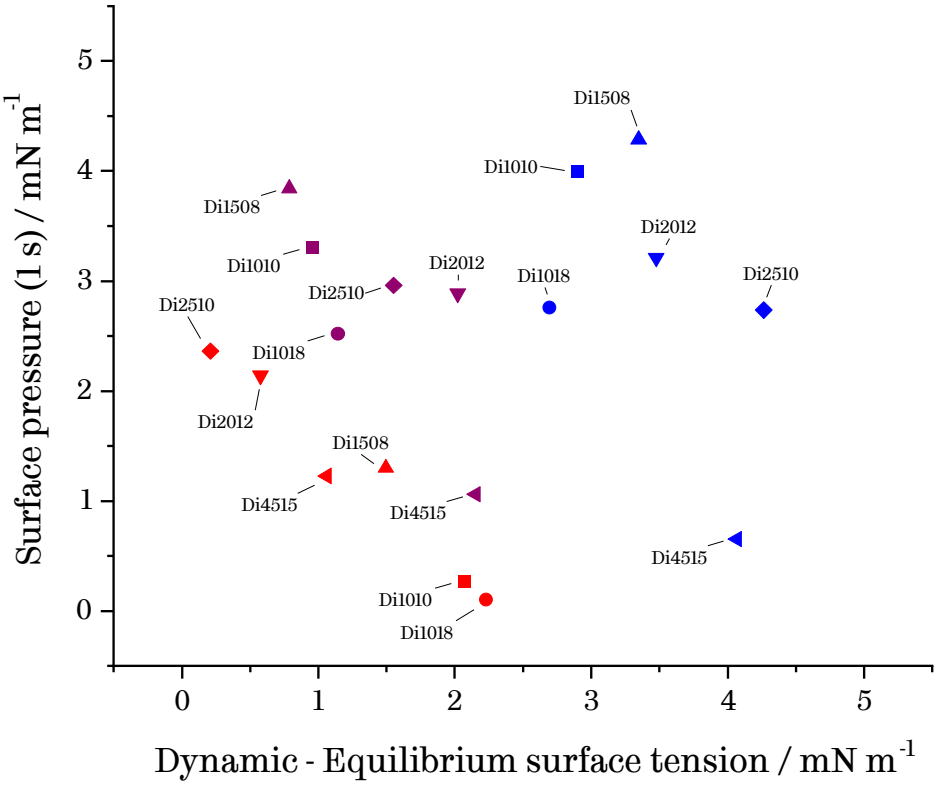

Figure 52. Surface pressure (after 1 s) vs dynamic *minus* equilibrium surface tension. Samples to the right are far from their equilibrium value, whereas samples to the left are close to equilibrium. Data for surface pressures at 1 s are ontained from bubble pressure tensiometry. Quasi-equilibrium was identified via Du Noüy ring tensiometry at 3000 s. All surfactants are compared at 1 % w/w. Colour is scaled with solvent composition, with red indicating 90% ethanol, purple 70% ethanol and blue 50% ethanol.

Surfactant/solvent combinations towards the top of Figure 52 show a rapid reduction in surface tension, whereas those at the bottom have slow reductions. Those to the left-hand side of the figure are close to their measured equilibrium values, whereas those to the right-hand side are far from them. Surfactant/solvent combinations in the bottom-left quadrant are both poor at reducing surface tension at short times, and also have little capacity to lower surface tension in the long term. Surfactants in the bottom right quadrant, by contrast, are farther from equilibrium and thus have the capacity to lower surface tension over longer times.

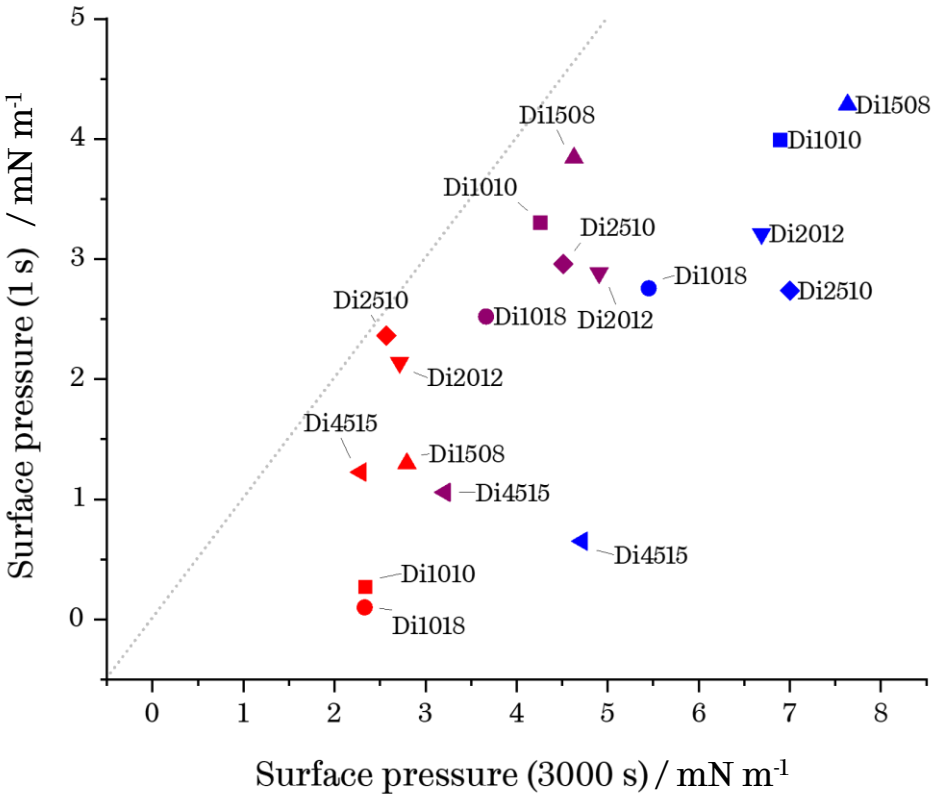

Figure 53. Surface pressure at 1 s versus surface pressure at 3000 s for the full range of surfactant and solvent compositions. Data for surface pressures at 1 s are taken from bubble pressure tensiometry. Surface pressures at 3000 s are taken from Du Noüy ring tensiometry. All surfactants are compared at 1 % w/w. Colour is scaled with solvent composition, with red indicating 90% ethanol, purple 70% ethanol and blue 50% ethanol. Dotted line indicates the function $y = x$ - *i.e.*, where surface pressures at the two times are equal.

Figure 53 shows this mapping slightly differently. Here, surfactant/solvent combinations to the right have high quasi-equilibrium surface pressures, and those towards the top of the plot exhibit rapid reductions in early surface pressures. The dotted line indicates (theoretical) equivalence between short-time and long-time surface pressures.

Both plots reveal several interesting relationships. The 90% ethanol mixtures tend to have lower surface pressures at both short and long times, with Di2510 and Di2012 already approaching equilibrium surface pressures after aging for 1 s. In addition, there is very little difference in equilibrium surface pressures for surfactants in 90% ethanol, as they approach the surface pressure corresponding with the surface tension difference between pure PDMS and the 90% ethanol/water mixture (~2.5 mN m^{-1}).

It is striking that smaller surfactants in these solutions (Di1010, Di1018, Di1508) appear to be capable of producing similar surface tensions as larger surfactants, but take longer to do so. This contrasts with the generally held view that smaller surfactants are more quickly able to migrate to interfaces and adsorb. This may be because the triblock copolymer in these surfactants may be completely soluble, and the surface-active species may instead be a low concentration of surface-active impurities - whose migration to the interface is much slower than a typical triblock surfactant.

By contrast, all surfactant solutions in 50% ethanol are far from equilibrium at 1 s, and their rightward position on both figures indicates that significant further reductions in surface tension are possible over longer time. This is consistent with the reasoning outlined in 2.3 and 2.4, and my findings on the relationship between the CMC and water/ethanol mixtures – in water-rich mixtures, surfactant adsorption at the interface is slowed by poorer solvent quality, with surfactants 'frozen' in relatively stable micelles. This is particularly striking for Di4515, which moves both down and rightward on the figure as its solvent mixture is changed from 90% to 50% ethanol, indicating poorer short-time surface pressures.

8.3.3 Relationship with foamability

Dynamic surface tension has been theoretically and empirically linked with foamability. Low dynamic surface tension for new surfaces can indicate the rapid formation of surface tension gradients, which give rise to robust, elastic foam films (see 1.3.2). Recent work by Petkova *et al.* has shown that dynamic surface tension at short times is a good predictor of foamability for a range of aqueous surfactant solutions.[18]

In order to explore the relationship between surface tension and foamability, models developed in 6.3.3 were used to predict the foamabilities of solutions used in surface tension tests. For the foam pump, foam volumes were interpolated using simple linear or quadratic models to maximise the reliability of these estimates. For syringe and vortex foaming approach, the full models discussed in 6.3.3 were applied. Comparisons were restricted to samples within the range in which the foamability models were fitted (typically 0.5-3% w/w surfactant).

There was no statistically significant relationship between the dynamic surface tension and the predicted foam volume from the foam pump ($R^2 = 0.00$ - see Figure 54) and vortex tests, and only a weak relationship for the syringe bubbling test. This is because the dynamic

surface tensions of these samples are not directly comparable, because they arise from three different solvent mixtures.

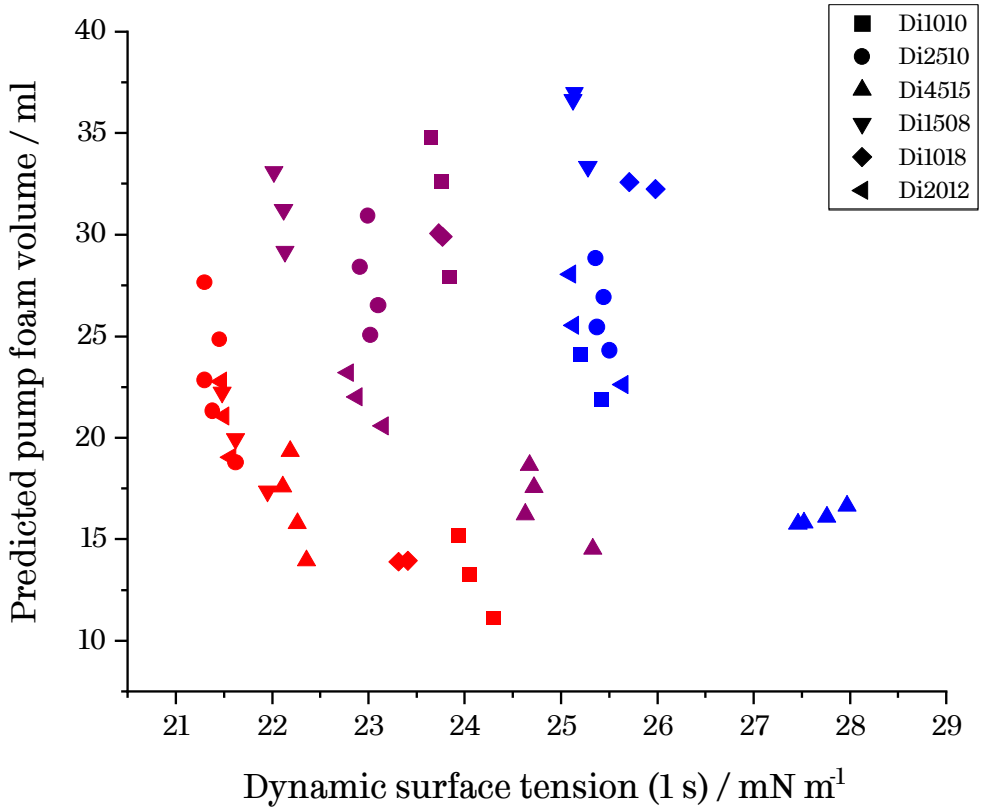

Figure 54. Predicted foam volume versus dynamic surface tension (at 1 second) for the full range of surfactant and solvent compositions. The dynamic surface tension at 1 second is not correlated with predicted foam volume using the pump method. Colour is scaled with solvent mixture, such that red indicates 90% ethanol and blue indicates 50% ethanol.

Figure 54 illustrates an example of Simpson's paradox, in which a true relationship between two variables is obscured by subgroup differences.[101] In this case, a clear, consistent curve is apparent, shifting gradually to higher surface tensions as the solvent mixture becomes more water-rich. This underlying relationship becomes clear when comparing the dynamic surface *pressure*, which accounts for differences in γ_{sol}. Here, the association is much stronger ($R^2 = 0.76$) – see Figure 55. When comparing dynamic surface pressure and foamability, all six surfactants across three solvent mixtures and concentrations collapse onto a single master curve.

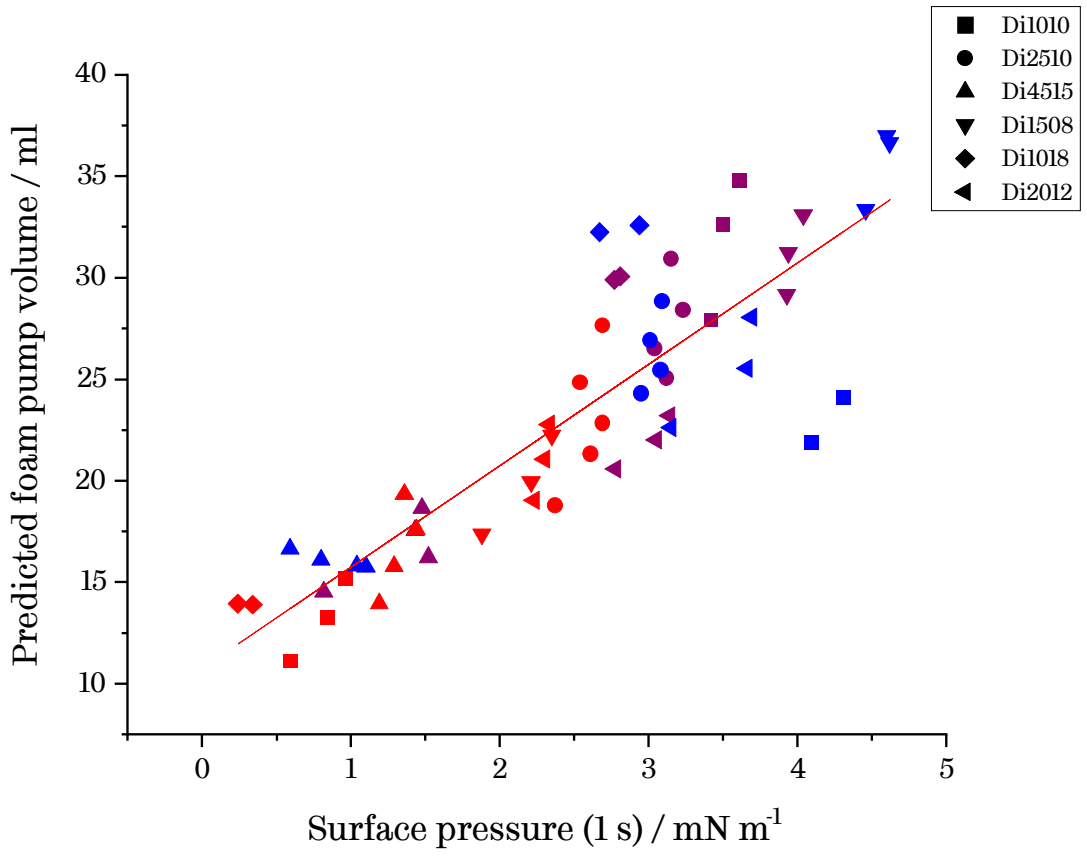

Figure 55. Predicted foam pump volume versus surface pressure for the full range of surfactant and solvent compositions. Surface pressure at 1 s predicts pump foam volume. Colour is scaled to solvent mixture, with red indicating 90% ethanol and blue indicating 50% ethanol.

A range of characteristic times can be chosen at which to compare the surface pressure. Combining data from ring and bubble pressure tensiometry, times in the range 100 ms – 3000 s were tested, and their predictive power with respect to foam volume was compared for three foaming methods.

As shown in Figure 56, this relationship varies significantly between foaming methods. The maximum R^2 for the foam pump method occurs within the range 0.5 – 1 s, which is consistent with the typical timescale of foam generation for the foam pump. Predictive power declines sharply afterwards. Sparging, by contrast, is best predicted by surface tension values between 10-3000 seconds. Predictive power for the vortexing method is generally poor, but better at short times than long. This may be a result of vortexing lacking a well-defined period of foam generation – rather, the foam is continuously generated and folded over several seconds, and a simple analysis of interfaces based on lifetime is not sufficient to predict foaming behaviour under such conditions.

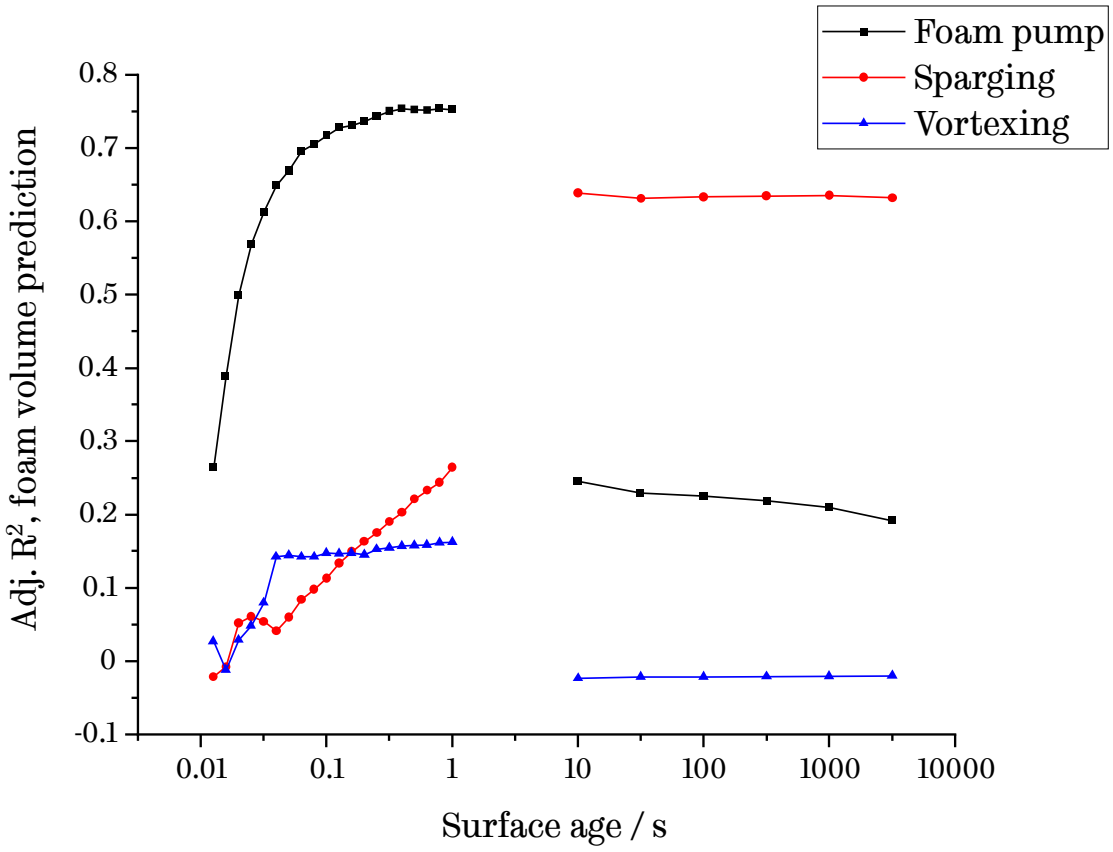

Figure 56. Relationship between adjusted R^2 value for the predicted foam volume and dynamic surface pressure, across a range of surface ages, for a combined dataset of Di1010, Di1018, Di1508, Di2012, Di2510 and Di4515 in 50, 70 and 90% ethanol/water mixtures. Dynamic surface pressure is predictive of foam volume for different foaming methods at different characteristic times. A break separates bubble pressure tensiometry data from Du Noüy ring tensiometry data.

This dramatic difference in predictive power is most likely due to the different timescales at work in the sparging and foam pump methods of foam generation. Bubbles are generated comparatively slowly in the sparging method, and their interfaces therefore have longer to approach equilibrium – thus long-time surface tensions are correlated with foam volumes. The foam pump method, by contrast, is a relatively high-speed method for interface generation and requires correspondingly fast surface tension decays. This finding is analogous to that of Patist *et al.* who compared capillary bubbling to hand-shaking.[102]

8.4 Time-concentration superposition

8.4.1 Theory

Figure 55 shows that a single master curve – based on surface pressure – can explain the foaming behaviour of six surfactants across a range of concentrations and for three solvent

compositions. This suggests a fundamental similarity between interfacial processes for all the surfactant samples tested.

Time-temperature superposition analysis is an analytical technique commonly applied to the rheology of polymers. The central insight of this approach is that there is a strong analogy between increasing the temperature and carrying out a particular deformation (for example, an oscillatory shear) at a faster rate. By carrying out a number of experiments over a given frequency range at different temperatures, it is possible to introduce a 'shift factor' which slides these curves in the frequency domain, such that a single, continuous curve can be constructed. This new curve predicts the behaviour of the polymer at frequencies which cannot or have not been tested.[103]

An analogous approach has been employed for the dilational rheology of surfactants by Bae *et al*.[104] By measuring the dilational rheology of surfactants at several concentrations, the authors were able to 'extend' the frequency range of their measurements by several orders of magnitude. The motivation this analysis is the same as that applied in time-temperature superposition – increasing the concentration of the surfactant can be thought of as increasing the *speed* of the adsorption process but otherwise leaves it unchanged.

Thus time-*concentration* superposition, by analogy, implies that the dynamic surface tension function at a certain concentration resembles the shape of the same functions at similar concentrations, and that it may be possible to construct a single master curve for the dynamic surface tension data presented in this Thesis.

8.4.2 Methods

Surface tension was measured between 100 ms and 1000 ms by the methods described in 8.3.2. Siloxane polyether surfactants were measured across a wide range of concentrations, and in three different water-ethanol mixtures.

Surface tension, γ, was normalised against γ_{sol}, the surface tension of the pure solvent mixture, to give a relative surface tension γ_{rel}.

For each set of dynamic surface tension data, a shift factor α is defined:

$$\log(t_{adj}) = \log(t) + \alpha$$

This has the qualitative effect of 'sliding' the surface tension curve horizontally on a surface tension / $\log(t)$ plot by α units. Each concentration-surfactant-solvent combination was assigned a single shift factor, by which all time points for that combination were shifted.

Shift factor values can be interpreted by comparison to the reference state used to construct the master curve. A shift factor of α implies that 1 ms in the test state is equivalent to 10^{α} ms in the reference state.

To construct a master curve, a non-linear generalised reduced gradient descent (GRG) algorithm was applied and implemented in Excel. The GRG algorithm aimed to maximise the R^2 fit statistic of a simple polynomial to the composite master curve. Several orders of polynomial were also tested for this process – but the master curve exhibited no meaningful change beyond a second-order polynomial. In some cases, higher order terms were used to generate more compact master curves.

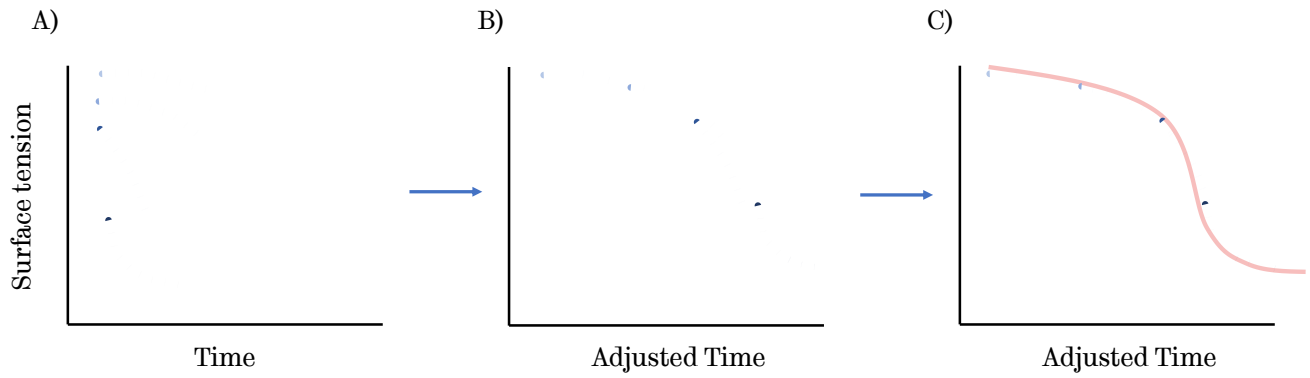

Figure 57. A schematic representation the process of creating a composite master curve from four sets of surface tension data. A) shows the raw surface tension data for four surface tension solutions at different concentrations. In B), data are manually offset to form a smooth curve. In C), the horizontal shifts of each dataset are optimised using generalised reduced gradient descent, in order to form a smooth curve given by a polynomial function (shown in red).

Master curves were generated for each surfactant-solvent combination, for each surfactant (incorporating all solvent mixtures and concentrations) and finally for all surfactants. For surfactant-solvent combination master curves, the reference mixture was defined by the data with the lowest mass fraction of surfactant. For surfactant master curves, the reference mixture was defined by the lowest mass fraction of surfactant in 90% ethanol. For the total master curve, the reference mixture was defined by the lowest mass fraction of Di1010 in 90% ethanol.

8.4.3 Results

This procedure produced smooth, compact master curves in all cases, with the fitted polynomial function typically reaching $R^2 > 0.99$. Rosen-Hua curves (see 8.1, Figure 58) fit these data well, providing confidence that they represent plausible dynamic surface tension decays. For many composite curves, the best fit can be achieved by setting the initial surface tension, $\gamma_0 = 0.97$, rather than unity – it is not clear why this is the case. All surfactant and surfactant-solvent composite curves are presented in Figure 60.

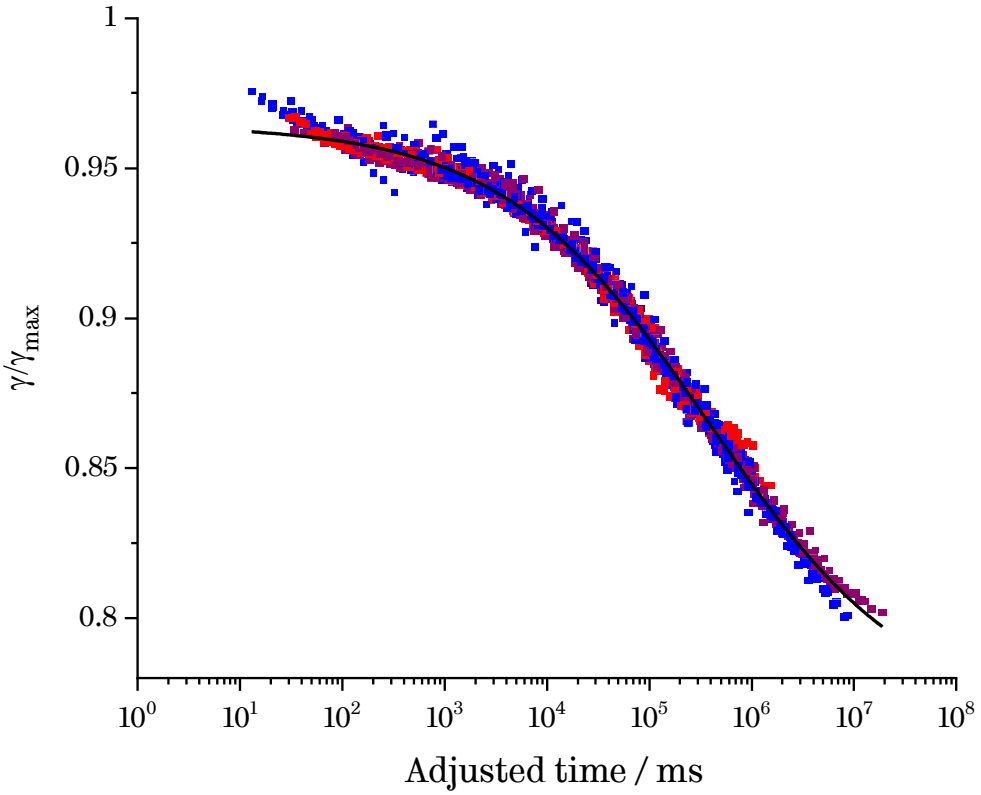

Figure 58. A master curve formed by time-concentration superposition of relative surface tension decays. This master curve includes all surfactants, in the time range 100 – 1000 ms, across a range of concentrations and for three different solvent mixtures. Symbol colour is scaled with solvent composition, where red is 90% ethanol and blue 50% ethanol. Data are fitted with the Rosen equation.

The shift factor, α, is (in part) a measure of the rate of surface tension reduction. As expected, therefore, α rose with surfactant concentration, and was higher in surfactants such as Di1508, which were effective at quickly reducing surface tension. Surfactants that performed poorly in ethanol-rich mixtures, such as Di1010 and Di1018, had significantly lower shift factors for 90% ethanol solutions than 50% or 70% ethanol – see Figure 59.

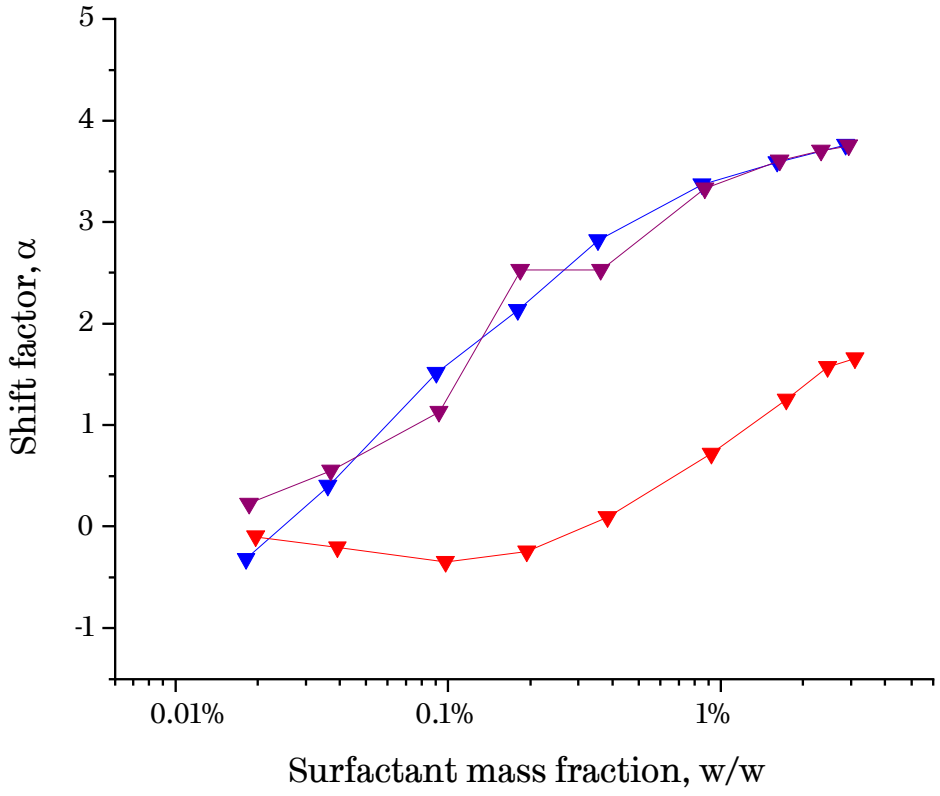

Figure 59. Time-concentration superposition shift factors versus surfactant concentration for Di1010 in three solvent compositions. Optimised shift factors for surfactants rise with concentration. Figure shows shift factors for Di1010 in the composite master curve. Symbol colour is scaled with solvent composition, where red is 90% ethanol, purple is 70% ethanol and blue is 50% ethanol.

For the master curve, the reference state was a dilute solution of Di1010 in 90% ethanol. Hence almost all optimised shift factors were larger than zero, as almost all conditions resulted in faster surface tension decay. For example, 1% w/w Di2510 in 90% ethanol has a shift factor of 2.7, suggesting that 1 ms in that state achieves the same (relative) surface tension reduction depression as ~470 ms in the reference state.

It was also possible to create smooth composite curves for all individual surfactants – see Figure 60, below. All such curves conformed well to the Rosen-Hua equation.

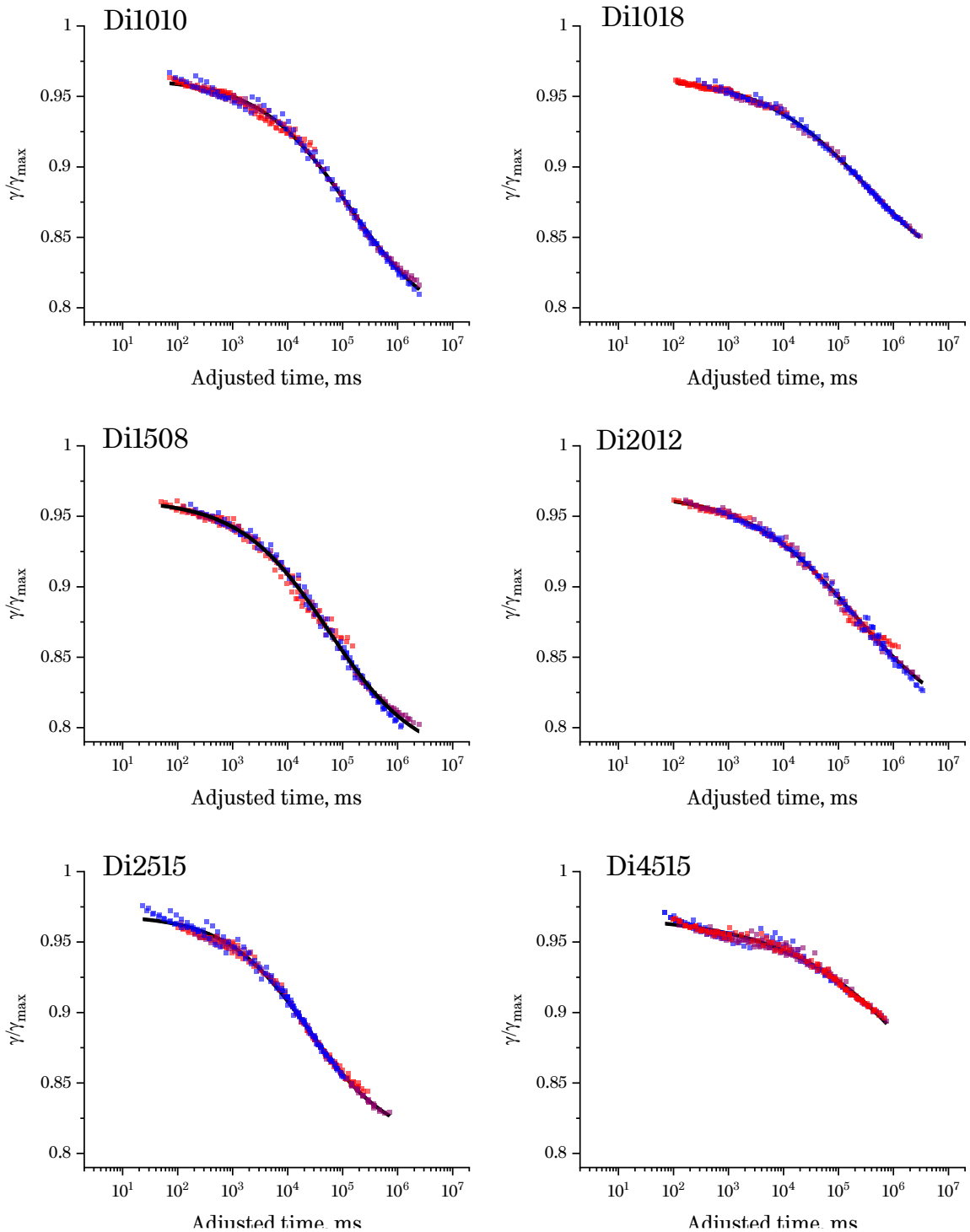

Figure 60. Time-concentration superposition curves for Di1010-Di4515. Colour is scaled to surfactant concentration, with low values indicated by red and high values by blue. Dark lines indicate the fitted numerical value derived from the Rosen-Hua equation.

The shift factor, α, correlates with predicted foam volumes in the foam pump test (see Figure 61. $R^2 = 0.66$). This aligns well with the results in 8.3.3 - both the shift factor and the dynamic surface pressure are normalised measures of the rate of DST decay.

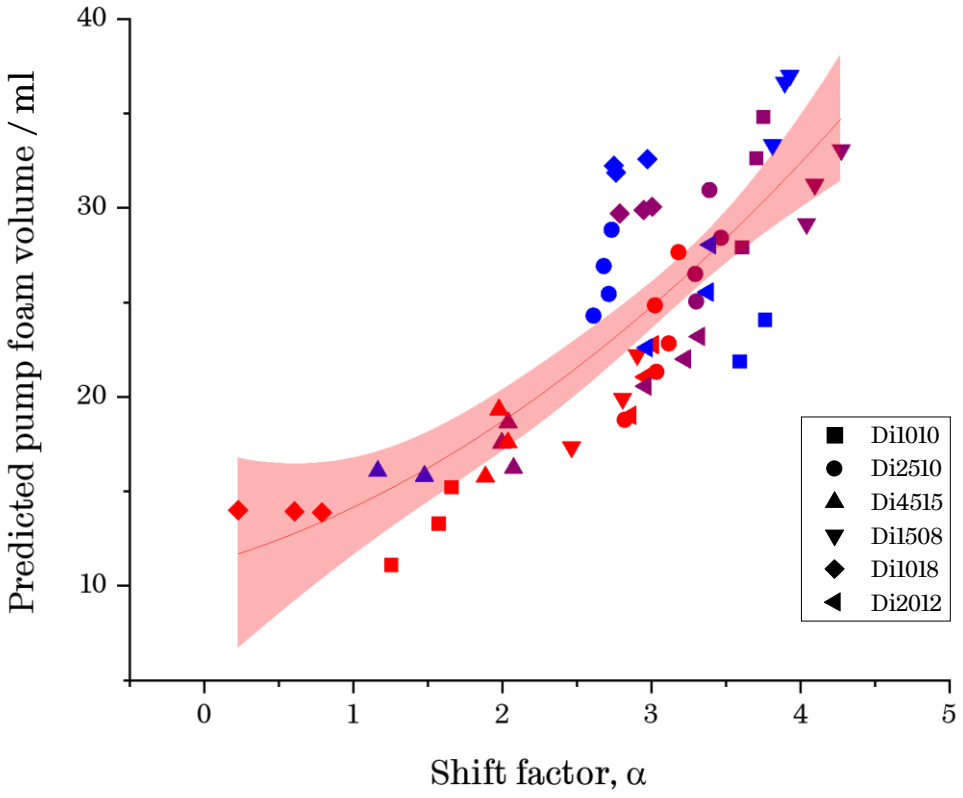

Figure 61. Foam volume versus time-concentration superposition shift factor for the full range of surfactant and solvent compositions. The optimised shift factor for a given surfactant/solvent/concentration combination is predictive of the foam volume generated in a foam pump test. Line of best fit is a quadratic polynomial. Shaded area represents 95% confidence interval. Symbol colour is scaled with solvent composition, where red is 90% ethanol and blue 50% ethanol.

The parameters of the Rosen-Hua equation have been associated with physical parameters by Filippov *et al*, who proposed the following relaxation function:

$$F(t) = \log\left[\frac{\gamma_0 - \gamma(t)}{\gamma(t) - \gamma_{eq}}\right] = n\log(t/t_{rel})$$

where $n = 1$ if adsorption is kinetically-controlled, and $n = 0.5$ if adsorption is diffusion-controlled.[105,106] This model was also applied to the surfactant master curves above. The values of γ_0 and γ_{eq} are fitted using the Rosen equation.

This model produces generally good fits, with all surfactants but Di4515 having $0.45 \leq n \leq 0.57$ (see Figure 62 and

Table 8). This suggests that the adsorption of these surfactants is diffusion-controlled, at least at short times. The anomalously low value of n for Di4515 is unlikely to be accurate characterisation of Di4515, as it suggests the surfactant undergoes a faster-than-diffusion adsorption processes. It is more likely to be a consequence of the anomalous shape of the Di4515 composite curve, which appears to feature a decline, plateau and second decline.

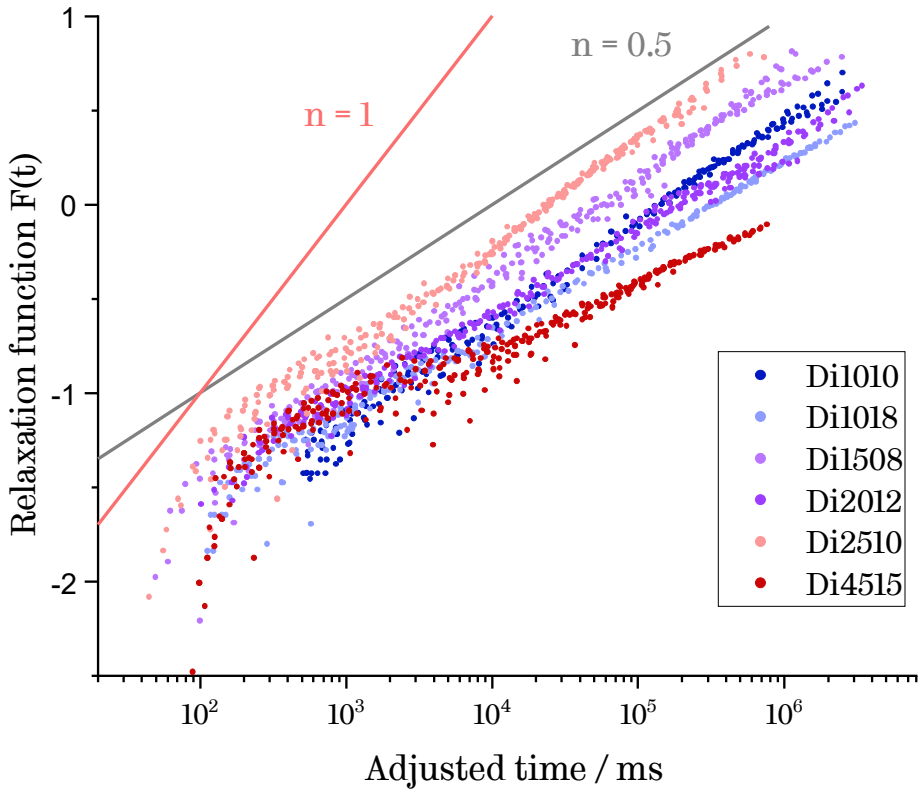

Figure 62. Relationship between the relaxation function proposed by Filippov and the adjusted time, when applied to the time-concentration superposition composite curves for surfactants Di1010-Di4515. The relaxation functions for the surfactant composite curve suggest that the adsorption process is diffusion-controlled. The black and red lines indicate the slopes of the function $n\ log\ (t/t_{rel})$ for $n = 0.5$ and $n = 1$, respectively.

Table 8. Fitted values of the Filippov relaxation function for composite master curves obtained for several surfactants.

Master curve	γ_0^{rel}	γ_{eq}^{rel}	n	t_{rel}, **ms**	$\mathbf{R^2}$
Di1010	0.960	0.780	0.54	1.46×10^5	0.99
Di1018	0.964	0.809	0.46	3.15×10^5	0.99
Di1508	0.962	0.776	0.54	5.50×10^4	0.99
Di2012	0.966	0.794	0.45	1.95×10^5	0.99
Di2510	0.969	0.806	0.57	2.44×10^4	0.98
Di4515	0.968	0.681	0.34	1.34×10^7	0.89

Attempts were made to apply the superposition approach to combined data from ring and bubble pressure tensiometry. In some cases, this approach was successful, producing smooth composite curves, but in other cases clear misalignments occurred – see Figure 63.

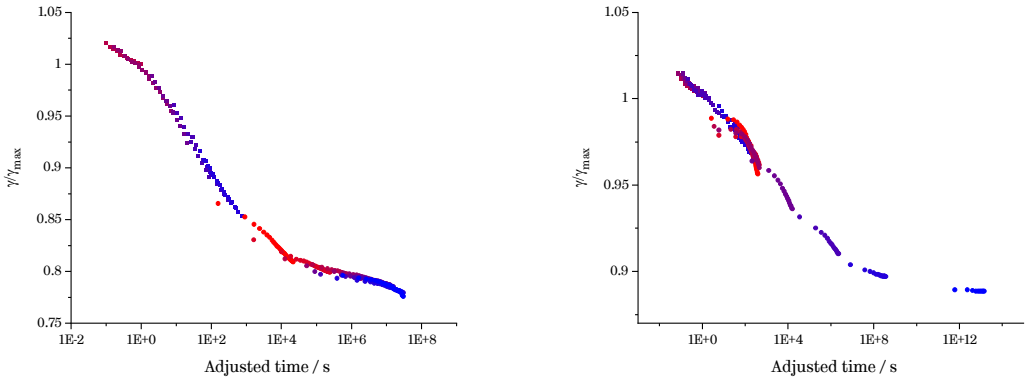

Figure 63. Superposition curves obtained for Di1010, combining bubble pressure and Du Noüy ring tensiometry data. Left: 90% ethanol. Right: 50% ethanol. Colour is scaled to surfactant concentration, with red implying low concentration and blue implying high.

In particular, low concentration Du Noüy ring tensiometry measurements, especially those featuring flat induction periods, could not normally be incorporated into the master curve.

9 Discussion

9.1 Substantive outcomes

This project aimed to link three levels of analysis: structure and composition of siloxane-based surfactants; analysis of micellar and interfacial behaviour and properties in various ethanol/water mixtures; and the behaviour and properties of the resulting foams. This was achieved using a range of analytical techniques, and it was shown that the degree of surface tension depression at characteristic times is a valuable tool for predicting foamability.

9.1.1 Molecular/surfactant properties

Siloxane polyethers were characterised, purified and (in one case) synthesised. As is commonly the case for technical grade surfactants, these materials proved to be polydisperse and to contain significant levels of contamination by surface-active impurities. Two methods of purification were examined – solvent extraction and foam fractionation. Both were effective in reducing the level of surface-active impurities.

The removal of PDMS-rich, surface-active impurities resulted in improved foamability, and their addition had a deleterious effect on foaming properties. This result supports similar findings by *e.g.* Patist *et al.*, who investigated the effects of surface-active impurities for aqueous solutions of sodium dodecyl sulfate.[102]

While both solvent extraction and foam fractionation proved effective, both would require significant optimisation and process design to be implementable on a large scale.

Surfactant solubility issues also arose during this research. Some EO-rich surfactants (Di4016 and Di4518) proved insoluble in water-ethanol mixtures, and a particularly EO-poor surfactant (Di4008) exhibited poor performance, most likely due to its low solubility. These results suggested an optimum range for nEO which should result in a soluble surfactant. It was found that nEO values equal to 16 or greater resulted in surfactants which would not disperse in water-ethanol mixtures, likely due to the formation of a crystalline EO phase. This result, to my knowledge, has not been reported elsewhere in the literature, and has no equivalent in the Pluronics literature.

9.1.2 Interfacial and solution properties

The influence of surfactant structure and solvent composition on the CMC of siloxane polyethers was investigated. The results agreed broadly with literature data for Pluronics – the length of the solvophobic block, in this case nPDMS, was the determining factor, dramatically lowering the CMC as it was increased. Adjusting the solvent quality also accorded with literature on siloxanes – improving the solvent quality for PDMS by increasing x_{eth} significantly increased the CMC.[47]

Dynamic surface tension measurements were carried out at both short surface ages (using BPT) and long surface ages (using PDT and Du Noüy ring tensiometry). Surface tension decayed faster at higher copolymer concentrations, with much of the surface tension reduction occurring within the first 1000 ms for higher concentrations. More water-rich mixtures produced significantly larger reductions in surface tension, particularly for shorter-chain surfactants (Di1010, Di1508, Di1018). Di4515, by contrast, produced slightly smaller reductions in surface tension in more water-rich mixtures. When comparing surfactant behaviour across solvent mixtures, surface pressure provides a convenient measure, removing effect of different γ_{sol} values to enable direct comparisons.

It is found that higher values of nPDMS and nPolyether result in lower surface activities. This finding aligns well with structure-property relations identified for Pluronics (see 2.3). While the literature on siloxane polyethers is less certain, these findings align with the majority of research - longer surfactants tend to exhibit lower surface activities (see 2.6). As expected, surfactants in more water-rich mixtures also take significantly longer to reach equilibrium, whereas equilibrium is attained relatively rapidly in ethanol-rich mixtures.

Time-temperature superposition methods were adapted to surface tension measurements, enabling the construction of composite curves which unified surface tension decay across a range of surfactants, solvent mixtures and concentrations – and in some cases, unifying bubble pressure and ring tensiometry data. This is analogous to the work of Bae *et al.*, who applied superposition analysis to dilational rheology of surfactant-laden interfaces.[104]

9.1.3 Foam properties

This thesis focused on foamability as the physical property of greatest importance, as it is believed that increasing this parameter has the largest practical benefit in the context of ABHR formulations. More voluminous foams are easier to handle and less wet-feeling, hence more convenient and appealing for users.

Experimental design and regularized regression were used to 'map' the foamability of solutions of siloxane polyethers across various water-ethanol mixtures. This work revealed that a complex set of interacting variables were responsible for the resultant foamability. A strong correlation between the ethanol content of the solvent mixture and the structure of the surfactant: lower nPDMS values performed better for water-rich solutions, and slightly higher nPDMS values are preferred for ethanol-rich solutions. These models were optimised to predict the ideal siloxane polyether for a range of water-ethanol mixtures.

The preferred solvent mixture for a given surfactant was shown to depend strongly on nPDMS, with more PDMS-rich surfactants exhibiting optimal performance in more ethanol-rich mixtures. It was also shown, however, that absolute performance declined when increasing both nPDMS and nEO.

Comparing foams generated by a foam pump, vortexing or sparging, the latter demonstrated very different foaming behaviour due to its slower rate of interface formation. This is consistent with studies by several researchers on the importance of foaming processes in determining foam properties.[33,81,107]

9.1.4 Linking surface and foam properties

It was demonstrated that 'dynamic surface pressure', *i.e.*, the surface pressure measured at surface age t, is a good predictor for foamability when t is close to a characteristic foaming time which depends on the foaming method. When $t = 500\ ms$, for example, dynamic surface pressure is a good predictor of performance in the foam pump test, whereas the dynamic surface pressure at $t = 10\ s$ is a good predictor for performance in the sparging test. These results quantitatively confirm the commonly held view that pumps correspond to a 'fast' foaming process whilst sparging is a slow one.

This result supports and extends the argument advanced by Petkova, Małysa and others (see 2.2.2) that *dynamic* surface properties are critical for understanding foaming behaviour. In addition, it shows that such a framework can be applied even when dealing with exotic surfactants and non-aqueous solvent mixtures. It also adds to a growing body of literature which highlights the importance of surfactant/process interactions in determining foaming performance.

The identification of dynamic surface *pressure* as a useful measure represents a slight divergence from research in this area. Petkova, for instance, demonstrated a link between foam volume and dynamic surface *tension* at short times – but these two approaches are

entirely compatible in my view. When γ_{sol} is fixed (e.g., when the solvent is water in all cases), they are essentially the same – but considering surface pressure better captures behaviour for non-aqueous solvent mixtures.

There are some qualitative differences between mine and Petkova's findings regarding the relationship between surface tension reduction and foamability. Petkova found a sharp threshold (~20 mN m^{-1} dynamic surface pressure, equivalent to 50 mN m^{-1}) for dynamic surface tension after 10 seconds, below which foamability in nonionic surfactants is poor. By contrast, siloxane-based surfactants exhibit a more gradual increase in foam volumes with respect to dynamic surface pressure.

As discussed in 2.5, water-ethanol mixtures represent something of an edge case for 'non-aqueous' foaming mixtures. At 50% ethanol, they retain significant aqueous character – such that conventional surfactants can still generate significant foam volumes.[51] As the ethanol content increases, the mixture becomes significantly less polar. In general, this work shows that siloxane surfactants in water-ethanol mixtures behave largely analogously to conventional nonionic surfactants in aqueous conditions.

9.2 Methodological developments

To the author's knowledge, this is the first attempt to systematically explore the behaviour of siloxane-based surfactants in non-aqueous media. The introduction of solvent polarity as an extra variable required the use of new methodological approaches, such as experimental design and regression modelling. Such methods allow fast and efficient exploration of systems with many possible variables, leading to new insights into their underlying mechanisms.

This is also the first application of superposition methods to dynamic surface tension measurements. This framework proved to be surprisingly successful in unifying disparate surface tension measurements into a single master curve, combining multiple surfactants, surfactant concentrations and solvent mixtures. The superposition approach highlights the underlying similarity of adsorption processes under various conditions and allowed the construction of an extended time series that was amenable to further analysis, *e.g.*, by the method of Filippov.[105,106]

9.3 Strengths

This project delivered on its principal aim – linking surfactant structure to surface properties, and in turn to foaming behaviour. It also developed complementary mechanistic and empirical frameworks, which can be applied to understand and predict foaming behaviour. The connection between dynamic surface pressure and foam performance may enable rapid screening of formulations in relatively small quantities, and without the need for full-scale foaming tests.

A further valuable output is a regression model, which can predict foam pump performance for siloxane polyether solutions across a wide range of conditions. This has a range of practical applications for both optimising ABHR formulations and designing new siloxane polyether surfactants.

A range of foaming methods – principally the foam pump and sparging – were investigated to probe the influence of the foaming process on the empirical model described above. The significant differences in behaviour observed between these methods emphasises the need to consider surfactant-process interactions in foaming science.

Finally, this work has begun to explore the interactions between (non-aqueous) solvent quality and surfactant structure on foaming. Given the practical importance of ethanol-based foams in ABHRs, it is hoped that this research provides new impetus to further explore and understand this area.

9.4 Key limitations

Several limitations reduced the scope of this work.

Most significantly, the project did not contain any primary research with users of ABHRs, but instead drew on prior results and my intuition to develop objectives for foam properties. Testing with users – before or after developing my model - might have shown whether my assumptions about foam quality agreed with user experiences and perceptions. User-assessed foam quality is unlikely to be solely determined by the volume of the foam, but may also depend on other aesthetic and use characteristics, and in principle could be quantified and modelled.

This limitation connects to a second area of weakness – a focus on foamability, and to a lesser extent stability, left several interesting foam properties unexplored. These areas include foam rheology, bubble size/size distribution and the rate of drainage.

Finally, it proved difficult to probe the mechanisms that govern the behaviour of surfactants. Despite significant effort (described in Chapter 5) to probe micelle dissolution kinetics, for example, no method proved to be sufficiently sensitive. It was also hoped that it would be possible to explore differences in surface elasticities using a pendant drop tensiometer (described in Chapter 7) but this instrument proved very difficult to use for this and other applications. Measuring the rates of kinetic processes and interfacial rheology would begin to identify the processes that determine surface tension reduction, and hence open an avenue for the more rational design of next-generation surfactants.

9.5 Future work

There are several avenues for future research which suggest themselves from this project.

It would be valuable to determine micelle dissolution rates and surface elasticities across the surfactants and solvent mixtures explored in this work. Investigations of the micellisation of siloxane surfactants might be possible using siloxane-modified dyes – which would ensure that said dyes are encapsulated – or could be investigated using a high-flux SAXS beamline equipped with stopped-flow apparatus. Surface elasticities might be determined using a pendant drop tensiometer built to higher specifications, but issues of needle wetting and rapid evaporation would most likely continue to make this work technically difficult.

A second avenue would expand the experimental space explored in Chapter 6. This expansion could include siloxane surfactants in mixtures, siloxane surfactants with different structures (e.g., graft or diblock copolymers) or with different chemical moieties (e.g., sugar-based solubilizing groups or mixed EO/PO chains). It could also investigate the effect of adjuvants present in common commercial formulations – moisturisers, cationic surfactants, preservatives, etc – on foaming performance.

Finally, one could explore the limits of the dynamic surface pressure/foam performance link by applying this model to other solvent mixtures, surfactants (e.g., fluorocarbon surfactants) and foaming methods.

10 References

1 D. Weaire and S. Hutzler, *The physics of foams. Clarendon*, Clarendon Press, Oxford, 1st edn., 1999.

2 Cantat, Isabelle, S. Cohen-Addad, F. Elias, F. Graner, R. Hohler, O. Pitois, F. Rouyer and A. Saint-Jalmes, *Foams: Structure and Dynamics*, Oxford University Press, Oxford, 1st edn., 2013.

3 S. E. Friberg, *Curr. Opin. Colloid Interface Sci.*, 2010, **15**, 359–364.

4 V. Croce, T. Cosgrove, C. A. Dreiss, G. Maitland, T. Hughes and G. Karlsson, *Langmuir*, 2004, **20**, 7984–7990.

5 M. Gradzielski, *Curr. Opin. Colloid Interface Sci.*, 2003, **8**, 337–345.

6 T. Gaudin, H. Lu, G. Fayet, A. Berthauld-Drelich, P. Rotureau, G. Pourceau, A. Wadouachi, E. Van Hecke, A. Nesterenko and I. Pezron, *Adv. Colloid Interface Sci.*, 2019, **270**, 87–100.

7 S. Chavda and P. Bahadur, *J. Mol. Liq.*, 2011, **161**, 72–77.

8 K. Shirahama and T. Kashiwabara, *J. Colloid Interface Sci.*, 1971, **36**, 65–70.

9 M. Li, Y. Rharbi, M. A. Winnik and K. G. Hahn, *J. Colloid Interface Sci.*, 2001, **240**, 284–293.

10 W. Drenckhan and A. Saint-Jalmes, *Adv. Colloid Interface Sci.*, 2015, **222**, 228–259.

11 M. Tupinamba Lima, S. N. Kurt-Zerdeli, D. Brüggemann, V. J. Spiering, M. Gradzielski and R. Schomäcker, *Colloids Surfaces A Physicochem. Eng. Asp.*, 2020, **588**, 124386.

12 D. Kawale, A. T. van Nimwegen, L. M. Portela, M. A. van Dijk and R. A. W. M. Henkes, *Colloids Surfaces A Physicochem. Eng. Asp.*, 2015, **481**, 328–336.

13 S. Hutzler, D. Lösch, E. Carey, D. Weaire, M. Hloucha and C. Stubenrauch, *Philos. Mag.*, 2011, **91**, 537–552.

14 A. Saint-Jalmes, *Soft Matter*, 2006, **2**, 836–849.

15 A. Patist, J. R. Kanicky, P. K. Shukla and D. O. Shah, *J. Colloid Interface Sci.*, 2002, **245**, 1–15.

16 K. Małysa, *Adv. Colloid Interface Sci.*, 1992, **40**, 37–83.

17 R. Höhler, S. Cohen-Addad and D. J. Durian, *Curr. Opin. Colloid Interface Sci.*, 2014, **19**, 242–252.

18 B. Petkova, S. Tcholakova, M. Chenkova, K. Golemanov, N. Denkov, D. Thorley and S. Stoyanov, *Adv. Colloid Interface Sci.*, 2020, **276**, 102084.

19 R. J. Pugh, *Adv. Colloid Interface Sci.*, 1996, **64**, 67–142.

20 H. A. Ritacco, *Adv. Colloid Interface Sci.*, 2020, **285**, 102282.

21 S. Marze, R. M. Guillermic and A. Saint-Jalmes, *Soft Matter*, 2009, **5**, 1937–1946.

22 A. L. Fameau and A. Saint-Jalmes, *Adv. Colloid Interface Sci.*, 2017, **247**, 454–464.

23 *WHO Guidelines on Hand Hygiene in Health Care*, 2009.

24 M. Winnefeld, M. A. Richard, M. Drancourt and J. J. Grob, *Br. J. Dermatol.*, 2000, **143**, 546–550.

25 A. P. Golin, D. Choi and A. Ghahary, *Am. J. Infect. Control*, 2020, **48**, 1062–1067.

26 V. Erasmus, T. J. Daha, H. Brug, J. H. Richardus, M. D. Behrendt, M. C. Vos and E. F. van Beeck, *Infect. Control Hosp. Epidemiol.*, 2010, **31**, 283–294.

27 L. Kingston, N. H. O'Connell and C. P. Dunne, *J. Hosp. Infect.*, 2016, **92**, 309–320.

28 R. E. Greenaway, K. Ormandy, C. Fellows and T. Hollowood, *J. Hosp. Infect.*, 2018, **100**, 195–201.

29 A. Berardi, D. R. Perinelli, H. A. Merchant, L. Bisharat, I. A. Basheti, G. Bonacucina, M. Cespi and G. F. Palmieri, *Int. J. Pharm.*, 2020, **584**, 119431.

30 K. Malysa and K. Lunkenheimer, *Curr. Opin. Colloid Interface Sci.*, 2008, **13**, 150–162.

31 A. Patist, B. K. Jha, S. G. Oh and D. O. Shah, *J. Surfactants Deterg.*, 1999, **2**, 317–324.

32 B. Petkova, S. Tcholakova and N. Denkov, *Colloids Surfaces A Physicochem. Eng. Asp.*, 2021, **626**, 127009.

33 L. Grossmann, P. Moll, C. Reichert and J. Weiss, *Food Res. Int.*, 2020, **129**, 108794.

34 P. Alexandridis and T. Alan Hatton, *Colloids Surfaces A Physicochem. Eng. Asp.*, 1995, **96**, 1–46.

35 R. Sedev, D. Exerowa and G. H. Findenegg, in *Colloid and Polymer Science*, D. Steinkopff-Verlag, 2000, vol. 278, pp. 119–123.

36 K. Khristov, B. Jachimska, K. Malysa and D. Exerowa, *Colloids Surfaces A Physicochem. Eng. Asp.*, 2001, **186**, 93–101.

37 B. R. Blomqvist, S. Folke and P. M. Claesson, *J. Dispers. Sci. Technol.*, 2006, **27**, 469–479.

38 B. B. Luokkala, S. Garoff, R. D. Tilton and R. M. Suter, *Langmuir*, 2001, **17**, 5917–5923.

39 N. Feng, T. Zhao, Y. Zhao, P. Song, G. Li and G. Zhang, *Colloids Surfaces A Physicochem. Eng. Asp.*, 2020, **586**, 124215.

40 P. Kanokkarn, T. Shiina, M. Santikunaporn and S. Chavadej, *Colloids Surfaces A Physicochem. Eng. Asp.*, 2017, **524**, 135–142.

41 M. A. Safarpour, A. A. Rafati, H. Gharibi and M. Rezaie, *J. Chinese Chem. Soc.*, 1999, **46**, 983–991.

42 L. A. Moreira and A. Firoozabadi, *Langmuir*, 2009, **25**, 12101–12113.

43 J. B. Huang, M. Mao and B. Y. Zhu, *Colloids Surfaces A Physicochem. Eng. Asp.*, 1999, **155**, 339–348.

44 S. K. Shah, S. K. Chatterjee and A. Bhattarai, *J. Mol. Liq.*, 2016, **222**, 906–914.

45 M. Bielawska, A. Chodzińska, B. Jańczuk and A. Zdziennicka, *Colloids Surfaces A Physicochem. Eng. Asp.*, 2013, **424**, 81–88.

46 R. Zana, C. Marques and A. Johner, *Adv. Colloid Interface Sci.*, 2006, **123**–**126**, 345–351.

47 Y. Lin and P. Alexandridis, *J. Phys. Chem. B*, 2002, **106**, 12124–12132.

48 P. Alexandridis and Y. Lin, *Macromolecules*, 2000, **33**, 5574–5587.

49 S. S. Soni, S. H. Panjabi and N. V. Sastry, *Colloids Surfaces A Physicochem. Eng. Asp.*, 2011, **377**, 205–211.

50 C. Blázquez, E. Emond, S. Schneider, C. Dalmazzone and V. Bergeron, *Oil Gas Sci. Technol.*, 2014, **69**, 467–479.

51 M. Miyashita, M. Akamatsu, K. Sakai and H. Sakai, *Chem. Lett.*, 2020, **49**, 453–456.

52 G. N. Sethumadhavan, A. D. Nikolov, D. T. Wasan, V. J. Srivastava, J. J. Kilbane and T. D. Hayes, *Ind. Eng. Chem. Res.*, 2003, **42**, 2634–2638.

53 B. M. Somosvári, N. Babcsán, P. Bárczy and A. Berthold, *Colloids Surfaces A Physicochem. Eng. Asp.*, 2007, **309**, 240–245.

54 B. Ning, Y. Wang, M. Zhang, Y. Bai, X. Tai, W. Wang and G. Wang, *J. Ind. Eng. Chem.*, 2021, **94**, 217–224.

55 A. L. Fameau, Y. Ma, M. Siebenbuerger and B. Bharti, *J. Colloid Interface Sci.*, 2021, **600**,

882–886.

56 R. M. Hill, *Curr. Opin. Colloid Interface Sci.*, 2002, **7**, 255–261.

57 P. Fang, Y. Bai, X. Ma, X. Tai, W. Wang and G. Wang, *J. Ind. Eng. Chem.*, 2018, **59**, 208–217.

58 Y. Bai, H. Liu, X. Ma, X. Tai, W. Wang, Z. Du and G. Wang, *J. Mol. Liq.*, 2018, **266**, 90–98.

59 J. Tan, Z. He, Y. Bai and P. Yan, *J. Dispers. Sci. Technol.*, 2020, **41**, 188–194.

60 J. Tan, M. Lin and Z. Ye, *J. Solution Chem.*, 2018, **47**, 2082–2093.

61 C. P. Chen, F. Lu and Q. X. Tong, *J. Mol. Liq.*, 2018, **266**, 504–513.

62 D. won Chung and J. C. Lim, *Colloids Surfaces A Physicochem. Eng. Asp.*, 2009, **336**, 35–40.

63 H. J. Liu, L. H. Lin and K. M. Chen, *J. Appl. Polym. Sci.*, 2002, **86**, 3005–3012.

64 B. Kanner, W. G. Reid and I. H. Petersen, *Ind. Eng. Chem. Prod. Res. Dev.*, 1967, **6**, 88–92.

65 J. Tan, Z. He, Y. Miao and M. Lin, *J. Surfactants Deterg.*, 2019, **22**, 875–883.

66 A. G. Kanellopoulos and M. J. Owen, *J. Colloid Interface Sci.*, 1971, **35**, 120–125.

67 H. J. Liu, L. H. Lin and K. M. Chen, *J. Appl. Polym. Sci.*, 2003, **88**, 1236–1241.

68 W. Noll, W. Büchner, H. J. Lücking and C. Sucker, *Kolloid-Zeitschrift Zeitschrift für Polym.*, 1972, **250**, 836–847.

69 B. Rippner Blomqvist, T. Wärnheim and P. M. Claesson, *Langmuir*, 2005, **21**, 6373–6384.

70 A. Wang, L. Jiang, G. Mao and Y. Liu, *J. Colloid Interface Sci.*, 2001, **242**, 337–345.

71 A. Patist, S. S. Bhagwat, K. W. Penfield, P. Aikens and D. O. Shah, *J. Surfactants Deterg.*, 2000, **3**, 53–58.

72 P. Johansson, R. Paberit, E. Rilby, J. Göhl, J. Swenson, Z. Refaa and H. Jansson, *ACS Appl. Energy Mater.*, 2020, **3**, 10578–10589.

73 A. Kelarakis, S. M. Mai, C. Booth and A. J. Ryan, *Polymer (Guildf).*, 2005, **46**, 2739–2747.

74 V. Bergeron, P. Cooper, C. Fischer, J. Giermanska-Kahn, D. Langevin and A. Pouchelon, *Colloids Surfaces A Physicochem. Eng. Asp.*, 1997, **122**, 103–120.

75 A. Genest, S. Binauld, E. Pouget, F. Ganachaud, E. Fleury and D. Portinha, *Polym. Chem.*, 2017, **8**, 624–630.

76 I. S. Khattab, F. Bandarkar, M. A. A. Fakhree and A. Jouyban, *Korean J. Chem. Eng.*, 2012, **29**, 812–817.

77 S. A. Onaizi, *Eur. Biophys. J.*, 2018, **47**, 631–640.

78 C. Tondre, J. Lang and R. Zana, *J. Colloid Interface Sci.*, 1975, **52**, 372–379.

79 J. Ilavsky and P. R. Jemian, *J. Appl. Crystallogr.*, 2009, **42**, 347–353.

80 V. Castelletto and I. W. Hamley, *Fibre Diffr. Rev.*, 2003, **11**, 36.

81 A. Patist, S. G. Oh, R. Leung and D. O. Shah, *Colloids Surfaces A Physicochem. Eng. Asp.*, 2001, **176**, 3–16.

82 R. Zana, *Adv. Colloid Interface Sci.*, 1995, **57**, 1–64.

83 P. Alexandridis, J. F. Holzwarth and T. A. Hatton, *Macromolecules*, 1994, **27**, 2414–2425.

84 I. N. Kurniasih, H. Liang, P. C. Mohr, G. Khot, J. P. Rabe and A. Mohr, *Langmuir*, 2015, **31**, 2639–2648.

85 D. Jacquemin, J. Preat, V. Wathelet and E. A. Perpète, *J. Chem. Phys.*, 2006, **124**, 074104.

86 H. Yoshioka, Y. Itoh, A. Kiyomori and Y. Oki, *Opt. Mater. Express*, 2016, **6**, 3417.

87 K. C. Shih, Z. Shen, Y. Li, M. Kröger, S. Y. Chang, Y. Liu, M. P. Nieh and H. M. Lai, *Soft Matter*, 2018, **14**, 7653–7663.

88 K. Hinkelmann, *Design and Analysis of Experiments*, Wiley, Hoboken, New Jersey, 8th ed., 2012, vol. 3.

89 V. R. Joseph, E. Gul and S. Ba, *Biometrika*, 2015, **102**, 371–380.

90 J. Antonakis and J. Dietz, *Pers. Individ. Dif.*, 2011, **50**, 409–415.

91 N. Mucic, A. Javadi, N. M. Kovalchuk, E. V. Aksenenko and R. Miller, *Adv. Colloid Interface Sci.*, 2011, **168**, 167–178.

92 J. E. Dennis and R. B. Schnabel, *Numerical Methods for Unconstrained Optimization and Nonlinear Equations*, Society for Industrial and Applied Mathematics, 1996.

93 T. Gaillard, M. Roché, C. Honorez, M. Jumeau, A. Balan, C. Jedrzejczyk and W. Drenckhan, *Int. J. Multiph. Flow*, 2017, **96**, 173–187.

94 P. Kanokkarn, T. Shiina, M. Santikunaporn and S. Chavadej, *Colloids Surfaces A Physicochem. Eng. Asp.*, 2017, **524**, 135–142.

95 J. Lang and R. Zana, *J. Phys. Chem.*, 1986, **90**, 5258–5265.

96 J. D. Berry, M. J. Neeson, R. R. Dagastine, D. Y. C. Chan and R. F. Tabor, *J. Colloid Interface Sci.*, 2015, **454**, 226–237.

97 M. Nagel, T. A. Tervoort and J. Vermant, *Adv. Colloid Interface Sci.*, 2017, **247**, 33–51.

98 Y. Touhami, G. H. Neale, V. Hornof and H. Khalfalah, *Colloids Surfaces A Physicochem. Eng. Asp.*, 1996, **112**, 31–41.

99 A. Daerr and A. Mogne, *J. Open Res. Softw.*, 2016, **4**, 3.

100 M. G. Muñoz, F. Monroy, F. Ortega, R. G. Rubio and D. Langevin, *Langmuir*, 2000, **16**, 1094–1101.

101 E. H. Simpson, *J. R. Stat. Soc. Ser. B*, 1951, **13**, 238–241.

102 A. Patist, T. Axelberd and D. O. Shah, *J. Colloid Interface Sci.*, 1998, **208**, 259–265.

103 C. W. Macosko, *Rheology: Principles, Measurements, and Applications*, Wiley, 1994.

104 J. E. Bae, J. B. Jung, K. Kim, S. M. Lee and N. G. Kang, *J. Colloid Interface Sci.*, 2019, **556**, 704–716.

105 L. K. Filippov, *J. Colloid Interface Sci.*, 1994, 163, 49–60.

106 L. K. Filippov, *J. Colloid Interface Sci.*, 1994, 164, 471–482.

107 B. Petkova, S. Tcholakova and N. Denkov, *Colloids Surfaces A Physicochem. Eng. Asp.*, 2021, **626**, 127009.

11 Appendices

General note on model structure:

Models presented below had the general structure:

$$y = \epsilon + \beta_0 + \sum_{i=1}^{4} \beta_i x_i + \sum_{j=1}^{4} \beta_j x_j^2 + \sum_{i,j=1}^{4} \beta_{ij} x_i x_j$$

Where x_n represents, (e.g.):

$x_1 = \text{ethanol volume fraction}$

$x_2 = \text{surfactant weight fraction}$

$x_3 = \text{push time, s}$

$x_4 = \text{surfactant [categorical]}$

β_0 represents the intercept, β_n represents the estimated coefficient for term n, y represents the outcome variable, and ϵ represents remaining error, unaccounted for by the model terms.

Categorical terms representing the identity surfactant had the following structure:

If [Surfactant] is Di1010 $\Rightarrow \beta_n = a$

...is Di1018 $\Rightarrow \beta_n = b$

...is Di1508 $\Rightarrow \beta_n = c$

etc

11.1 Doping Model

Fit by standard least squares, with only first-order terms: intercept, calculated concentration of triblock in Di2510 sample, concentration of 'natural' PDMS oligomer and concentration of added PDMS oligomer.

Model structure:

$$y = \epsilon + \beta_0 + \sum_{i=1}^{3} \beta_i x_i$$

Where x_i represents:

$x_1 =$ triblock molar concentration

$x_2 =$ natural PDMS oligomer molar concentration

$x_3 =$ added PDMS oligomer molar concentration

Term	Estimate	Std Error	t Ratio	Prob>|t|
Intercept	15.26	1.94	7.85	0.000
Triblock Concentration	1.94	0.40	4.81	0.001
Natural PDMS	-4.32	2.61	-1.66	0.132
Added PDMS	-8.99	1.51	-5.94	0.000

11.2 Foam pump naïve model

Fit by standard least squares. Includes all first-order, quadratic and second-order interaction terms for: surfactant [categorical], ethanol fraction, surfactant weight fraction and push time, except an interaction term between push time and surfactant.

Model structure:

$$y = \epsilon + \sum_{i=1}^{4} \beta_i x_i + \sum_{j=1}^{4} \beta_j x_j^2 + \sum_{i,j=1}^{4} \beta_{ij} x_i x_j$$

Where:

$x_1 =$ ethanol volume fraction

$x_2 =$ surfactant weight fraction

$x_3 =$ push time, s

$x_4 =$ surfactant [categorical]

The terms representing the identity surfactant had the following structure:

$$\text{If [Surfactant] is Di1010} \Rightarrow \beta_n = a$$
$$\ldots \text{is Di1018} \Rightarrow \beta_n = b$$
$$\ldots \text{is Di1508} \Rightarrow \beta_n = c$$

$$etc \ldots$$

Term	Estimate	Std Error	t Ratio	Prob>|t|
Intercept	23.09	0.65	35.67	0.000
Surfactant[Di1010]	10.29	0.45	22.84	0.000
Surfactant[Di1018]	4.60	0.31	15.02	0.000
Surfactant[Di1508]	11.02	0.39	27.93	0.000
Surfactant[Di2012]	4.97	0.25	20.00	0.000
Surfactant[Di2510]	8.27	0.26	31.47	0.000
Surfactant[Di3012]	-4.36	0.37	-11.75	0.000
Surfactant[Di3514]	-5.65	0.36	-15.74	0.000
Surfactant[Di4016]	-12.57	0.40	-31.65	0.000
Surfactant[Di4515]	-0.59	0.24	-2.43	0.015

Ethanol Fraction	-10.79	0.67	-16.02	0.000
Surfactant weight fraction	164.98	8.36	19.74	0.000
Push Time	3.82	0.65	5.84	0.000
(Push Time-0.51521)*(Push Time-0.51521)	-45.36	4.98	-9.10	0.000
(Ethanol Fraction-0.70089)*(Ethanol Fraction-0.70089)	-54.20	5.23	-10.37	0.000
(Surfactant weight fraction-0.03144)*(Surfactant weight fraction-0.03144)	-2708.45	352.67	-7.68	0.000
(Ethanol Fraction-0.70089)*(Surfactant weight fraction-0.03144)	230.85	35.87	6.44	0.000
Surfactant[Di1010]*(Ethanol Fraction-0.70089)	-19.02	2.04	-9.34	0.000
Surfactant[Di1018]*(Ethanol Fraction-0.70089)	-41.54	1.72	-24.17	0.000
Surfactant[Di1508]*(Ethanol Fraction-0.70089)	-22.43	1.72	-13.00	0.000
Surfactant[Di2012]*(Ethanol Fraction-0.70089)	2.63	1.42	1.85	0.064
Surfactant[Di2510]*(Ethanol Fraction-0.70089)	9.68	1.37	7.07	0.000
Surfactant[Di3012]*(Ethanol Fraction-0.70089)	15.29	2.24	6.84	0.000
Surfactant[Di3514]*(Ethanol Fraction-0.70089)	9.27	2.00	4.64	0.000
Surfactant[Di4016]*(Ethanol Fraction-0.70089)	13.02	2.28	5.71	0.000
Surfactant[Di4515]*(Ethanol Fraction-0.70089)	20.08	1.48	13.56	0.000
Surfactant[Di1010]*(Surfactant weight fraction-0.03144)	311.44	32.06	9.71	0.000
Surfactant[Di1018]*(Surfactant weight fraction-0.03144)	-98.50	21.00	-4.69	0.000
Surfactant[Di1508]*(Surfactant weight fraction-0.03144)	87.00	30.58	2.84	0.005
Surfactant[Di2012]*(Surfactant weight fraction-0.03144)	96.32	15.73	6.12	0.000
Surfactant[Di2510]*(Surfactant weight fraction-0.03144)	140.20	12.65	11.08	0.000
Surfactant[Di3012]*(Surfactant weight fraction-0.03144)	-86.33	28.77	-3.00	0.003
Surfactant[Di3514]*(Surfactant weight fraction-0.03144)	-65.29	23.10	-2.83	0.005
Surfactant[Di4016]*(Surfactant weight fraction-0.03144)	-140.02	26.21	-5.34	0.000
Surfactant[Di4515]*(Surfactant weight fraction-0.03144)	-1.46	17.38	-0.08	0.933

Variable importance was assessed by Monte Carlo simulation, using independent uniform inputs. The resulting output, shown below, describes the degree of variability in the predicted response (in this case, foam volume) based on the variation of the factor in question. Effects are separated into direct effects of the variable (the ‘main’ effect) and effects that act through interactions with other variables (the ‘total’ effect).

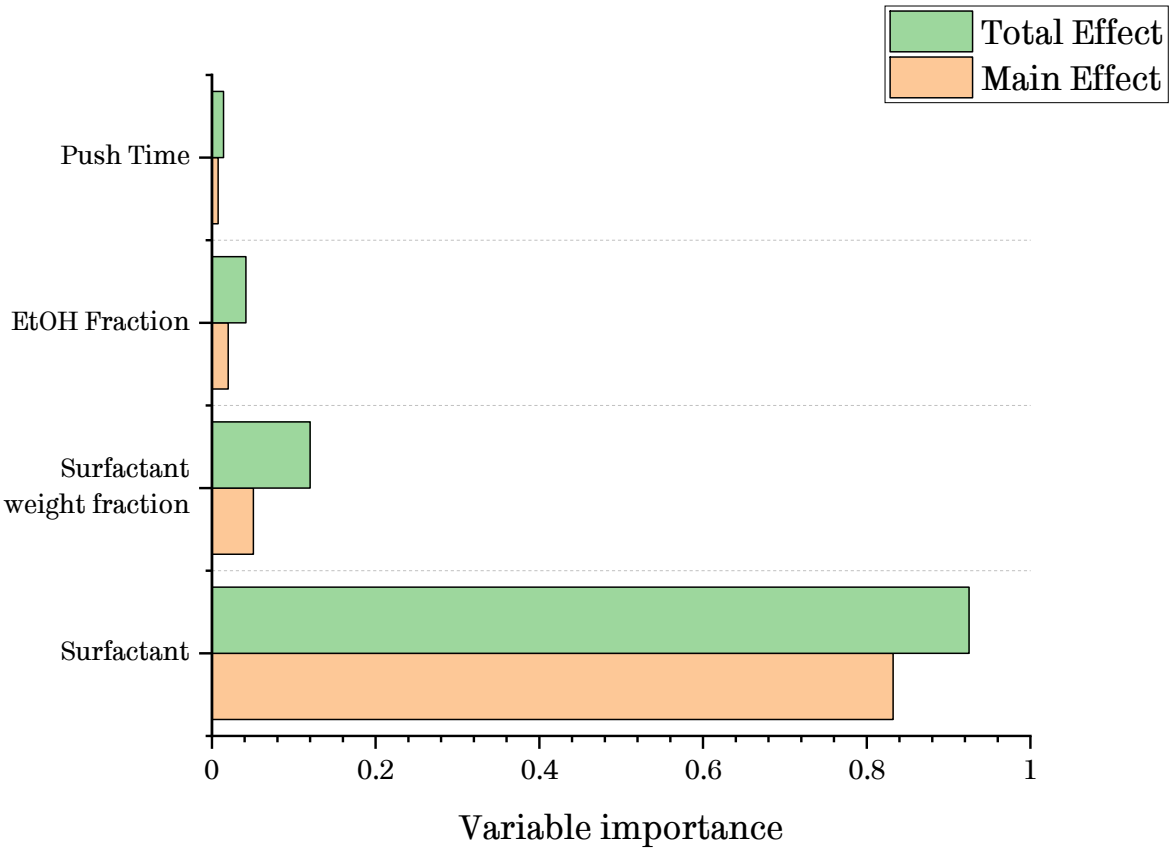
Total Effect
Main Effect
Push Time
EtOH Fraction
Surfactant
weight fraction
Surfactant
0
0.2
0.4
0.6
0.8
1
Variable importance

11.3 Foam pump informed model

Fit by elastic net regularisation. Includes first order terms: nPDMS, nEO, ethanol fraction, push time and polymer weight fraction. Includes quadratic and second-order interaction terms for all terms.

Model structure:

$$y = \epsilon + \sum_{i=1}^{4} \beta_i x_i + \sum_{j=1}^{4} \beta_j x_j^2 + \sum_{i,j=1}^{4} \beta_{ij} x_i x_j$$

Where:

$x_1 =$ ethanol volume fraction

$x_2 =$ surfactant weight fraction

$x_3 =$ push time, s

$x_4 = \mathrm{PDMS}_n$

$x_5 = \mathrm{EO}_n$

Term	Estimate	Std Error	Wald Chi Square	Prob > Chi Square
Intercept	51.60	1.06	2364.99	0.000
PDMS Units 2	-0.51	0.02	597.40	0.000
PEG Units 2	-1.33	0.05	674.43	0.000
Ethanol Fraction	-9.85	0.90	118.94	0.000
Push Time	4.19	0.93	20.13	0.000
Surfactant weight fraction	217.76	8.55	648.28	0.000
(PDMS Units -25.0074)*(PDMS Units -25.0074)	-0.03	0.00	117.18	0.000
(PDMS Units -25.0074)*(PEG Units -11.5405)	0.00	0.00	0.00	1.000
(PEG Units -11.5405)*(PEG Units -11.5405)	0.22	0.03	61.50	0.000
(PDMS Units -25.0074)*(Ethanol Fraction-0.70834)	1.11	0.09	148.57	0.000
(PEG Units -11.5405)*(Ethanol Fraction-0.70834)	0.00	0.00	0.00	1.000
(Ethanol Fraction-0.70834)*(Ethanol Fraction-0.70834)	-68.39	7.32	87.41	0.000
(PDMS Units -25.0074)*(Push Time-0.50677)	0.00	0.00	0.00	1.000
(PEG Units -11.5405)*(Push Time-0.50677)	0.00	0.00	0.00	1.000

(Ethanol Fraction-0.70834)*(Push Time-0.50677)	-19.47	5.49	12.57	0.000
(Push Time-0.50677)*(Push Time-0.50677)	-30.97	7.21	18.47	0.000
(PDMS Units -25.0074)*(Surfactant weight fraction-0.03077)	0.00	0.00	0.00	1.000
(PEG Units -11.5405)*(Surfactant weight fraction-0.03077)	-53.24	3.05	305.53	0.000
(Ethanol Fraction-0.70834)*(Surfactant weight fraction-0.03077)	253.13	41.96	36.39	0.000
(Push Time-0.50677)*(Surfactant weight fraction-0.03077)	352.33	37.40	88.76	0.000
(Surfactant weight fraction-0.03077)*(Surfactant weight fraction-0.03077)	-590.44	328.15	3.24	0.072

Variable importance was assessed as above.

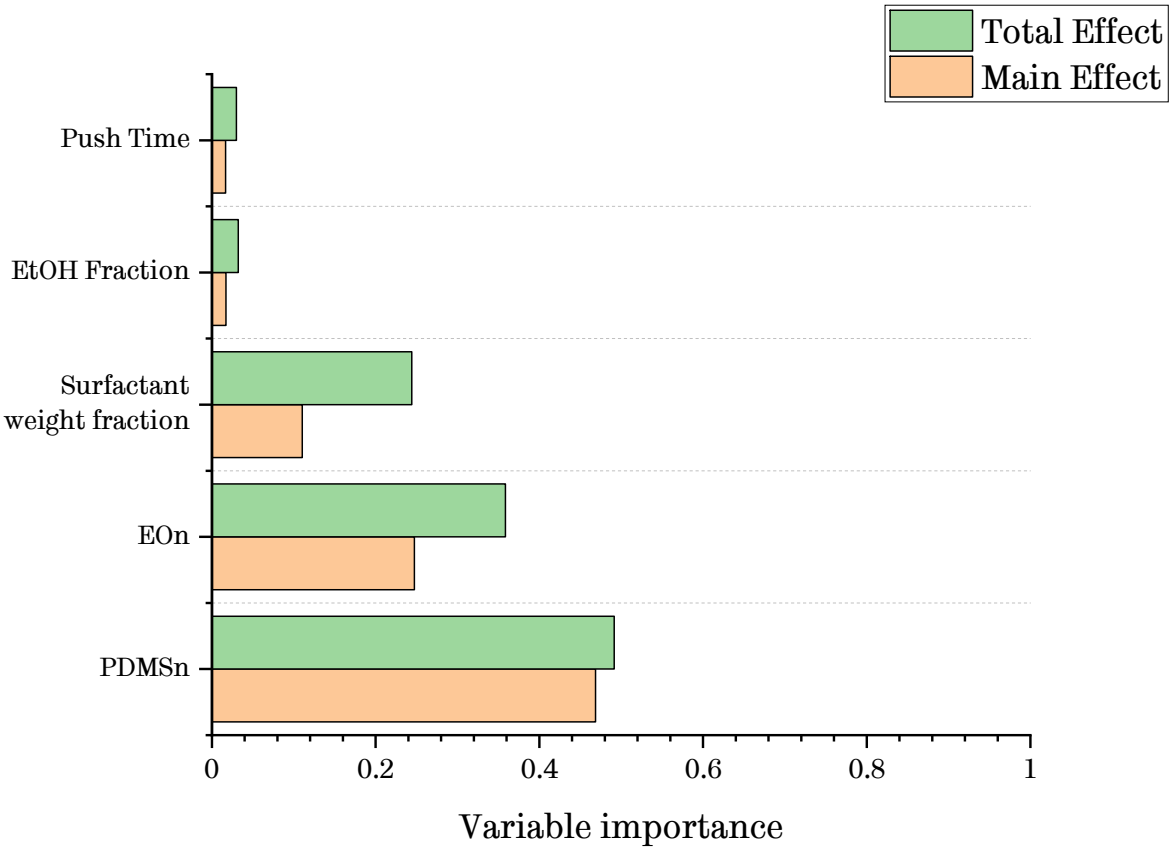

11.4 Sparging foam volume model

Fitted by elastic net regularised regression. Included surfactant [categorical variable], ethanol fraction, push speed, polymer weight fraction. Also included all quadratic terms and second-order interactions.

Effects of surfactants are measured by comparison to Di4515.

Model structure:

$$y = \epsilon + \sum_{i=1}^{4} \beta_i x_i + \sum_{j=1}^{4} \beta_j x_j^2 + \sum_{i,j=1}^{4} \beta_{ij} x_i x_j$$

Where:

$x_1 = \text{ethanol volume fraction}$

$x_2 = \text{surfactant weight fraction}$

$x_3 = \text{push speed, ml / s}$

$x_4 = \text{surfactant [categorical]}$

The terms representing the identity surfactant had the following structure:

$$\text{If [Surfactant] is Di1010} \Rightarrow \beta_n = a$$
$$\ldots \text{is Di1018} \Rightarrow \beta_n = b$$
$$\ldots \text{is Di1508} \Rightarrow \beta_n = c$$
$$etc \ldots$$

Term	Estimate	Std Error	Wald Chi Square	Prob > Chi Square
Intercept	63.40	4.81	173.44	0.000
Surfactant[Di1010-Di4515]	-4.96	1.52	10.65	0.001
Surfactant[Di1018-Di4515]	-3.03	1.41	4.60	0.032
Surfactant[Di1508-Di4515]	0.00	0.00	0.00	1.000
Surfactant[Di2012-Di4515]	-3.45	1.57	4.85	0.028
Surfactant[Di2510-Di4515]	0.00	0.00	0.00	1.000

Push speed	0.00	0.00	0.00	1.000
Ethanol fraction	-17.36	6.00	8.37	0.004
Surfactant weight fraction	0.00	0.00	0.00	1.000
Surfactant[Di1010-Di4515]*(Push speed-86.0096)	-0.32	0.05	35.05	0.000
Surfactant[Di1018-Di4515]*(Push speed-86.0096)	-0.06	0.04	1.60	0.206
Surfactant[Di1508-Di4515]*(Push speed-86.0096)	0.03	0.05	0.32	0.570
Surfactant[Di2012-Di4515]*(Push speed-86.0096)	-0.05	0.04	1.34	0.247
Surfactant[Di2510-Di4515]*(Push speed-86.0096)	0.00	0.00	0.00	1.000
(Push speed-86.0096)*(Push speed-86.0096)	0.00	0.00	0.54	0.464
Surfactant[Di1010-Di4515]*(Ethanol fraction-0.68942)	-51.88	8.15	40.47	0.000
Surfactant[Di1018-Di4515]*(Ethanol fraction-0.68942)	-32.49	9.33	12.12	0.000
Surfactant[Di1508-Di4515]*(Ethanol fraction-0.68942)	-46.93	11.08	17.93	0.000
Surfactant[Di2012-Di4515]*(Ethanol fraction-0.68942)	-16.16	11.66	1.92	0.166
Surfactant[Di2510-Di4515]*(Ethanol fraction-0.68942)	0.00	0.00	0.00	1.000
(Push speed-86.0096)*(Ethanol fraction-0.68942)	-0.57	0.11	25.53	0.000
(Ethanol fraction-0.68942)*(Ethanol fraction-0.68942)	-125.52	42.51	8.72	0.003
Surfactant[Di1010-Di4515]*(Surfactant weight fraction-0.02619)	83.17	44.73	3.46	0.063
Surfactant[Di1018-Di4515]*(Surfactant weight fraction-0.02619)	119.44	55.02	4.71	0.030
Surfactant[Di1508-Di4515]*(Surfactant weight fraction-0.02619)	0.00	0.00	0.00	1.000
Surfactant[Di2012-Di4515]*(Surfactant weight fraction-0.02619)	218.80	6.909	12.87	0.000
Surfactant[Di2510-Di4515]*(Surfactant weight fraction-0.02619)	-150.54	49.26	9.34	0.002
(Push speed-86.0096)*(Surfactant weight fraction-0.02619)	0.69	0.92	0.57	0.452
(Ethanol fraction-0.68942)*(Surfactant weight fraction-0.02619)	45.21	113.41	0.16	0.690

(Surfactant weight fraction-0.02619)*(Surfactant weight fraction-0.02619)	3164.12	1252.70	6.38	0.012

11.5 Sparging foam half-life model

Fitted by elastic net regularised regression, using a gamma distribution. Included surfactant [categorical variable], ethanol fraction, push speed, polymer weight fraction. Also included all quadratic terms and second-order interactions.

Effects of surfactants are measured by comparison to Di4515.

Model structure:

$$y = \exp\left[\epsilon + \sum_{i=1}^{4} \beta_i x_i + \sum_{j=1}^{4} \beta_j x_j^2 + \sum_{i,j=1}^{4} \beta_{ij} x_i x_j\right]$$

Where:

$x_1 = \text{ethanol volume fraction}$

$x_2 = \text{surfactant weight fraction}$

$x_3 = \text{push speed, ml / s}$

$x_4 = \text{surfactant [categorical]}$

The terms representing the identity surfactant had the following structure:

$$\text{If [Surfactant] is Di1010} \Rightarrow \beta_n = a$$
$$\ldots \text{is Di1018} \Rightarrow \beta_n = b$$
$$\ldots \text{is Di1508} \Rightarrow \beta_n = c$$

$$etc \ldots$$

Term	Estimate	Std Error	Wald Chi Square	Prob > Chi Square
Intercept	6.23	0.16	1559.20	0.000
Surfactant[Di1010-Di4515]	0.00	0.00	0.00	1.000
Surfactant[Di1018-Di4515]	-0.17	0.09	3.74	0.053
Surfactant[Di1508-Di4515]	-0.32	0.07	19.49	0.000
Surfactant[Di2012-Di4515]	-0.08	0.08	0.93	0.335
Surfactant[Di2510-Di4515]	0.00	0.00	0.00	1.000
Push speed	0.00	0.00	0.00	1.000
Ethanol fraction	-2.81	0.22	161.82	0.000
Surfactant weight fraction	0.00	0.00	0.00	1.000
Surfactant[Di1010-Di4515]*(Push speed-86)	-0.01	0.00	86.74	0.000
Surfactant[Di1018-Di4515]*(Push speed-86)	-0.01	0.00	15.63	0.000
Surfactant[Di1508-Di4515]*(Push speed-86)	0.00	0.00	0.00	1.000
Surfactant[Di2012-Di4515]*(Push speed-86)	-0.01	0.00	20.62	0.000
Surfactant[Di2510-Di4515]*(Push speed-86)	0.00	0.00	0.35	0.553
(Push speed-86)*(Push speed-86)	0.00	0.00	19.56	0.000
Surfactant[Di1010-Di4515]*(Ethanol fraction-0.69143)	-4.01	0.43	86.77	0.000
Surfactant[Di1018-Di4515]*(Ethanol fraction-0.69143)	0.00	0.00	0.00	1.000
Surfactant[Di1508-Di4515]*(Ethanol fraction-0.69143)	-2.50	0.52	23.22	0.000
Surfactant[Di2012-Di4515]*(Ethanol fraction-0.69143)	0.00	0.00	0.00	1.000
Surfactant[Di2510-Di4515]*(Ethanol fraction-0.69143)	-0.93	0.49	3.63	0.057
(Push speed-86)*(Ethanol fraction-0.69143)	-0.01	0.01	5.72	0.017
(Ethanol fraction-0.69143)*(Ethanol fraction-0.69143)	0.00	0.00	0.00	1.000
Surfactant[Di1010-Di4515]*(Surfactant weight fraction-0.02595)	0.00	0.00	0.00	1.000
Surfactant[Di1018-Di4515]*(Surfactant weight fraction-0.02595)	4.92	2.87	2.95	0.086
Surfactant[Di1508-Di4515]*(Surfactant weight fraction-0.02595)	0.00	0.00	0.00	1.000
Surfactant[Di2012-Di4515]*(Surfactant weight fraction-0.02595)	11.08	1.88	34.72	0.000
Surfactant[Di2510-Di4515]*(Surfactant weight fraction-0.02595)	0.00	0.00	0.00	1.000
(Push speed-86)*(Surfactant weight fraction-0.02595)	0.00	0.00	0.00	1.000
(Ethanol fraction-0.69143)*(Surfactant weight fraction-0.02595)	25.04	6.73	13.83	0.000
(Surfactant weight fraction-0.02595)*(Surfactant weight fraction-0.02595)	0.00	0.00	0.00	1.000

11.6 Vortexing foam volume model

Fitted by standard least squares regression. Contains Surfactant [categorical variable], ethanol fraction, surfactant weight fraction. All quadratic terms and first-order interactions.

Model structure:

$$y = \epsilon + \sum_{i=1}^{3} \beta_i x_i + \sum_{j=1}^{3} \beta_j x_j^2 + \sum_{i,j=1}^{3} \beta_{ij} x_i x_j$$

Where:

$x_1 =$ ethanol volume fraction

$x_2 =$ surfactant weight fraction

$x_3 =$ surfactant [categorical]

The terms representing the identity surfactant had the following structure:

$$\text{If [Surfactant] is Di1010} \Rightarrow \beta_n = a$$
$$\text{... is Di1018} \Rightarrow \beta_n = b$$
$$\text{... is Di1508} \Rightarrow \beta_n = c$$

$$etc \ldots$$

Term	Estimate	Std Error	t Ratio	Prob>|t|
Intercept	7.37	0.16	45.04	0.000
Surfactant[Di1010]	-0.20	0.14	-1.40	0.165
Surfactant[Di1018]	0.12	0.14	0.83	0.409
Surfactant[Di1508]	0.23	0.16	1.48	0.143
Surfactant[Di2012]	-0.30	0.13	-2.33	0.022
Surfactant[Di2510]	0.68	0.16	4.37	0.000
Surfactant[Di4515]	-0.53	0.14	-3.81	0.000
Ethanol fraction	-0.19	0.09	-2.15	0.035
Surfactant weight fraction	1.95	0.12	16.03	0.000
Surfactant[Di1010]*(Ethanol fraction-0.69143)	0.07	0.17	0.44	0.661
Surfactant[Di1018]*(Ethanol fraction-0.69143)	-1.06	0.18	-5.90	0.000
Surfactant[Di1508]*(Ethanol fraction-0.69143)	1.00	0.23	4.39	0.000
Surfactant[Di2012]*(Ethanol fraction-0.69143)	-0.19	0.16	-1.16	0.251

Surfactant[Di2510]*(Ethanol fraction-0.69143)	-0.38	0.22	-1.74	0.085
Surfactant[Di4515]*(Ethanol fraction-0.69143)	0.56	0.18	3.17	0.002
(Ethanol fraction-0.69143)*(Ethanol fraction-0.69143)	-0.38	0.18	-2.08	0.040
Surfactant[Di1010]*(Surfactant weight fraction-0.02595)	-0.13	0.19	-0.71	0.482
Surfactant[Di1018]*(Surfactant weight fraction-0.02595)	-0.87	0.20	-4.38	0.000
Surfactant[Di1508]*(Surfactant weight fraction-0.02595)	0.88	0.30	2.97	0.004
Surfactant[Di2012]*(Surfactant weight fraction-0.02595)	-0.13	0.19	-0.67	0.504
Surfactant[Di2510]*(Surfactant weight fraction-0.02595)	0.53	0.21	2.50	0.014
Surfactant[Di4515]*(Surfactant weight fraction-0.02595)	-0.28	0.19	-1.48	0.143
(Ethanol fraction-0.69143)*(Surfactant weight fraction-0.02595)	0.21	0.11	1.85	0.068
(Surfactant weight fraction-0.02595)*(Surfactant weight fraction-0.02595)	-0.86	0.23	-3.72	0.000

11.7 Double syringe half-life model

Fitted by elastic net regularised regression, using a gamma distribution. Incorporated Sample size, container size, ethanol fraction and surfactant weight fraction as first-order variables.

Model structure:

$$y = \exp\left[\epsilon + \sum_{i=1}^{5} \beta_i x_i\right]$$

Where:

$x_1 =$ ethanol volume fraction

$x_2 =$ liquid/gas ratio

$x_3 =$ surfactant weight fraction

$x_4 =$ container area [categorical]

$x_5 =$ sample size, ml

Term	Estimate	Std Error	Wald Chi Square	Prob > Chi Square
Intercept	7.82	0.60	171.75	0.000
Container Area[7.07-3.14]	0.83	0.15	32.43	0.000
Sample Size	-0.25	0.07	12.16	0.000
Liquid/Gas Ratio	-1.64	0.62	7.00	0.008
Ethanol Fraction	-2.16	0.75	8.29	0.004
Surfactant weight fraction	6.23	2.84	4.82	0.028

11.8 Surface pressure model

Model structure:

$$y = \epsilon + \sum_{i=1}^{3} \beta_i x_i + \beta_3 x_3^2$$

Where:

$x_1 =$ ethanol volume fraction

$x_2 = \mathrm{PDMS}_n$

$x_3 = \mathrm{EO}_n$

Term	Estimate	Std Error	t Ratio	Prob>|t|
Intercept	11.61688	0.614634	18.90048	7.74E-11
nPDMS	0.007205	0.019095	0.377348	0.712003
nPolyether	-0.1042	0.027588	-3.77706	0.002306
Ethanol fraction	-8.93404	0.65677	-13.603	4.58E-09
(nPolyether -14.6667)*(nPolyether 14.6667)	0.003268	0.003685	0.886883	0.391254